Bottomonium and B Physics with Lattice NRQCD b Quarks

Brian Colquhoun

School of Physics and Astronomy

Submitted in fulfilment of the requirements for the

Degree of Doctor of Philosophy

University of Glasgow

February 2015

Abstract

Lattice Nonrelativistic QCD (NRQCD) is a formalism that allows b quarks to be simulated in their bound states in lattice QCD. It requires only a relatively straightforward evolution equation and is therefore much faster than other lattice QCD formalisms. We perform calculations using radially improved NRQCD for mesons that contain b quarks on gluon field configurations generated by the MILC collaboration with $2 + 1 + 1$ flavours of sea quarks, and including light quarks down to their physical masses.

We calculate properties of bottomonium mesons; in particular, the Υ and η_b. The kinetic mass of these states over a range of momenta is calculated and shown to be stable. We determine the Υ and Υ' leptonic widths for the first time in lattice QCD after determining a renormalisation factor matching NRQCD to QCD using temporal moments of the meson correlators. We also compare these temporal moments to continuum temporal moments derived from q^2-derivative moments of the b quark polarisation function in continuum QCD perturbation theory. Finally, we use the NRQCD moments to determine the mass of the b quark and the contribution of a b quark loop to the hadronic piece of the muon anomalous magnetic moment.

The same NRQCD action can be used to simulate the b quark in heavy-light mesons. We present results here for the form factor $f_0(q^2_{\text{max}})$ of the semileptonic $B \to \pi\ell\nu$ decay. We show that the soft pion theorem, which states that $f_0(q^2_{\text{max}}) = f_B/f_\pi$ in the chiral limit, holds. This was uncertain previously as simulations were carried out with light quarks that were much heavier than their physical masses. The lattice gluon field configurations with physical light quarks allow us to overcome this issue and simulate at the physical pion mass.

Finally, we briefly discuss the decays $B_s \to K\ell\nu$ and the fictitious $B_s \to \eta_s$ decay. These processes again utilise NRQCD b quarks.

Contents

List of Tables

List of Figures

Acknowledgements

I would like to thank my PhD supervisor, Christine Davies, for her support, guidance and patience. I also want to thank all of those who were PhD students during my time with Glasgow's PPT group: Kate Elliot, Gordon Donald, Dan Coumbe, António Morais, Ben Galloway, Liam Moore, Stacey Melville, Bipasha Chakraborty and Michael Russell. Thanks, too, to my friends in the particle physics experiment group; in particular, Will Breaden Madden, Gavin Kirby and Stephen Ogilvy.

Particular thanks go to Rachel Dowdall for her infinite patience in explaining the ins and outs of various pieces of code that she laboured over and how they relate to the physics. I would also like to thank Jonna Koponen for discussions on various aspects of lattice QCD and in sharing the same woes in fitting meson correlators.

Additionally, thanks to the other PPT members, past and present, from my time in the group: Christoph Englert, Jack Laiho, David Miller, Tania Robbens and Chris White.

Finally, thanks to my friends and family who live in a world entirely disparate from physics research, who allowed me to inhabit that alternative universe, however briefly.

I am grateful to the MILC collaboration who generated the gauge configurations that were used throughout this thesis. The MILC collaboration kindly make these configurations freely available.

This work was performed using the Darwin Supercomputer of the University of Cambridge High Performance Computing Service (http://www.hpc.cam.ac.uk/), provided by Dell Inc. using Strategic Research Infrastructure Funding from the Higher Education Funding Council for England and funding from the Science and Technology Facilities Council.

It doesn't make a difference how beautiful your guess is; it doesn't make a difference how smart you are, who made the guess or what his name is. If it disagrees with experiment it's wrong. That's all there is to it.

– Richard P. Feynman

Declaration

With the exception of chapters 1, 2 and 3, which contain introductory material, all work in this thesis was carried out by the author unless otherwise explicitly stated.

Chapter 1

The Standard Model

Our current best understanding of particle physics is described by the Standard Model [1]. It describes the quarks and leptons, along with their anti-particles, and the gauge bosons that mediate the strong, electromagnetic and weak forces that act between them.

The quarks and leptons are spin-$1/2$ particles, collectively known as fermions. They obey Fermi-Dirac statistics, meaning that they observe the Pauli exclusion principle, which forbids two identical fermions from occupying the same quantum state. Fermions interact with each other via the integer spin gauge bosons. Bosons obey Bose-Einstein statistics, so are not constrained by the Pauli exclusion principle as the fermions are. The gauge bosons are photons, denoted γ, which mediate the electromagnetic force, gluons, denoted g, which mediate the strong force, and Z and $W^{\pm}$ bosons, which mediate the weak force.

The final particle of the Standard Model is the Higgs Boson, the most recently observed of the fundamental particles, discovered in 2012 by the ATLAS [2] and CMS [3] groups at the Large Hadron Collider in CERN. It was predicted as a result of work by several independent groups in 1964 [4–6], culminating in a Nobel prize in 2013 for Peter Higgs – after whom it gets its most commonly used name – and François Englert. This was the most recent of several Nobel prizes for work relating to the Standard Model, which further highlights its success.

1.1 The Weak Interaction

The weak interaction takes place between different quark flavours and is the force responsible for radioactive β decay. Understanding this area of the Standard Model could provide

valuable insights into what may lie beyond.

The flavour-changing interactions between quarks of different flavours occur via the emission of a $W^{\pm}$ boson. In the Standard Model, the interactions are necessarily charged at tree level, and any flavour changing neutral currents (FCNCs) would hint at physics beyond the Standard Model.

The strength of the interaction that takes place between various flavours of quarks is given by the Cabibbo-Kobayashi-Maskawa (CKM) matrix,

$$M_{CKM} = \begin{pmatrix} V_{ud} & V_{us} & V_{ub} \\ V_{cd} & V_{cs} & V_{cb} \\ V_{td} & V_{ts} & V_{tb} \end{pmatrix}. \tag{1.1}$$

This is a unitary matrix whose elements are determined by comparing experimental data to theoretical predictions. If this matrix was found not to be unitary it would imply the existence of physics beyond the Standard Model. Consequently, the CKM matrix is of much interest in both experimental and theoretical physics.

1.2 Quantum Chromodynamics

The gauge theory of the strong interaction in the Standard Model is quantum chromodynamics (QCD). It describes the interactions that take place between the quarks and gluons, collectively known as partons. The QCD Lagrangian is given by [7],

$$\mathcal{L} = \sum_f \overline{\psi}_f (iD_\mu \gamma_\mu - m_f)\psi_f - \frac{1}{4} F^a_{\mu\nu} F^{\mu\nu a} \tag{1.2}$$

where the sum is over quark flavour, f, m_f is the mass of the quark, and D_μ is the gauge invariant derivative, equivalent to $\partial_\mu - ig_s A_\mu$, with g_s the QCD coupling constant and A_μ the gluon fields. The index a runs from 1 to 8, corresponding to eight linearly independent matrices. $F^a_{\mu\nu}$ is the gluon field strength tensor, where

$$F^a_{\mu\nu} = \partial_\mu A^a_\nu - \partial_\nu A^a_\mu - g_s f_{abc} A^b_\mu A^c_\nu \tag{1.3}$$

and where f_{abc} are the structure constants of the SU(3) group.

QCD is a non-abelian gauge theory that results in the self interaction of the gluons and in the strong force being asymptotically free [8–10]. This is in contrast to QED,

the gauge theory that describes the electromagnetic interaction, whose gauge bosons do not self-interact. A further feature of QCD is that quarks and gluons cannot be seen as free particles but instead form colour-singlet objects called hadrons. This phenomenon is known as color confinement.

What this means for calculating processes that involve QCD is that when the energy is sufficiently low, perturbative QCD calculations cannot be carried out as an expansion in α_s as it is too large. Lattice QCD provides a nonperturbative way of calculating QCD processes in this case.

1.3 Path Integrals

The path integral formulation was proposed by R. P. Feynman in 1948 [11] and forms the basis of calculations in Lattice QCD. This approach allows one to determine an amplitude for some event by summing over all possible paths between the initial and final event. The path integral expectation for an operator $\mathcal{O}$ can be written,

$$\langle \mathcal{O} \rangle = \frac{1}{\mathcal{Z}} \int \mathcal{D}\phi \mathcal{O} \exp\left(i \int \mathrm{d}^4 x \mathcal{L}(\phi, \partial\phi) \right) \tag{1.4}$$

where $\mathcal{Z}$ is the partition function,

$$\mathcal{Z} = \int \mathcal{D}\phi \exp\left(i \int \mathrm{d}^4 x \mathcal{L}(\phi, \partial\phi) \right). \tag{1.5}$$

The $\mathcal{D}$ denotes that the integral is over all possible values of the fields in the Lagrangian and has, as a consequence, an infinite number of degrees of freedom. In order to produce meaningful results it is necessary to introduce some form of regularisation. This is achieved in this thesis through the introduction of a space-time lattice that imposes a momentum cut-off to allow the calculation of low energy phenomenology.

1.4 Mesons

Bound states of quarks and antiquarks, held together by the strong force, are known as hadrons. The kinds of hadrons that have been observed at experiments are baryons, comprising three quarks or three antiquarks, and mesons, comprising of a quark and an antiquark. The work in this thesis focusses entirely on physics involving mesons, and those that appear in the various calculations are now discussed briefly.

1.4.1 The Υ Spectrum

Bottomonium mesons are those that contain – as its valence quarks – a b quark and its antiquark, $\overline{b}$. The first experimentally discovered states were low lying Υ particles at Fermilab in 1977 [12, 13], and so the system of bottomonium states is also referred to as the Υ spectrum.

Throughout the thesis, the Υ – the state which transforms as a vector – and the η_b – which transforms as a pseudoscalar – will be the mesons that are referred to extensively. The ground state η_b was observed much later than the Υ, not having been detected until 2008 by the BABAR collaboration [14, 15]. Lattice QCD work had already reached an era in which it could provide accurate calculations, so this presented one of several opportunities to offer up predictions[1], where the mass splitting between the experimentally observed $\Upsilon(1S)$ and the unobserved $\eta_b(1S)$ was calculated [16].

The notation Υ will be used to refer to the Υ in the ground state where it is clear, otherwise the notation Υ, Υ', ... will be used to refer to the ground state, first radially excited state, and so on. This is analogously true for the η_b meson. Also useful is the quark model notation, $^{2S+1}L_J$, for total quark and antiquark spin $S = 0$ or 1, relative angular momentum L and total angular momentum or spin of the hadron, $\mathbf{J} = \mathbf{L} + \mathbf{S}$.

Figure 1.1 shows the masses of the η_b and Υ mesons and their excited states. The red line shows the $B\overline{B}$ threshold, which is the mass above which it is possible for the bottomonium meson to decay into a B meson and its antiparticle. This sort of decay of the $b\overline{b}$ state is a result of having enough energy for the creation of a light $q\overline{q}$ pair to give the two final state mesons.

1.4.2 Heavy-Light Mesons

Heavy-light mesons are those that are made of a heavy quark (antiquark) and a light antiquark (quark).

In this thesis results for the decays of a heavy-light meson – where the heavy quark is exclusively a b quark – to a meson where both quark and antiquark are light will be presented. In particular, the B mesons, which comprise a b antiquark (or quark) and

[1] Many of the calculations presented in this thesis are *postdictions* (or retrodictions), i.e. the tools of lattice QCD are used to give results for particle properties already observed experimentally.

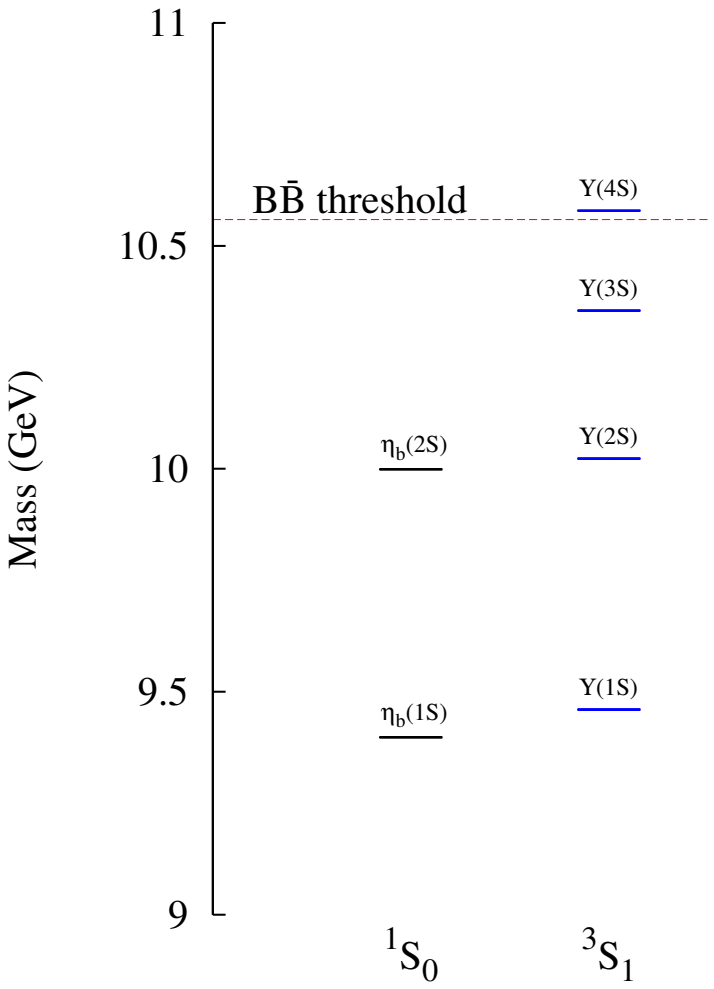

Figure 1.1: Part of the bottomonium spectrum. The $\eta_b(^1S_0)$ and $\Upsilon(^3S_1)$ states are shown. The red dotted line is the $B\overline{B}$ threshold above which the Υ can undergo a strong decay to a B and a $\overline{B}$ as a result of the creation of an additional $q\bar{q}$ pair.

either an up or down quark (or antiquark), and the B_s meson, which comprises a strange quark and a b antiquark, will be discussed.

1.4.3 π, K and η_s

In chapter 5, results for properties of decays of B and B_s mesons are given. These processes have lighter mesons in the final state so these mesons are introduced very briefly here.

The Pion

The π mesons, or pions, are the lightest mesons in particle physics, comprising a light quark and a light antiquark. There are three types of pion: the neutral pion, π^0; the positively charged pion π^+; and its antiparticle, the negatively charged π^-. They participate in semileptonic $B \to \pi\ell\nu$ decays discussed in this thesis.

The Kaon

The K mesons or kaons are mesons that contain a light quark and a strange antiquark. In this thesis they are used in calculations of the $B_s \to K\ell\nu$ semileptonic decays, which features the same $b \to u$ weak transition that appears in the $B \to \pi\ell\nu$ process.

The η_s Meson

The η_s comprises an s quark and its antiquark, and although it does not exist in the real world, by not including disconnected pieces of the correlation function it can be simulated in lattice QCD. Then through the use of chiral perturbation theory and results for the π and K mesons it is possible to determine the mass and decay constant of this fictitious meson [17–19]. This can then allow one to accurately tune the mass of the valence s quark for use in subsequent lattice QCD calculations. Additionally, the spacing between points on the lattice are not known in advance, and although not the method used for the results in this thesis, it is possible to determine the lattice spacing from properties of this fictitious meson.

Chapter 2

Lattice QCD

In 1974, Kenneth Wilson [20] showed that it was possible to regularise QCD by discretising space-time and thus reducing the infinite degree of freedom of QCD to a finite number of degrees of freedom that would become numerically calculable. Increased computing power in recent years has allowed for a wealth of physics to be studied on the lattice with great accuracy.

On the lattice, fermion fields, ψ, are confined to the lattice points, x_μ, while the gluons, U are defined on the links between them. This discretisation means that derivatives simply become differences on the lattice,

$$\begin{aligned}
\Delta_\mu \psi(x) &= \frac{1}{a}(U_\mu(x)\psi(x+a\hat{\mu}) - \psi(x)) \\
\Delta^*_\mu \psi(x) &= \frac{1}{a}(\psi(x) - U^\dagger_\mu(x-a\hat{\mu})\psi(x-a\hat{\mu})) \\
\Delta^{(\pm)}_\mu \psi(x) &= \frac{1}{2}(\Delta_\mu \psi(x) + \Delta^*_\mu \psi(x)) \\
&= \frac{1}{2a}(U_\mu(x)\psi(x+a\hat{\mu}) - U^\dagger_\mu(x-a\hat{\mu})\psi(x-a\hat{\mu})).
\end{aligned} \tag{2.1}$$

As we will see, the U fields – the gluons – are required in the derivatives for gauge covariance.

2.1 Gluons on the Lattice

Gluon fields, $U_\mu(x)$, are defined on the links between the lattice points as $SU(3)$ fields,

$$U(x, x+\hat{\mu}) = U_\mu(x) = e^{iagA_\mu(x+a\hat{\mu})} \tag{2.2}$$

where $U_\mu(x)$ denotes the link from x to $x+\hat{\mu}$. The conjugate of this field, $U_\mu^\dagger(x)$ is the link from $x+\hat{\mu}$ to x.

The gluons and quarks fields transform as,

$$U_\mu(x) \rightarrow \Lambda(x)U_\mu(x)\Lambda^{-1}(x+\hat{\mu}) \tag{2.3}$$

$$\psi(x) \rightarrow \Lambda(x)\psi(x) \tag{2.4}$$

$$\overline{\psi}(x) \rightarrow \overline{\psi}(x)\Lambda^{-1}(x) \tag{2.5}$$

where $\Lambda \in \mathrm{SU}(3)$. It is clear from this that any closed loop of links is gauge invariant. The simplest example of such an object is the plaquette,

$$U_{\mathrm{plaq}} = U_\mu(x)U_\nu(x+\hat{\mu})U_\mu^\dagger(x+\hat{\nu})U_\nu^\dagger(x), \tag{2.6}$$

which is a 1×1 square lattice loop. Similarly, a quark and antiquark with any string of U fields between them is also clearly gauge invariant.

The simplest way in which to construct the purely gluonic piece of the QCD action is through the use of these plaquettes to give the Wilson action,

$$S_g = \beta \sum_{\mathrm{plaq}} \left(1 - \frac{1}{3}\mathrm{Re}\left[\mathrm{Tr}U_{\mathrm{plaq}}\right]\right), \tag{2.7}$$

where $\beta = 6/g$. In the continuum limit $a \rightarrow 0$, we get

$$\frac{1}{4}\int \mathrm{d}^4x F^a_{\mu\nu}F^{\mu\nu}_a, \tag{2.8}$$

which is the form of the pure gauge piece of the QCD Lagrangian.

2.1.1 Improving the Gauge action

In order to get physical results from lattice calculations, it is necessary to perform extrapolations to the continuum, where $a \rightarrow 0$. It is not a trivial task due to the presence of discretisation effects that necessarily appear when continuum equations are approximated on a space-time lattice [21]. A programme of improvement was proposed by Symanzik [22], which seeks to add counterterms order by order in the lattice spacing, a, to deal with these errors and improve the approach to the continuum.

The gauge action of equation 2.7 has errors at $\mathcal{O}(a^2)$. The errors at this order can be dealt with by adding more terms to the action to subtract them. It is possible to do this in

various ways but, following [23], two six link Wilson loop terms can be used: a rectangle, $U_{\rm rt}$ and a parallelogram, $U_{\rm pg}$. These can be combined with the original Wilson action to give the improved Wilson action [24, 25]:

$$\begin{aligned} S_G &= \beta \sum_{\rm plaq} \left(1 - \frac{1}{3}{\rm Re}\left[{\rm Tr}U_{\rm plaq}\right]\right) \\ &+ \beta_{\rm rt} \sum_{\rm rt} \left(1 - \frac{1}{3}{\rm Re}\left[{\rm Tr}U_{\rm rt}\right]\right) \\ &+ \beta_{\rm pg} \sum_{\rm pg} \left(1 - \frac{1}{3}{\rm Re}\left[{\rm Tr}U_{\rm pg}\right]\right), \end{aligned} \tag{2.9}$$

where $\beta_{\rm rt}$ and $\beta_{\rm pg}$ are determined in perturbation theory in such a way that the latter two terms cancel out the $\mathcal{O}(a^2)$ errors from the first term.

2.2 Fermion Discretisation

The simplest way in which a fermion can be placed on the lattice is by considering what is known as the naïve lattice action,

$$S_q = \sum_x \bar{\psi}(x)(\gamma_\mu \Delta_\mu + m)\psi(x), \tag{2.10}$$

for a quark with mass m. γ_μ are the Dirac γ matrices,

$$\gamma_0 = \begin{pmatrix} 1 & 0 \\ 0 & -1 \end{pmatrix} \qquad \gamma_i = \begin{pmatrix} 0 & \sigma_i \\ \sigma_i & 0 \end{pmatrix}, \tag{2.11}$$

where σ_i are the Pauli matrices,

$$\sigma_x = \begin{pmatrix} 0 & 1 \\ 1 & 0 \end{pmatrix} \qquad \sigma_y = \begin{pmatrix} 0 & -i \\ i & 0 \end{pmatrix} \qquad \sigma_z = \begin{pmatrix} 1 & 0 \\ 0 & -1 \end{pmatrix}. \tag{2.12}$$

There is a problem that surfaces with the naïve quark action that becomes clear if we look at the inverse of the free lattice propagator, which is the case when the U fields all have value 1. This is given by,

$$S^{-1}(p) = m + \sum_\mu \frac{i\gamma_\mu \sin p_\mu a}{a}, \tag{2.13}$$

which in the limit $m \to 0$ has 16 zeros at $p = (0,0,0,0)$, $p = (\pi/a, 0, 0, 0)$, $\ldots$, $p = (\pi/a, \pi/a, \pi/a, \pi/a)$ owing to the $\sin p_\mu a$ piece. This is known as the *doubling problem* since

the number of fermions that appear is 2^d in d dimensions, so for the purpose of the work presented here in four dimensions it means there are 15 extra copies, or doublers, of the same quark flavour rather than the one desired.

2.2.1 Wilson Quarks

The first attempt to address the issue was implemented by Wilson himself when he included an additional term in the fermion action to give [26, 27],

$$S_q^{(W)} = S_q - \sum_x \overline{\psi}(x)\frac{ra}{2}\Delta_\mu^2\psi(x), \tag{2.14}$$

with Wilson parameter r, which is usually set to 1.

The inverse of the propagator for this new action is,

$$S^{-1}(p) = m + \sum_\mu i\gamma_\mu \frac{\sin p_\mu a}{a} + \frac{2r}{a}(\cos p_\mu a - 1), \tag{2.15}$$

where this new third term means that all quarks except the one where $p_\mu = 0$ retains a nonzero mass in the continuum limit and thus decouples from the theory. Unfortunately, this discretisation suffers in that chiral symmetry is now lost explicitly as result [28, 29].

2.2.2 Cloverleaf Fields

The Symanzik improvement discussed previously applies to the improvement of the fermions as well as the gluons in lattice QCD calculations. When using Wilson fermions, errors appear at $\mathcal{O}(a)$ due to the appearance of several dimension 5 operators [30]. Most can be absorbed into the scaling of the fermion mass, but the operator $i\psi\sigma_{\mu\nu}F^{\mu\nu}\psi$ remains. This can be addressed by the addition of an extra term that cancels it [30, 31], giving the Wilson clover action,

$$S = S_W - \frac{iaC_{SW}\kappa r}{4}\overline{\psi}(x)\sigma_{\mu\nu}\hat{F}_{\mu\nu}\psi(x), \tag{2.16}$$

where C_{SW} is a coefficient with the value 1 at tree level, and κ is the hopping parameter,

$$\kappa = \frac{1}{2ma + 8r}. \tag{2.17}$$

The cloverleaf operator is defined on the lattice such that

$$gF_{\mu\nu}^{(c)}(x) = -\frac{1}{4a^2}\sum_{\text{plaq}(x,\mu\nu)} \mathcal{I}\left[U_{\text{plaq}(x,\mu\nu)}\right], \tag{2.18}$$

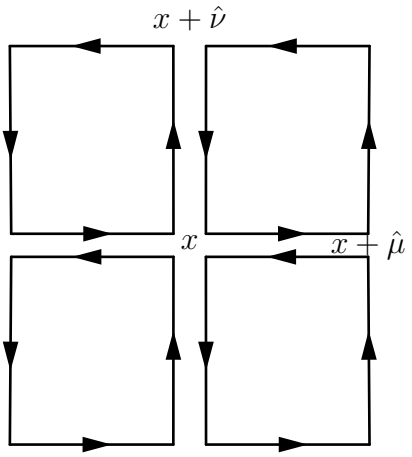

Figure 2.1: The cloverleaf operator in lattice QCD centered at site x on the $\mu - \nu$ plane.

where the sum is over all plaquettes P in the plane (μ, ν) containing site x and

$$\mathcal{I}\left[U_{\text{plaq}}\right] \equiv \frac{U_{\text{plaq}} - U_{\text{plaq}}^{\dagger}}{2i} - \frac{1}{3}\text{Im}[\text{Tr}U_{\text{plaq}}]. \tag{2.19}$$

A diagram of this arrangement is shown in figure 2.1, making it clear why it is referred to as the clover term.

2.2.3 Staggered Quarks

The process of staggering quarks addresses the doubling problem by reducing the number of tastes from 16 to 4. This is achieved by the introduction of a staggered transformation,

$$\psi(x) \to \Omega(x)\chi(x) \qquad \overline{\psi}(x) \to \overline{\chi}(x)\Omega^{\dagger}(x), \tag{2.20}$$

with,

$$\Omega(x) \equiv \gamma_x \equiv \prod_{\mu=0}^{3} (\gamma_\mu)^{x_\mu}, \tag{2.21}$$

where x_μ is a four component vector with $x_\mu \in \mathbb{Z}$. The naive action of 2.10 can now be rewritten as,

$$S_{\text{staggered}} = \sum_x \overline{\chi}(x)((-1)^{x_\mu^<}\Delta_\mu + m)\chi(x), \tag{2.22}$$

where we have introduced the notation,

$$x_\mu^< = \sum_{\nu<\mu} x_\mu. \tag{2.23}$$

The result of this staggering process is that the four components of the spinor $\chi(x)$ are precisely the same. For this reason the number of tastes has been reduced by a factor of

four, which makes simulating them on the lattice cheaper. Although the doubling problem is somewhat improved, it still leaves three unwanted tastes; but unlike Wilson fermions, a remnant chiral symmetry is maintained.

Oscillations

The naïve quark action given in equation 2.10 is invariant under the doubling transformation,

$$\begin{aligned} \psi &\rightarrow i\gamma_5\gamma_\mu(-1)^{x_\mu}\psi(x) \\ &= \gamma_5\gamma_\mu \exp\left(ix_\mu\pi\right)\psi(x). \end{aligned} \tag{2.24}$$

This transformation can be applied multiple times in different directions, giving:

$$\psi(x) \rightarrow \mathcal{B}_\zeta(x)\psi(x), \qquad \overline{\psi}(x) \rightarrow \overline{\psi}(x)\mathcal{B}_\zeta^\dagger(x), \tag{2.25}$$

with

$$\begin{aligned} \mathcal{B}_\zeta(x) &\equiv \gamma_{\overline{\zeta}}\,(-1)^{\zeta\cdot x} \\ &\propto \prod_\mu \left(\gamma_5\gamma_\mu\right)^{\zeta_\mu} \exp\left(ix\cdot\zeta\pi\right), \end{aligned} \tag{2.26}$$

where ζ is a vector with $\zeta_\mu \in \mathbb{Z}$ and $\overline{\zeta}$ is related to ζ by,

$$\begin{aligned} \overline{\zeta}_\mu &\equiv \zeta^> + \zeta^< = \sum_{\nu\neq\mu}\zeta_\nu \bmod 2 \\ &= \begin{cases} \zeta_\mu & \text{if } \zeta^2 \text{ even} \\ (\zeta_\mu + 1) \bmod 2 & \text{if } \zeta^2 \text{ odd.} \end{cases} \end{aligned} \tag{2.27}$$

As described previously, the 16 doublers that result here are reduced to 4 upon applying the staggered transformation given in equation 2.20.

For the B meson, we could construct a pseudoscalar operator,

$$J_5(x) = \overline{\psi}(x)\gamma_5\Psi_b(x), \tag{2.28}$$

for a b quark Ψ – which is not a staggered quark – and light staggered quark, ψ. It is usual to create correlators in lattice QCD simulations, which for the pseudoscalar is,

$$C_{\mathrm{PS}}(t) \equiv \sum_{\vec{x}} \langle 0|J_5(\vec{x},t)J_5(0,0)|0\rangle. \tag{2.29}$$

By summing over space to give zero three momentum, the spatial doublers cancel out. However, doublers still appear in time, so the staggered quark can have energy $E \approx 0$ or $E \approx \pi$ meaning the current J_5 couples to $\zeta = 0$ and $\zeta = (1, 0, 0, 0)$. The staggered quark field with $E \approx \pi$ can be transformed back to a low energy field using equation 2.24,

$$\overline{\psi}(x)|_{E\approx\pi} \rightarrow \overline{\psi}(x)\,(i\gamma_5\gamma_0)\,(-1)^t\,, \tag{2.30}$$

and by inserting this into the current J_5 we get,

$$\overline{\psi}\gamma_5\Psi_b|_{E\approx\pi} \rightarrow \overline{\psi}\,(i\gamma_5\gamma_0)\,\gamma_5\Psi_b\,(-1)^t = -\overline{\psi}i\gamma_0\Psi_b\,(-1)^t\,. \tag{2.31}$$

The implication is that, as well as getting the $J^P = 0^-$ state desired, J_5 also couples to the parity partner: the $J^P = 0^+$ state.

The meson correlator constructed from the pseudoscalar currents is then,

$$C_{PS}(t) = |\langle 0|\overline{\psi}\gamma_5\Psi_b|0^-\rangle|^2 \mathrm{e}^{-E_- t} - (-1)^t\,|\langle 0|\overline{\psi}i\gamma_0\Psi_b|0^-\rangle|^2 \mathrm{e}^{-E_+ t}, \tag{2.32}$$

where E_- and E_+ are the energies for the O^- and O^+ states respectively. The second term on the right oscillates from one time slice to the next, which must be taken into consideration when extracting properties of the mesons when fitting a full set of correlators.

In addition to the oscillations in heavy-light mesons, oscillations can appear when both quarks are staggered. At zero momentum the oscillatory pieces cancel for local pseudoscalar currents when the masses of the quark and antiquark are the same, but remain when they differ. The π and η_s mesons discussed in this thesis therefore do not contain oscillations since they contain degenerate mass quarks and are at zero momentum, but the K meson does, since it contains a u/d and an s.

2.2.4 Improved and Highly Improved Staggered Quarks

The naïve staggered quark formulation suffers from large discretisation errors of $\mathcal{O}(a^2)$. The obvious source of error here is in the discretisation of the derivatives in the action, but a second source of errors comes from taste-exchanging interactions as a result of the staggered quark discretisation. Taste changing interactions involve a low energy quark emitting a gluon and changing taste as a result. This gluon can then be absorbed by another quark and it, too, changes taste. This process is shown in figure 2.2. These tastes look like the original low energy quarks because of the doubling symmetry.

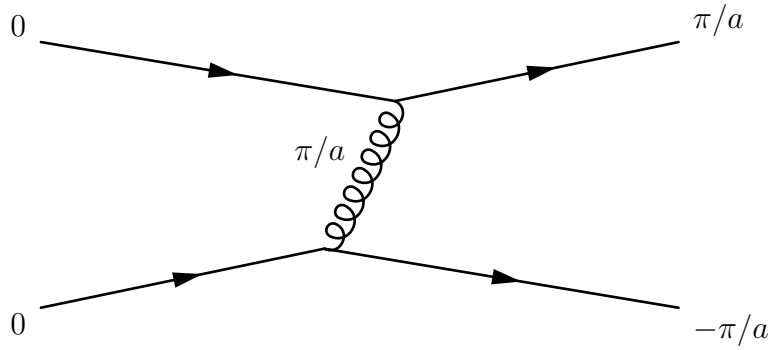

Figure 2.2: A taste changing interaction. A low energy quark emits a gluon with energy π/a, which is then absorbed by another quark; both quarks change taste as a result.

The $\mathcal{O}(a^2)$ taste-changing errors are dealt with again via Symanzik improvement through the introduction of *fattened* links, which have either three, five or seven links [32]. The introduction of the Naik term, which is comprised of three links [33], offers improvement of the usual a^2 errors of the derivatives. Further improvement can be achieved through the use of tadpole improvement (discussed in chapter 3), giving rise to the Asq-Tad action.

More recently [34], the HPQCD collaboration developed a method for removing all $\mathcal{O}(a^2)$ errors and tree-level $(am)^4$ errors at leading order in the quark's velocity, v/c. In addition to this, one-loop taste changing interactions are reduced. These sorts of fermions on the lattice are called Highly Improved Staggered Quarks (HISQ) and have been shown to give very small discretisation errors, even when simulating quarks as heavy as charm quarks.

2.2.5 Heavy Quarks on the Lattice

Since heavy quarks have a different mass scale than light quarks, they often have to be treated differently when simulated on the lattice. The same methods, if applied to quarks that are too heavy, can result in discretisation errors that are completely unmanageable, growing as powers of the heavy quark mass, am_Q. Fortunately, various methods for modelling heavy quarks are available and reviews of these can be found in [35–37]. In the next chapter, Nonrelativistic QCD (NRQCD) will be discussed in detail, as that is the heavy quark formulation used in the remainder of this thesis, but here other possibilities are mentioned briefly.

Relativistic Heavy Quarks

It is currently possible to directly give charm quarks a full relativistic treatment in lattice QCD, but this is not a viable option with bottom quarks [36]. Instead, it is possible to simulate a range of quark masses, m_q, where $m_c < m_q < m_b$ on a range of lattice ensembles. Determining the behaviour of the bottom quark is then a case of extrapolating to m_b from these lighter masses [38]. The disadvantage of this method is that errors from the extrapolation exist. The advantages are that all relativistic effects are included and allows comparison with nonrelativistic treatments of heavy quarks on the lattice. The HPQCD collaboration currently uses the HISQ discretisation to simulate heavy quarks in this way, giving a complementary method to the work presented in this thesis.

Heavy Quark Effective Theory

Heavy Quark Effective Theory (HQET) [39–43] is a method used by the ALPHA collaboration in which the static limit of the heavy quark is considered at lowest order, i.e. in the limit $m_b \to \infty$. This is a method that can be applied when there is a single heavy quark in either the initial or final state, or both. Correction operators in $1/m_b$ can then be inserted systematically to the desired order.

2.3 Gauge Configurations

The gauge configurations used throughout this thesis were generated by the MILC collaboration and include the effects of $2+1+1$ flavours of quarks in the sea [44, 45] using the HISQ formalism. The gauge action is improved through $\mathcal{O}(\alpha_s a^2)$ [46]. The $2+1+1$ refers to u, d, s and c quarks, where the masses of the u and d quarks are degenerate in our lattice calculations. The u and d quarks have in the past been simulated at masses that are much heavier than their physical masses. This is the case for some of the ensembles here, where the light quark mass, m_l, is set to $m_s/5$ or $m_s/10$. However, the MILC collaboration have also generated state-of-the-art HISQ configurations with physical m_l, which are used in some of these calculations.

All relevant details for all of the configurations used are contained in table 2.1. The lattice spacing, a for the configurations used are ≈ 0.15 fm, ≈ 0.12 fm and ≈ 0.09 fm, which are referred to as very coarse, coarse and fine ensembles respectively. The lattice

Set	a_Υ (fm)	am_l	am_s	am_c	$L \times T$	$n_{\rm cfg}$
1	0.1474(5)(14)(2)	0.013	0.065	0.838	16×48	1020
2	0.1463(3)(14)(2)	0.0064	0.064	0.828	24×48	1000
3	0.1450(3)(14)(2)	0.00235	0.0647	0.831	32×48	1000
4	0.1219(2)(9)(2)	0.0102	0.0509	0.635	24×64	1053
5	0.1195(3)(9)(2)	0.00507	0.0507	0.628	32×64	1000
6	0.1189(2)(9)(2)	0.00184	0.0507	0.628	48×64	1000
7	0.0884(3)(5)(1)	0.0074	0.037	0.440	32×96	1008
8	0.0873(2)(5)(1)	0.0012	0.0363	0.432	64×96	621

Table 2.1: Parameters for the gauge configurations. The lattice spacings given here were determined using the splitting between the $\Upsilon(2S)$ and $\Upsilon(1S)$ states and are referred to in the text as very coarse, coarse and fine for $a \approx 0.15$fm, $a \approx 0.12$fm and $a \approx 0.09$fm respectively. The first error quoted is a result of the statistics and fitting; the second error comes from the remaining systematics that result from the NRQCD action that is used; the final error is from experiment and from the effect of electromagnetism, not included in the NRQCD calculation. The values for the sea quark masses, am_q, are detailed, where m_s and m_c are tuned as closely to their physical values as possible, and the degenerate u and d quark masses, m_l, range from $m_s/5$ to their physical values ($\approx m_s/27.5$). Also given are the spatial and temporal lattice extents, L and T, and the number of configurations in each lattice ensemble, $n_{\rm cfg}$.

spacing is not known a priori and must be determined after the ensembles have been generated. This can be done in various ways, but the values given here were determined by using the mass splitting between $\Upsilon(1S)$ and $\Upsilon(2S)$ [18].

Chapter 3

NRQCD

3.1 Motivation

One way of studying the physics of b quarks on the lattice is by using a method known as lattice Nonrelativistic QCD (NRQCD) [47]. It is easy to see that simulating b quarks using a nonrelativistic method is a reasonable thing to do. We start by observing that the mass splittings between bottomonium mesons are much less than their masses. The mass splitting between the $\Upsilon(1S)$ and $\Upsilon(2S)$ is approximately 600 MeV, which should be of the order of the average kinetic energy. So the squared velocity of the Υ is $v^2_\Upsilon \approx 0.1$; we can be confident that b quarks can be simulated nonrelativistically.

For heavy quarks, there are three scales to consider in a lattice QCD calculation:

- $m_h \sim$ mass
- $m_h v \sim$ 3-momentum
- $m_h v^2 \sim$ kinetic mass.

where m_h is the heavy quark mass and v its velocity. The lattice has to be large compared to $1/m_h v^2$, but also have a lattice spacing that is small compared with $1/m_h$. For the Υ, $m_h/m_h v^2 \sim 10$ so in order to treat b quarks relativistically in a way that the systematic errors from finite lattice spacing and finite volume are reasonably small, one would perhaps expect to have lattice sizes five or ten times as large in each dimension, so up to $(100)^4$ in size. With NRQCD we *explicitly* remove the mass term in the Lagrangian, thus removing the mass scale. The result is to allow a lattice size to be reduced by a factor of $(1/v^4)$,

which for the case of the Υ is ~ 100. This leads to a much more reasonable lattice size, allowing NRQCD calculations to be done with lattices that have been available for a number of years, and which can now include the effects of quarks in the sea where even the u/d quarks have physical mass.

3.2 Constructing NRQCD

3.2.1 Foldy-Wouthuysen-Tani Transformation

By carrying out a series of Foldy-Wouthuysen-Tani (FWT) transformations [48, 49] for successive powers of $1/m_h$ it is possible to obtain a nonrelativistic formalism for heavy quarks where the quark and antiquark fields are decoupled. Starting from the Dirac Lagrangian, which can be written,

$$\mathcal{L} = \bar{\Psi}\left(i\gamma^0 D_0 + i\gamma^j D_j - m_h\right)\Psi, \tag{3.1}$$

we aim to cancel the $i\gamma^j D_j$ piece since it is this that connects the quark and antiquarks [50–52]. Such operators are referred to as odd, while those that contain only diagonal pieces – and thus connect only quarks with quarks and antiquarks with antiquarks – are referred to as even operators. An appropriate choice of field redefinition to this end would be,

$$\Psi \rightarrow \exp\left(\frac{1}{2m_h} i\gamma^j D_j\right)\Psi \tag{3.2}$$

$$\bar{\Psi} \rightarrow \bar{\Psi}\exp\left(\frac{1}{2m_h} i\gamma^j D_j\right). \tag{3.3}$$

Applying these transforms to equation 3.1 gives,

$$\mathcal{L} = \bar{\Psi}\left(i\gamma^0 D_0 - m_h\right)\Psi + \sum_{n=1}^{\infty}\frac{1}{m_h^n}\bar{\Psi}\mathcal{O}^{(1)}\Psi, \tag{3.4}$$

so $i\gamma^j D_j$ is indeed cancelled. However, additional terms result from this transformation in an infinite sum of higher powers of $1/m_h$ with $\mathcal{O}^{(1)}$ containing odd operators. The introduction of a further field redefinition removes the odd operators at $1/m_h$, leaving them only at order $1/m_h^2$ and higher. This procedure can be repeated until one obtains any desired order in $1/m_h$, but the here we restrict the discussion to terms up to order $1/m_h^2$.

We also want to remove the mass term in this Lagrangian, so it is necessary to introduce one further field redefinition:

$$\Psi \rightarrow \exp\left(-im_h x^0 \gamma^0\right) \Psi \tag{3.5}$$

$$\bar{\Psi} \rightarrow \bar{\Psi} \exp\left(im_h x^0 \gamma^0\right). \tag{3.6}$$

Ultimately, by carrying out successive FTW transformations and defining two component fields by,

$$\Psi = \begin{pmatrix} \psi \\ \chi \end{pmatrix}, \qquad \bar{\Psi} = \begin{pmatrix} \psi^\dagger & \chi^\dagger \end{pmatrix} \tag{3.7}$$

we can reach the Langrangian,

$$\begin{aligned} \mathcal{L} &= \psi^\dagger \left[iD_0 + \frac{\mathbf{D}^2}{2m_h} + \frac{g}{2m_h} \boldsymbol{\sigma} \cdot \mathbf{B} + \frac{g}{8m^2} \left(\mathbf{D} \cdot \mathbf{E} - \mathbf{E} \cdot \mathbf{D} \right) + \frac{ig}{8m_h^2} \boldsymbol{\Sigma} \cdot \left(\mathbf{D} \times \mathbf{E} - \mathbf{E} \times \mathbf{D} \right) \right] \psi \\ &+ \chi^\dagger \left[iD_0 + \frac{\mathbf{D}^2}{2m_h} - \frac{g}{2m_h} \boldsymbol{\sigma} \cdot \mathbf{B} - \frac{g}{8m^2} \left(\mathbf{D} \cdot \mathbf{E} - \mathbf{E} \cdot \mathbf{D} \right) + \frac{ig}{8m_h^2} \boldsymbol{\Sigma} \cdot \left(\mathbf{D} \times \mathbf{E} - \mathbf{E} \times \mathbf{D} \right) \right] \chi \\ &+ \mathcal{O}\left(\frac{1}{m_h^3} \right), \end{aligned} \tag{3.8}$$

where,

$$\Sigma^j = \begin{pmatrix} \sigma^j & 0 \\ 0 & \sigma^j \end{pmatrix} \tag{3.9}$$

and $\mathbf{E}$ and $\mathbf{B}$ are the chromoelectric and chromomagnetic fields respectively, the QCD equivalent of the electric and magnetic fields that arise in QED.

3.2.2 Power Counting

It is possible to pick appropriate terms for the NRQCD action through power counting, a thorough derivation of which is given by Lepage et al [53]. In this case, one selects the terms required to a given order in the square of the velocity of the b quark, v^2.

The starting point is the Schrödinger theory from which the leading terms originate,

$$S_0 = \int d^4x \psi^\dagger(x) \left(iD_t + \frac{\mathbf{D}^2}{2m_h} \right) \psi(x). \tag{3.10}$$

The terms here appear at v^2 in the power counting. As mentioned previously, correction terms are added until the desired accuracy is achieved, and so another set of terms suppressed by a further factor of v^2 can be added. The following order v^4 terms are the only

such terms that are bilinear in the quark field:

$$\begin{aligned}\partial\mathcal{L}_{\text{bilinear}} &\equiv c_1\frac{1}{m_h^3}\psi^\dagger\mathbf{D}^4\psi \\ &+ c_2\frac{g}{m_h^2}\psi^\dagger\left(\mathbf{D}\cdot\mathbf{E}-\mathbf{E}\cdot\mathbf{D}\right)\psi \\ &+ c_3\frac{ig}{m_h^2}\psi^\dagger\boldsymbol{\sigma}\cdot\left(\mathbf{D}\times\mathbf{E}-\mathbf{E}\times\mathbf{D}\right)\psi \\ &+ c_4\frac{g}{m_h}\psi^\dagger\boldsymbol{\sigma}\cdot\mathbf{B}\psi. \end{aligned} \tag{3.11}$$

Deliberately excluded from the above are terms involving the quark time derivative, D_t, as they make the numerical calculation of the quark propagator more complicated. However, it is possible to deal with this issue by looking at the field equation for ψ,

$$iD_t\psi(x) \sim \frac{-\mathbf{D}^2}{2m_h}\psi(x), \tag{3.12}$$

which allows us to substitute iD_t terms for $-\mathbf{D}^2/2m_h$.

Each of these terms is preceded by a coefficient c_i, each of which are determined in such a way that NRQCD matches QCD through v^4 [53]. Matching appropriately for QCD in the continuum and making the substitutions,

$$x^0_{(M)} = -ix^0_{(E)} \tag{3.13}$$

$$\partial_0^{(M)} = i\partial_0^{(E)} \tag{3.14}$$

$$D_0^{(M)} = iD_0^{(E)}, \tag{3.15}$$

one obtains a Lagrangian for NRQCD in Euclidean space for tree level values of c_i given as,

$$\begin{aligned}\mathcal{L}_{\text{cont}} &= \psi^\dagger\left(D_t-\frac{\mathbf{D}^2}{2m_h}\right)\psi+\frac{1}{8m_h^3}\psi^\dagger\mathbf{D}^4\psi+\frac{ig}{8m_h^2}\left(\mathbf{D}\cdot\mathbf{E}-\mathbf{E}\cdot\mathbf{D}\right) \\ &- \frac{g}{8m_h^2}\boldsymbol{\sigma}\cdot\left(\mathbf{D}\times\mathbf{E}-\mathbf{E}\times\mathbf{D}\right)-\frac{g}{2m_h}\boldsymbol{\sigma}\cdot\mathbf{B}. \end{aligned} \tag{3.16}$$

3.3 Lattice NRQCD

We now proceed to place the NRQCD action on the lattice by appropriately discretising the formalism and introducing additional discretisation improvement terms.

The covariant derivatives are replaced with differences as described in chapter 2 such that:

$$a\Delta_\mu^{(+)} \equiv U_{x,\mu}\psi(x+a\hat{\mu})-\psi(x) \tag{3.17}$$

$$a\Delta_\mu^{(-)} \equiv \psi(x) - U^\dagger_{x-a\mu,\mu}\psi(x-a\hat{\mu}) \tag{3.18}$$

$$\Delta^{(\pm)} \equiv \frac{1}{2}(\Delta^{(+)} + \Delta^{(-)}), \tag{3.19}$$

and the lattice Laplacian is given as,

$$\Delta^{(2)} \equiv \sum_i \Delta_i^{(+)}\Delta_i^{(-)} = \Delta_i^{(-)}\Delta_i^{(+)}. \tag{3.20}$$

The covariant derivatives of the cloverleaf field definition of $F_{\mu\nu}$ are given by,

$$a\Delta_\rho^{(+)}F_{\mu\nu}^{(c)} \equiv U_{x,\rho}F_{\mu\nu}^{(c)}(x+a\hat{\rho})U^\dagger_{x,\rho} - F_{\mu\nu}^{(c)} \tag{3.21}$$

$$a\Delta_\rho^{(-)}F_{\mu\nu}^{(c)} \equiv F_{\mu\nu}^{(c)} - U^\dagger_{x-a\hat{\rho},\rho}F_{\mu\nu}^{(c)}(x-a\hat{\rho})U_{x-a\hat{\rho}}, \tag{3.22}$$

which completes the elements needed in order to construct the NRQCD action on the lattice.

3.3.1 Discretisation Improvement

Spatial Improvement

An improved spatial difference operator can be introduced for D_i that is now correct through to a^4, rather than a^2 errors given in the leading kinetic terms,

$$\tilde{\Delta}_i^{(\pm)} \equiv \Delta_i^{(\pm)} - \frac{a}{6}\Delta_i^{(+)}\Delta_i^{(\pm)}\Delta_i^{(-)}. \tag{3.23}$$

From here a new Laplacian operator can be introduced:

$$\tilde{\Delta}^{(2)} = \Delta^{(2)} - \frac{a^2}{12}\sum_i \left[\Delta_i^{(+)}\Delta_i^{(-)}\right]^2. \tag{3.24}$$

Temporal Improvement

The temporal derivatives in NRQCD are not as straightforward to deal with as the spatial derivatives because the quark propagation plays out through a Schrödinger equation. This allows a time evolution equation to be solved, rather than a more complicated boundary value problem, which is much less costly when running numerical simulations. If we were to try to improve the temporal derivative using the same sort of procedure as in the previous section, higher order time derivatives would mean a loss of the simplicity of this evolution equation.

Instead we should look directly at the time evolution equation. By deliberately omitting the gauge fields for the time being,

$$\begin{aligned} G(\mathbf{x}, t+a) &= \left(1 - \frac{aH_0}{2n}\right)^{2n} G(\mathbf{x}, t) \\ &= e^{aH_{\text{eff}}} G(\mathbf{x}, t), \end{aligned} \tag{3.25}$$

with the effective Hamiltonian,

$$\begin{aligned} H_{\text{eff}} &\equiv -\frac{2n}{a} \ln\left(1 - \frac{aH_0}{2n}\right) \\ &= H_0 + \frac{a}{4n} H_0^2 + \cdots . \end{aligned} \tag{3.26}$$

If we subtract the second term from the Hamiltonian we will correct for the leading error in the temporal derivative.

Tadpole Improvement

Since the links representing the gluon fields in lattice QCD are given by $\exp(igA_\mu)$, they do not exhibit the behaviour of their continuum values in QCD, instead introducing terms that have problematic ultraviolet divergences. In order to solve this problem we undertake tadpole improvement [54].

It is possible to do this in a gauge invariant way by taking the fourth root of the average plaquette,

$$u_{0,P} \equiv \frac{1}{3} \langle \text{ReTr} U_{\text{pl}} \rangle^{\frac{1}{4}}, \tag{3.27}$$

but it is has been shown to further reduce errors to use the average of the gauge links in Landau gauge [55–59],

$$u_{0,L} \equiv \frac{1}{3} \langle \text{ReTr} U_\mu \rangle, \qquad \partial_\mu A^\mu = 0. \tag{3.28}$$

It is the latter procedure that has been used in determining the tadpole improvement factor used in the calculations in this thesis. In either case, all links, U_μ, are then divided through by u_0, giving a better matching between the lattice and the continuum.

3.3.2 Evolution Equation & Lattice NRQCD action

One of the strengths of the NRQCD formalism is that, when it is used to simulate quarks on the lattice, it is very cheap compared to other formalisms. This is because rather than

a complicated boundary problem, it operates through a comparatively simple evolution equation:

$$G(\mathbf{x}, t+a) = \left(1 - \frac{aH_0}{2n}\right)^n \left(1 - \frac{a\delta H}{2}\right) U_\mu^\dagger(\mathbf{x}, t) \left(1 - \frac{a\delta H}{2}\right) \left(1 - \frac{aH_0}{2n}\right)^n G(\mathbf{x}, t) \quad (3.29)$$

where the form of the NRQCD Hamiltonian terms used throughout are,

$$\begin{aligned} aH =& aH_0 + a\delta H; \\ aH_0 =& -\frac{\Delta^{(2)}}{2am_b}, \\ a\delta H =& -c_1 \frac{\left(\Delta^{(2)}\right)^2}{8\left(am_b\right)^3} + c_2 \frac{ig}{8\left(am_b\right)^2} \left(\nabla \cdot \tilde{\mathbf{E}} - \tilde{\mathbf{E}} \cdot \nabla\right) \\ & - c_3 \frac{g}{8\left(am_b\right)^2} \sigma \cdot \left(\tilde{\nabla} \times \tilde{\mathbf{E}} - \tilde{\mathbf{E}} \times \tilde{\nabla}\right) \\ & - c_4 \frac{g}{2am_b} \sigma \cdot \tilde{\mathbf{B}} + c_5 \frac{a^2 \Delta^{(4)}}{24am_b} - c_6 \frac{a\left(\Delta^{(2)}\right)^2}{16n\left(am_b\right)^2}. \end{aligned} \quad (3.30)$$

Here m_b is the bare b quark mass, and the chromoelectric and chromomagnetic fields $\tilde{\mathbf{E}}$ and $\tilde{\mathbf{B}}$ have been constructed from an improved cloverleaf operator by making the following replacement to the standard cloverleaf operator [60]:

$$F_{\mu\nu}(x) \to \frac{5}{3} F_{\mu\nu}(x) - \frac{1}{6} \Big[U_\mu(x) F_{\mu\nu}(x + a\hat{\mu}) U_\mu^\dagger(x) \quad (3.31)$$

$$+ U_\mu^\dagger(x - a\hat{\mu}) F_{\mu\nu}(x - a\hat{\mu}) U_\mu(x - a\hat{\mu}) \quad (3.32)$$

$$- (\mu \Leftrightarrow \nu) \Big] + \frac{1}{3} \left(\frac{1}{u_0^2} - 1\right) F_{\mu\nu}(x). \quad (3.33)$$

These have also been tadpole improved such that,

$$\mathbf{E} \to \frac{\mathbf{E}}{u_0^4} \quad (3.34)$$

$$\mathbf{B} \to \frac{\mathbf{B}}{u_0^4}. \quad (3.35)$$

The parameter n in the action is a number included purely for stability. The quark modes with the highest energy cannot be modelled accurately if the temporal lattice spacing is too large for the quark mass m_b. In lattice units, the free quark theory would require $mb > 3$, which can be achieved by increasing the temporal lattice spacing. However, by instead inserting n, it allows for simulating quarks with mass of order $3/n$ and larger and this doesn't affect the results at low momentum, so is suitable for calculations presented here. For the calculations throughout this thesis it is set as $n = 4$.

In the $a\delta H$ piece, the first four terms are the lattice versions of the equivalent NRQCD terms derived for the continuum and given in equation 3.16. The last two terms are those given earlier for temporal and spatial improvement of the leading term, H_0, respectively.

The coefficients, c_i, can, in principle, be determined order by order in α_s as an expansion of the form $c_i = 1 + c_i^{(1)}(\alpha_s) + \mathcal{O}(\alpha_s^2)$ in perturbation theory. The HPQCD collaboration has recently been using a mix of tree level values, which are 1 for all coefficients, and their $\mathcal{O}(\alpha_s)$ improved values [18, 61, 62]. In the discussions of the results, the values used in the calculations will be given explicitly, as these were updated as research proceeded and sometimes varied in order to get a handle on their effects. It is important to note that the values of the coefficients depend on the values of α_s and am_b, so they must be determined for each lattice spacing.

Although not included in the work in this thesis, an NRQCD action to $\mathcal{O}(v^6)$ has been used in other studies [63,64], including work by the HPQCD collaboration [61], which also included 4-quark operators.

3.4 Meson Correlators

Using the NRQCD action derived, propagators for the quarks and antiquarks are created on the lattice and combined with appropriate operators to make meson correlation functions. This is done through the use of interpolating operators,

$$\mathcal{O}(\mathbf{x_1}) = \sum_{\mathbf{x_2}} \psi^\dagger \Gamma(\mathbf{x_1} - \mathbf{x_2}) \chi^\dagger(\mathbf{x_2}) \tag{3.36}$$

where $\psi^\dagger$ and $\chi^\dagger$ create a quark and antiquark respectively, and Γ is

$$\Gamma(\mathbf{x_1} - \mathbf{x_2}) = \Omega\phi(|\mathbf{x_1} - \mathbf{x_2}|). \tag{3.37}$$

Ω is chosen with the correct quantum numbers for the meson. For the vector meson, Υ, the Pauli spin matrix σ_i is used, while the pseudoscalar in NRQCD requires just the unit matrix. ϕ is a smearing function used to help extract excited meson states and will be discussed more completely in the next section.

The propagation of the meson from 0 to t is given by the 2-point correlation function,

$$C^{(2\mathrm{pt})}(t) \;=\; \langle 0|\mathcal{O}(t)\mathcal{O}^\dagger(0)|0\rangle$$

$$= \sum_{\mathbf{y_1},\mathbf{y_2}} \mathrm{Tr}\left[G^\dagger(\mathbf{y_1},t)\Gamma^{(sk)}(\mathbf{y_1}-\mathbf{y_2})\tilde{G}(\mathbf{y_2},t)\right], \tag{3.38}$$

where

$$\tilde{G}(\mathbf{y},t) \equiv \sum_{\mathbf{x}} G(\mathbf{y}-\mathbf{x},t)\Gamma^{(sc)}(\mathbf{x}), \tag{3.39}$$

which creates the quark or antiquark from the vacuum at time 0 and then annihilates them at t. The trace here is over spin and color. The notation in the indices of the Γ operator, sc and sk indicate whether this smearing is at the source or the sink.

3.4.1 Smearing

The use of a combination of smearing functions in our lattice QCD calculations allow us better determine excited states when fitting correlators. Smearing functions are functions of spatial position and there is a choice in which function to use. At large times, the ground state of the meson dominates, but the use of the smearing functions can introduce time-dependences at short times. The advantage with that is that this can be exploited to extract the properties of the excited states.

The smearing functions that we have used for the NRQCD b quarks are 'hydrogen-wavefunction' smearings [18]. We used two different radii at each lattice spacing, which were adjusted so as to keep the same physical size on each ensemble. In addition to this, we used point sources, which are δ functions. Combinations of the point sources and smearings for the quarks and antiquarks allow a matrix of correlators to be constructed, the elements of which can be fitted simultaneously to extract the energies. In some cases, only the point sources need to be fitted, and this results in good determinations of the ground state energies from a much faster fit, but poorer results for the excited states.

Random Wall Sources

Statistical accuracy can be achieved through the use of random wall sources [19, 65]. By using a random number on each spatial point of the lattice, it is possible to simulate L^3 quark/antiquark pairs rather than just one. This is done by choosing a random number, η_a, from U(1) for the quark source at each lattice site, which is multiplied with the smearing. The antiquark source on the same lattice site is then assigned the complex conjugate, $\eta_b = \eta_a^\dagger$, such that when the quark and antiquark propagators are combined, those with

the correct pairing of random numbers will create the meson correlators, while the other combinations will cancel on the average.

The random wall source method allows this increase in statistical accuracy whilst not increasing computing cost; it would clearly be prohibitively expensive to run code L^3 times to create the equivalent number of meson correlators individually.

3.5 Fitting

In order to extract the matrix elements and energies of the correlators we need a suitable method for fitting them to theoretical expectations. The results for all correlators in this thesis were determined through constrained curve fitting [66], where a Bayesian approach was taken, allowing a large amount of data to be fitted efficiently. From theory, we want to fit to our correlators to the form

$$C(t) = \sum_{n=0}^{n_{\text{exp}}-1} A_n e^{-E_n t}, \tag{3.40}$$

where the sum is over the number of exponentials included in the fit, the amplitude A_n is – up to normalisation factors – the square of the matrix element $\langle n|\mathcal{O}|0\rangle$, and E_n is the energy, with $E_n > E_{n-1}$. In principle there are an infinite number of terms, but assuming the excited energy states are well behaved, they become negligibly small at large t.

The normal procedure is to minimise the value of $\chi^2(A_n, E_n)$ by varying A_n and E_n. In the procedure here, χ^2 is augmented such that,

$$\chi^2_{\text{aug}} \equiv \chi^2 + \chi^2_{\text{prior}}, \tag{3.41}$$

where

$$\chi^2_{\text{prior}} \equiv \sum_n \frac{(A_n - \tilde{A}_n)^2}{\tilde{\sigma}_{A_n}} + \sum_n \frac{(E_n - \tilde{E}_n)^2}{\tilde{\sigma}_{E_n}}. \tag{3.42}$$

Here, $\tilde{A}$ and $\tilde{E}$ are prior values given for the matrix elements and energies respectively, while $\tilde{\sigma}_{A_n}$ and $\tilde{\sigma}_{E_n}$ are their corresponding widths. This new value of χ^2_{aug} is then minimised in a fit to all the available data.

The prior values are picked to be reasonable inputs into the fit based on previous understanding. The number of exponential terms in the fit is increased until the results converge for the first few terms that we are interested in, and these constraints mean that

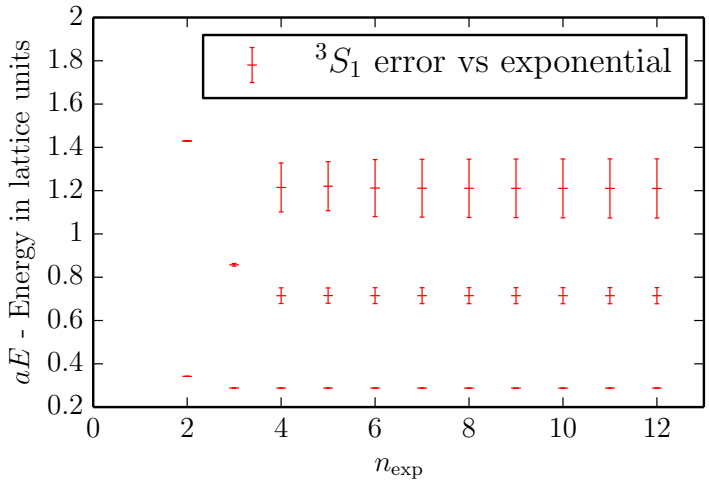

Figure 3.1: Errors against the number of exponentials in the fit of an Υ correlator. The ground state energy is found by the third exponential. By $n_{\text{exp}} = 6$ the energy and error for the ground state and first two excited states have stabilised.

this convergence can occur with only a few terms, depending on how complicated the fit is.

As an example of this convergence, figure 3.1 shows the the energies against the number of exponentials in the fit for the Υ meson at rest on very coarse set 1 using a point source. The ground state energy is found by the third exponential quickly followed by the first and then second excited states. It is not until the sixth exponential that the values converge properly for all three states, as evidence by the stability in the size of the errors. In this example, $\tilde{E}_0 = 0.3 \pm 0.15$ and $d\tilde{E} = 0.45 \pm 0.22$, where $d\tilde{E}$ is the prior for the splitting between each energy level. Energies are defined so that there is a 'ladder' of them with the lowest energy being the ground state energy by definition, followed by the first excited state, etc.

The same behaviour can be seen for the amplitudes from the fits as shown for $\sqrt{A}$ in figure 3.2. Since the amplitude is from the same term in equation 3.40, it is expected that it would converge at the same rate as the energy. In contrast to the energies, the central value for the amplitude for the first excited state here is lower than that for the ground state and this is perfectly allowed.

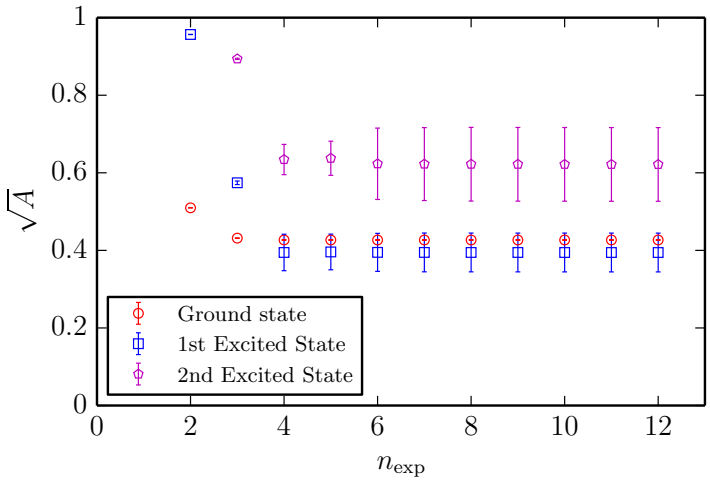

Figure 3.2: $\sqrt{A}$ against the number of exponentials in the fit of an Υ correlator. As with the E_0, $\sqrt{A_0}$ is found by the third exponential as it would be since they are from the same term in the expansion. By $n_{\text{exp}} = 6$, $\sqrt{A}$ for the ground state and first two excited states have stabilised. The priors, $\tilde{A}_n$, were all chosen to be 0.1 ± 1.0

Chapter 4

Bottomonium Physics: The Υ and Υ' Leptonic Widths and m_b

Bottomonium mesons, which are those comprised of a valence b quark and its antiparticle – specifically the vector meson, Υ, and the pseudoscalar, η_b – are discussed here. Studying the Υ spectrum on the lattice using NRQCD allows the b quark to be tuned for use in calculations of properties of other states and offers a method by which to tune the lattice spacing. Indeed, it is the results from the Υ spectrum calculations that are used for b quark parameters and lattice spacings used in calculations of heavy-light decays in chapter 5 [18].

The parameters for the valence b quarks used in the lattice QCD calculations are contained in table 4.1. am_b is the quark mass in lattice units and has been tuned as in [18]. We have also deliberately mistuned the b quark on set 1 in some cases, which will be made clear. This gives the advantage of allowing comparisons with calculations with a properly tuned am_b to allow for estimates of the effect of the errors. u_{0L} is the tadpole parameter, i.e. the mean gluon link, in Landau gauge and c_i are the coefficients in the NRQCD action at their $\mathcal{O}(\alpha_s)$ values, while those not listed are kept at the tree level of 1. The coefficient c_4 is also used at the tree level value in some cases, and again this will be made explicit for the appropriate calculations.

4.1 Kinetic Mass

The absence of a mass term in the NRQCD action means that the energy is offset, so the ground state energy does not correspond to the meson mass, although energy differences

Set	am_b	u_{0L}	c_1	c_4	c_5	c_6
1	3.297	0.8195	1.36	1.22	1.21	1.36
2	3.263	0.82015	1.36	1.22	1.21	1.36
3	3.25	0.819467	1.36	1.22	1.21	1.36
4	2.66	0.834	1.31	1.20	1.16	1.31
5	2.62	0.8349	1.31	1.20	1.16	1.31
6	2.62	0.834083	1.31	1.20	1.16	1.31
7	1.91	0.8525	1.21	1.16	1.12	1.21
8	1.89	0.851805	1.21	1.16	1.12	1.21

Table 4.1: Parameters used in the NRQCD action given in equation 3.30. am_b is the bare lattice mass of the b quark and u_{0L} is the Landau link. The parameters $c_{1,4,5,6}$ listed are the coefficients from the action and include $\mathcal{O}(\alpha_s)$ corrections. The other c_i have their tree level value of 1. There are cases where the values differ from those given here. They will be made clear in the text.

still correspond to mass differences. The result is therefore that the mass of the meson cannot be accessed directly like it can with other lattice QCD formalisms.

It is possible, however, to determine the zero of energy by calculating the *kinetic mass* in lattice units, aM_{kin}, of a meson with a particular momentum by using the energy difference between it and the same meson at rest. If a fully relativistic dispersion relation is considered:

$$aE(P) = \sqrt{a^2P^2 + a^2M_{\text{kin}}^2}, \tag{4.1}$$

where $aE(P)$ is the energy of the meson with lattice momentum aP, then,

$$aM_{\text{kin}} = \frac{a^2P^2 - (a\Delta E)^2}{2a\Delta E}. \tag{4.2}$$

Here, $a\Delta E$ is the energy difference between that of the meson with momentum $\mathbf{P}$, $aE(\mathbf{P})$, and the energy of the meson at rest, $aE(\mathbf{0})$.

In carrying out this calculation, Υ and η_b two-point correlators at various meson momenta are fitted simultaneously alongside the correlators of the mesons at rest. This allows correlations to be taken into account while fitting and improves the precision of $a\Delta E$. All of the results come from the use of point sources at the source and sink, with a random wall as described in section 3.4.1.

$Pa\ (2\pi/L)$	$aE(^1S_0,\vec{p})$	$aE(^3S_1,\vec{p})$	$aM_{\rm Kin}(\Upsilon)$	$aM_{\rm Kin}(\eta_b)$	$\overline{aM}_{\rm Kin}(1S)$
(0,0,0)	0.25075(6)	0.28525(8)	-	-	-
(1,1,1)	0.28195(6)	0.31696(10)	7.2777(171)	7.4007(90)	7.3084(148)
(2,2,1)	0.34321(9)	0.37925(15)	7.3365(93)	7.4603(54)	7.3675(81)
(3,0,0)	0.34229(8)	0.37841(13)	7.4023(73)	7.5364(42)	7.4358(64)

Table 4.2: Ground state energies and kinetic mass results in lattice units for the Υ and η_b on the very coarse ensemble set 1 with $c_{1,5,6}$ set to their $\mathcal{O}(\alpha_s)$ improved values.

$Pa\ (2\pi/L)$	$aE(^1S_0,\vec{p})$	$aE(^3S_1,\vec{p})$	$aM_{\rm Kin}(\Upsilon)$	$aM_{\rm Kin}(\eta_b)$	$\overline{aM}_{\rm Kin}(1S)$
(0,0,0)	0.26096(4)	0.29243(6)	-	-	-
(1,0,0)	0.26684(4)	0.29838(6)	5.7467(184)	5.8175(71)	5.7644(151)
(1,1,0)	0.27273(4)	0.30434(6)	5.7478(165)	5.8186(66)	5.7655(137)
(1,1,1)	0.27860(4)	0.31030(7)	5.7420(169)	5.8172(70)	5.7608(140)
(2,0,0)	0.28438(4)	0.31611(8)	5.7775(66)	5.8387(25)	5.7928(54)
(2,1,1)	0.29610(4)	0.32799(8)	5.7642(92)	5.8339(38)	5.7817(76)
(2,2,1)	0.31348(6)	0.34555(14)	5.7781(129)	5.8440(70)	5.7946(105)
(3,0,0)	0.31335(6)	0.34536(14)	5.7982(119)	5.8589(44)	5.8134(96)

Table 4.3: Ground state energies and kinetic mass results in lattice units for the Υ and η_b on the coarse ensemble set 4 with $c_{1,5,6}$ set to their $\mathcal{O}(\alpha_s)$ improved values.

The results of the kinetic mass calculations and the energies of the ground state Υ and η_b from our NRQCD calculation are given in table 4.2 for the very coarse lattice, set 1. The coefficients, c_1, c_5 and c_6 are set to their $\mathcal{O}(\alpha_s)$ improved values. The notation (p_x, p_y, p_z) is used to denote the momentum of the meson, where p_i is in units of $2\pi/L$ and it is to be understood to include an average over all possible permutations of that momentum with the same $p_x^2 + p_y^2 + p_z^2$. Table 4.3 contains the equivalent results for the coarse ensemble, set 4, while in table 4.4 the results where all coefficients are set to their tree level value of 1 are given [18]. Finally, results for the fine ensemble, set 7, are given in tables 4.5 and 4.6 for the values of $c_{1,5,6}$ at their $\mathcal{O}(\alpha_s)$ improved values and where the coefficients are set to 1 respectively.

Plots of these results against the square of the momentum in lattice units are shown in figures 4.1, 4.2 and 4.3 for sets 1, 4 and 7. It can be seen that the points where the momen-

$Pa\ (2\pi/L)$	$aE(^1S_0, \vec{p})$	$aE(^3S_1, \vec{p})$	$aM_{\text{Kin}}(\Upsilon)$	$aM_{\text{Kin}}(\eta_b)$	$\overline{aM}_{\text{Kin}}(1S)$
(0,0,0)	0.25529(4)	0.28626(6)	-	-	-
(1,0,0)	0.26119(4)	0.29220(7)	5.7157(245)	5.7733(100)	5.7301(203)
(1,1,1)	0.27309(4)	0.30426(7)	5.7027(166)	5.7665(69)	5.7187(137)
(2,0,0)	0.27890(4)	0.31007(9)	5.7387(67)	5.7879(23)	5.7510(55)
(2,2,1)	0.30830(8)	0.33977(17)	5.7317(148)	5.7871(71)	5.7456(123)
(3,0,0)	0.30814(6)	0.33957(14)	5.7528(105)	5.8049(33)	5.7658(84)

Table 4.4: Ground state energies and kinetic mass results in lattice units for the Υ and η_b on the coarse ensemble set 4 with $c_{1,5,6}$ set to 1.

$Pa\ (2\pi/L)$	$aE(^1S_0, \vec{p})$	$aE(^3S_1, \vec{p})$	$aM_{\text{Kin}}(\Upsilon)$	$aM_{\text{Kin}}(\eta_b)$	$\overline{aM}_{\text{Kin}}(1S)$
(0,0,0)	0.25827(3)	0.28390(5)	-	-	-
(1,0,0)	0.26278(3)	0.28844(4)	4.2447(148)	4.2782(65)	4.2531(124)
(1,1,0)	0.26727(4)	0.29299(6)	4.2514(172)	4.2864(90)	4.2602(147)
(1,1,1)	0.27173(3)	0.29747(5)	4.2562(135)	4.2871(61)	4.2639(112)
(2,0,0)	0.27620(3)	0.30199(5)	4.2515(29)	4.2914(14)	4.2615(24)
(2,2,1)	0.29850(4)	0.32451(6)	4.2523(44)	4.2920(23)	4.2622(37)
(3,0,0)	0.29847(3)	0.32447(6)	4.2538(41)	4.2951(19)	4.2641(35)

Table 4.5: Ground state energies and kinetic mass results in lattice units for the Υ and η_b on the fine ensemble set 7 with $c_{1,5,6}$ set to their $\mathcal{O}(\alpha_s)$ improved values.

$Pa\ (2\pi/L)$	$aE(^1S_0, \vec{p})$	$aE(^3S_1, \vec{p})$	$aM_{\text{Kin}}(\Upsilon)$	$aM_{\text{Kin}}(\eta_b)$	$\overline{aM}_{\text{Kin}}(1S)$
(0,0,0)	0.24652(3)	0.27153(5)	-	-	-
(1,0,0)	0.25107(3)	0.27610(4)	4.2222(143)	4.2441(64)	4.2277(120)
(1,1,1)	0.26010(3)	0.28518(5)	4.2304(133)	4.2516(62)	4.2357(112)
(2,0,0)	0.26461(3)	0.28974(5)	4.2253(28)	4.2548(14)	4.2327(24)
(2,2,1)	0.28713(4)	0.31244(6)	4.2225(44)	4.2516(23)	4.2298(37)
(3,0,0)	0.28712(4)	0.31246(7)	4.2154(57)	4.2510(28)	4.2243(48)

Table 4.6: Ground state energies and kinetic mass results in lattice units for the Υ and η_b on the fine set 7 ensemble with $c_{1,5,6}$ set to 1.

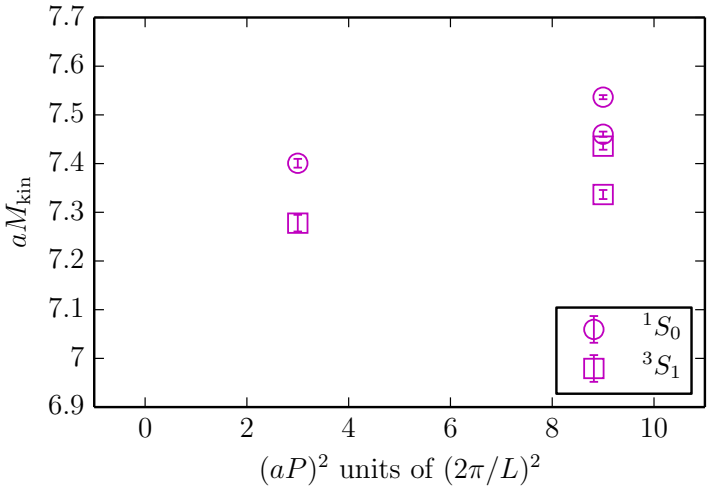

Figure 4.1: Kinetic mass of the Υ and η_b mesons for various values of lattice momentum on the very coarse ensemble, set 1. The values of the coefficients, $c_{1,5,6}$ in the action have been tuned to their $\mathcal{O}(\alpha_s)$ values while the others are set to their tree level values of 1.

tum is directed along one axis are slightly higher than those where the momentum is directed along multiple axes. This is a result of rotational symmetry breaking down because of discretisation effects on the lattice. This is most obvious for the points corresponding to mesons with $aP = (2, 2, 1)$ and $aP = (3, 0, 0)$ as they both have $P^2a^2 = 9(2\pi/L)^2$, where the $aP = (3, 0, 0)$ point is the higher of the two in each case.

The hyperfine splitting is the difference in mass between the Υ and the η_b mesons and the results here show a larger kinetic mass for the η_b than the Υ, which is the opposite of the experimental result. The energy difference $\Delta E(0)$, however, has the correct sign and it is this result that is used for accurate determination of the hyperfine splitting. The reason for the wrong sign in the kinetic masses is that the $\sigma \cdot \tilde{\mathbf{B}}$ term is only included at leading order in the action used, and relativistic corrections are needed to give a more accurate kinetic mass. This issue is rectified when v^6 terms containing v^2 corrections to the $\sigma \cdot \tilde{\mathbf{B}}$ term are added to the NRQCD action. This was demonstrated in [61], but for the discussion here these terms are not included.

In order to deal with this problem without these additional terms it is useful to consider the spin-averaged kinetic mass given by,

$$\overline{M}_{\rm Kin}(1S) = \frac{(3M_{\rm Kin}(\Upsilon) + M_{\rm Kin}(\eta_b))}{4}, \tag{4.3}$$

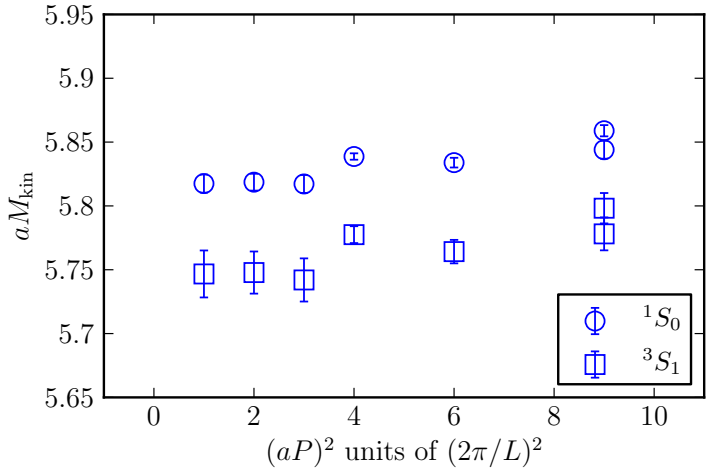

Figure 4.2: Kinetic mass of the Υ and η_b mesons for various values of lattice momentum on the coarse ensemble. The values of the coefficients, $c_{1,5,6}$ in the action have been tuned to their $\mathcal{O}(\alpha_s)$ values while the others are set to their tree level values of 1.

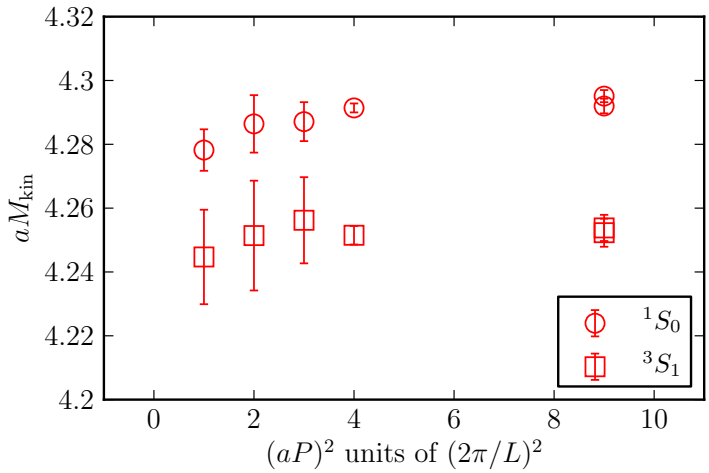

Figure 4.3: Kinetic mass of the Υ and η_b mesons for various values of lattice momentum on the fine ensemble. The values of the coefficients, $c_{1,5,6}$ in the action have been tuned to their $\mathcal{O}(\alpha_s)$ values while the others are set to their tree level values of 1.

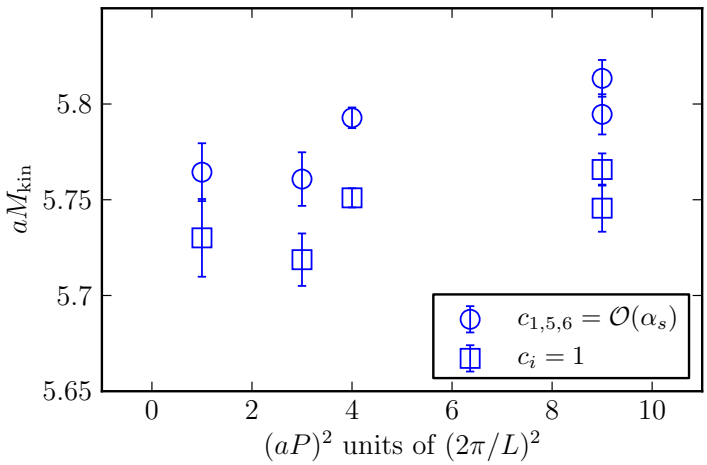

Figure 4.4: Spin averaged values of the kinetic mass for the Υ and η_b mesons for various values of lattice momentum on the coarse ensemble. The two sets of points correspond the coefficients, $c_{1,5,6}$ in the action having been tuned to their $\mathcal{O}(\alpha_s)$ values and where all coefficients are set to their tree level values of 1.

as this cancels out spin dependent effects. For this reason, we tune m_b based on this mass.

Figures 4.4 and 4.5 show results for the spin-averaged kinetic mass on the coarse and fine ensembles respectively. Each plot has points corresponding to the results where the coefficients in the action all have value 1 and where $c_{1,5,6}$ have their $\mathcal{O}(\alpha_s)$ improved values. Notice that the results with improved coefficients have higher kinetic mass results than those at tree level as a result of renormalising the p^4 term. A consequence in the shift in kinetic mass is that the tuned am_b needs to change in order that the kinetic mass matches the experimental bottomonium mass.

Returning to the results for (3,0,0) and (2,2,1) with the same value of $P^2a^2 = 9(2\pi/L)^2$, a comparison between the energies of these points shows the effect of lattice discretisation on rotational symmetry. The difference in the energy between the two momenta are plotted in figure 4.6 against the square of the lattice spacing in fm, using sets 1, 4 and 7. The points correspond to each of the Υ and η_b mesons with their tree level coefficients c_i and the usual $\mathcal{O}(\alpha_s)$ improved values. The use of the improved values can be seen to slightly reduce this energy splitting. As the lattice spacing becomes finer, this effect becomes smaller since it is a discretisation effect, and has all but disappeared by the time the spacing is $a \approx 0.09$ fm.

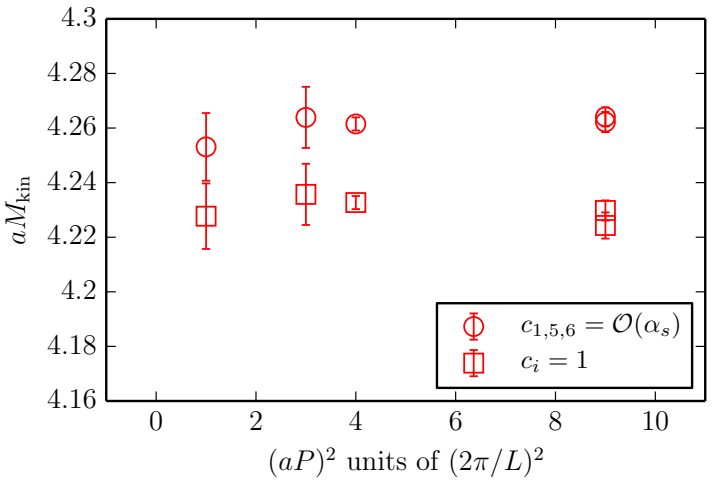

Figure 4.5: Spin averaged values of the kinetic mass for the Υ and η_b mesons for various values of lattice momentum on the fine ensemble. The two sets of points correspond the coefficients, $c_{1,5,6}$ in the action having been tuned to their $\mathcal{O}(\alpha_s)$ values and where all coefficients are set to their tree level values of 1.

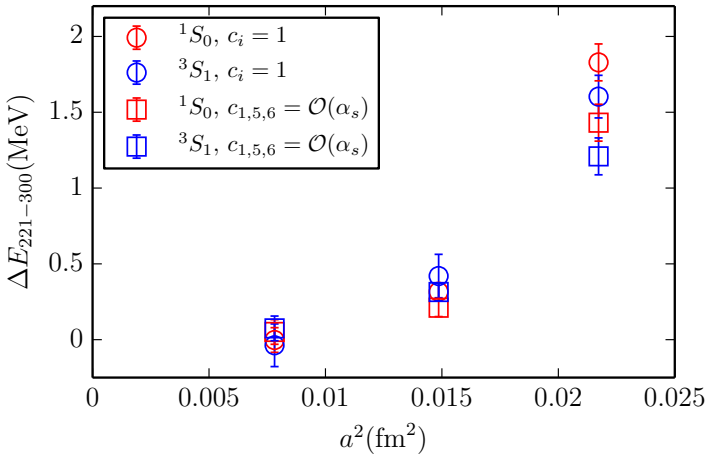

Figure 4.6: The energy difference in MeV between mesons with momenta (2,2,1) and (3,0,0) given in units of $(2\pi/L)$ plotted against the square of the lattice spacing in fm. The η_b and Υ results are shown here where c_i=1 and where $c_{1,5,6}$ are given their $\mathcal{O}(\alpha_s)$-improved values.

4.2 Amplitudes

The amplitude A_n defined in equation 3.40 can be split into a source and a sink component, such that,

$$C(t) = \sum_{n=0}^{n_{\text{exp}-1}} c(\phi_{\text{sc}}, n)c^*(\phi_{sk}, n)e^{-E_n t}, \tag{4.4}$$

where $\phi_{\text{sc/sk}}$ is the smearing at the source/sink. These amplitude components then relate to the matrix element that creates the meson from the vacuum:

$$c(\phi, n) = \frac{\langle 0|\mathcal{O}^{(\phi)}|b\bar{b}\rangle}{\sqrt{2M}}, \tag{4.5}$$

where $\mathcal{O}$ is the interpolating operator for the state as in equation 3.36. Additionally, for the vector meson Υ, due to polarisation vectors, the correct form of the two-point function with momentum P and momentum components p_i, p_j would be expected to be of the form [67],

$$C^{ij}(P, t) = \sum_{n=0}^{n_{\text{exp}-1}} A_n e^{-E_n t}\left(\delta_{ij} + \frac{p_i p_j}{M_\Upsilon^2}\right). \tag{4.6}$$

This means that there are nine correlators that can be fitted for the Υ, corresponding to the possible polarisation combinations. They all have the same energies, but the amplitudes can and do differ depending on the meson momentum. The results for the off-diagonal matrix elements, e.g. the xy element, were expected to be very small but this could not be determined; the amplitudes were consistent with zero. Unless otherwise stated, results given are those for the xx elements.

In the results in the remainder of the chapter, there are a mixture of those that utilised only point sources and those which used matrix fits of various combinations of smearings in order to extract the properties of excited states. It will be stated explicitly in the text which smearings were used for each result.

4.2.1 NRQCD Relativistic Covariance

The amplitudes that are obtained from the fits have to be matched to full QCD in order to determine the correct matrix elements for creating the bottomonium mesons from the vacuum. This is because the NRQCD action is to a finite order, so relativistic effects are missing. With the addition of more terms, NRQCD behaves more and more relativistically.

For example, the v^4 terms in the NRQCD action are required – as we will see – in order to properly introduce binding energy into the meson kinetic mass [18].

First we will match the NRQCD operators to continuum operators. Throughout this section the correlation functions use local sources at the source and sink, with operators $\chi^\dagger\psi$ and $\chi^\dagger\sigma_x\psi$ for the η_b and the Υ respectively. A random wall source is used to generate correlators with zero and finite momentum.

For local current operators the expectation is to get the following relativistically covariant behaviour:

$$\langle 0|\psi^\dagger\gamma_5\psi|\eta_b(\mathbf{p})\rangle = \text{constant} \tag{4.7}$$

$$\langle 0|\psi^\dagger\gamma_5\gamma_0\psi|\eta_b(\mathbf{p})\rangle \propto E(\mathbf{p}) \tag{4.8}$$

$$\langle 0|\psi^\dagger\gamma_i\psi|\Upsilon(\mathbf{p},\lambda)\rangle \propto \epsilon(\mathbf{p},\lambda), \tag{4.9}$$

where $\epsilon(\mathbf{p},\lambda)$ is the polarisation vector for the Υ.

The start point to match the currents is with the spinors,

$$\begin{aligned} u(\mathbf{p}) &= \begin{pmatrix} \psi \\ \dfrac{\sigma\cdot\mathbf{p}}{E+m}\psi \end{pmatrix}\sqrt{\frac{E+m}{2E}} \\ v(\mathbf{p}) &= \begin{pmatrix} \dfrac{\sigma\cdot\mathbf{p}}{E+m}\chi \\ \chi \end{pmatrix}\sqrt{\frac{E+m}{2E}} \end{aligned} \tag{4.10}$$

where the ψ and χ are the quark and antiquark Pauli spinors respectively and the normalisation is nonrelativistic so it is appropriate for NRQCD [68].

Making use of the gamma matrices,

$$\gamma^0 = \begin{pmatrix} 1 & 0 \\ 0 & -1 \end{pmatrix}, \quad \gamma^i = \begin{pmatrix} 0 & \sigma^i \\ \sigma^i & 0 \end{pmatrix}, \quad \gamma^5 = \begin{pmatrix} 0 & 1 \\ 1 & 0 \end{pmatrix}, \tag{4.11}$$

the tree-level matrix element $\langle 0|J^{\mathrm{QCD}}|\bar{b}b\rangle$ is

$$\bar{v}(\mathbf{p})\gamma_5 u(\mathbf{p}) \tag{4.12}$$

$$\bar{v}(\mathbf{p})\gamma_0\gamma_5 u(\mathbf{p}) \tag{4.13}$$

$$\bar{v}(\mathbf{p})\gamma_i u(\mathbf{p}) \tag{4.14}$$

with quark and antiquark momenta,

$$\begin{aligned} \mathbf{p} &= \frac{1}{2}\mathbf{P} + \mathbf{k}, \\ \mathbf{p} &= \frac{1}{2}\mathbf{P} - \mathbf{k}, \end{aligned} \tag{4.15}$$

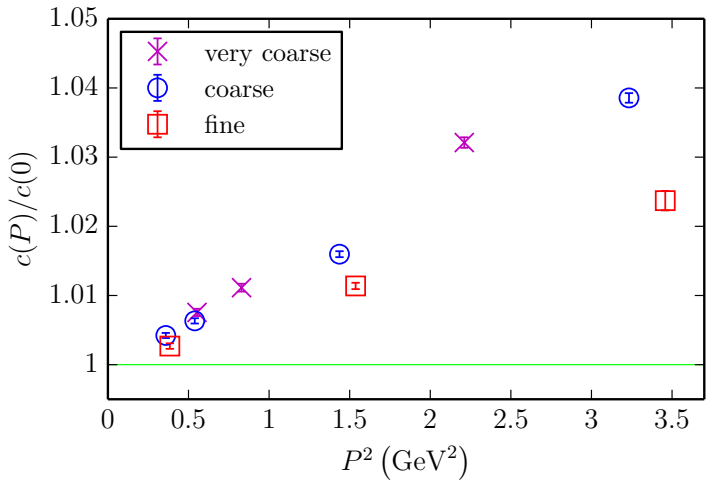

Figure 4.7: The ratios $c(\mathbf{P})/c(0)$ for the leading current of the η_b plotted against P^2 in GeV^2. Points are shown for all three ensembles with $m_l/m_s = 0.2$: very coarse set 1, coarse set 4 and fine set 7. The green line shows the expected relativistic behaviour, which in this case is constant.

for meson momentum $\mathbf{P}$ and internal momentum $\mathbf{k}$. Here we want to study the $\mathbf{P}$ dependence of these ratios, so $\mathbf{k} = 0$, making the calculation simpler. The internal momentum $\mathbf{k}$ relates to relativistic corrections to the currents, which are implemented through derivatives operators on the fields. Corrections to the currents will be discussed in the next section.

For the local currents used here, expanding $\bar{v}(\mathbf{P})\Gamma u(\mathbf{P})$ – where Γ is the appropriate combination of gamma matrices to create the meson state – in powers of $\mathbf{P}$ gives,

$$\bar{v}(\mathbf{P})\gamma_5 u(\mathbf{P}) = \chi^\dagger \psi \frac{m_b}{E} \tag{4.16}$$

$$\bar{v}(\mathbf{P})\gamma_0\gamma_5 u(\mathbf{P}) = \chi^\dagger \psi \tag{4.17}$$

$$\bar{v}(\mathbf{P})\gamma_i u(\mathbf{P}) = \frac{E+m}{2E}\chi^\dagger \left[\sigma_i + \frac{\sigma\cdot\mathbf{P}/2}{E+m}\sigma_i\frac{\sigma\cdot\mathbf{P}/2}{E+m}\right]\psi \tag{4.18}$$

with $E \equiv E(\mathbf{P})$. In the first case, only a straightforward factor that is a function of $\mathbf{P}$ is required to be multiplied with the NRQCD operator for matching. No additional factors are needed in the second case where the η_b is treated like a temporal axial current. The third case is the most complicated owing to the fact that the meson has an associated polarisation as well as the meson momentum.

In the first instance we look at just the raw local amplitudes, $c(\mathbf{P})$ to observe how

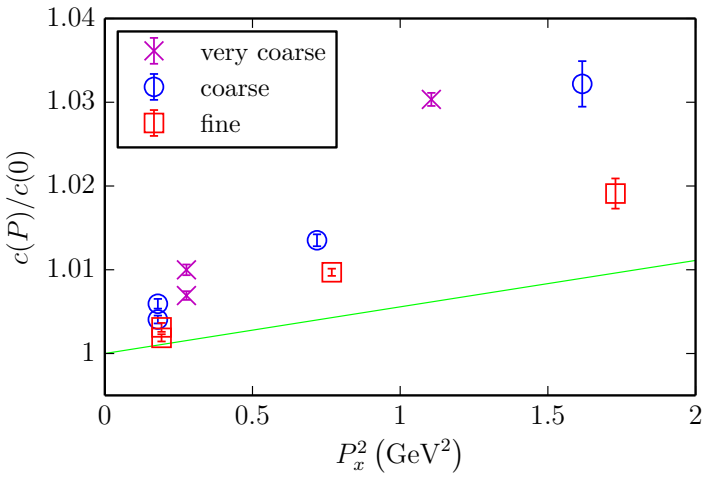

Figure 4.8: The ratio $c(\mathbf{P})/c(0)$ for the leading current of the Υ with x polarisation momentum P_x plotted against P_x^2 in GeV^2. Points are shown for all three ensembles with $m_l/m_s = 0.2$: very coarse set 1, coarse set 4 and fine set 7. The green line shows the expected relativistic behaviour, which in the case of the vector, Υ, is $\sqrt{1 + P_x^2/M_\Upsilon^2}$.

the NRQCD mesons behave with momentum P. The ratio $c(\mathbf{P})/c(0)$ is plotted for the η_b meson in figure 4.7 and for the x polarisation[1] of the Υ in figure 4.8. The η_b plot shows the ratio against P^2 in GeV^2 and the Υ plot is against P_x^2 in GeV^2, each for the very coarse, coarse and fine ensembles with $m_l/m_s = 0.2$.

The amplitudes in this case do not exhibit the correct relativistic behaviour, growing too quickly with P. The matching factors from equation 4.18 can then be applied to see whether the expected results of equations 4.7 to 4.9 are obtained. Figure 4.9 shows the amplitude ratios for the η_b with

$$\tilde{c}(\mathbf{P}) = c(\mathbf{P}) \frac{m_b}{\sqrt{P^2/4 + m_b^2}} \tag{4.19}$$

for each of the three ensembles with $m_l/m_s = 0.2$. The result is that as the lattice spacing becomes smaller the dependence on P vanishes as expected.

For the temporal axial current the matching factor is 1, so the amplitudes from the η_b correlators should already exhibit the behaviour expected of growing as E/M_{η_b}. Figure 4.10 shows that this does occur.

[1]For most of the results presented, the x polarisation will be used unless explicitly stated.

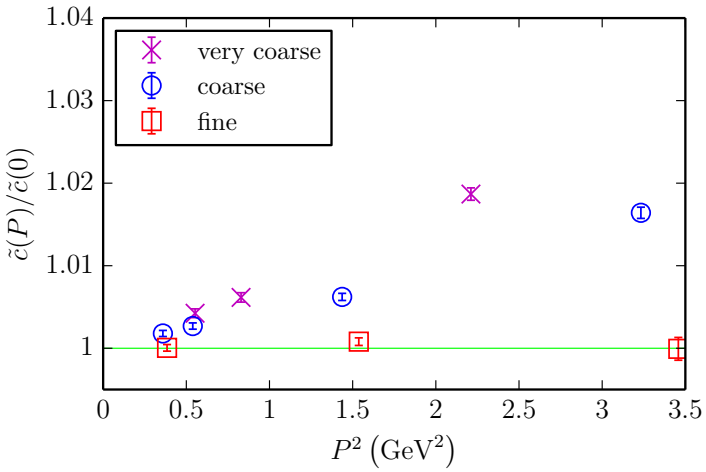

Figure 4.9: The ratios of the zero momentum amplitudes and amplitudes for mesons with momentum P from the leading current plotted against P^2 in GeV^2 for the η_b, with the factor $\frac{m_b}{E}$ included. Points are shown for all three ensembles: very coarse, coarse and fine. The green line shows the expected relativistic behaviour for the η_b, which is constant.

Finally, the corrected vector amplitude is,

$$\tilde{c}(\mathbf{P}) = c(\mathbf{P}) \left[\frac{m_b}{E} + \frac{P_x}{E(E+m_b)} \right] \tag{4.20}$$

with $E = \sqrt{P + m_b}$. The result of applying this factor on the x polarisation of the Υ is shown in figure 4.11. As with the other cases, as the lattice spacing becomes finer, the ratio of amplitudes approaches agreement with the expected relativistic behaviour. The green line on this plot comes from the completeness relation for the polarisation and is $\sqrt{1 + P_x/M_\Upsilon}$.

4.2.2 Excluding Radiative Correction Terms

The NRQCD action exhibits relativistic behaviour – as would be expected – when relativistic terms are added. To demonstrate this, the effect of the full v^4 action given in 3.30 is contrasted with an action using just H_0 plus the discretisation terms – the only parts of δH remaining are those led by the coefficients c_5 and c_6, both set to their tree level value of 1 – which gives a v^2 action. As discussed in 3.3.1, the effect of the c_5 and c_6 terms is to remove spatial and temporal discretisation errors from H_0 so they remain included in the v^2 action.

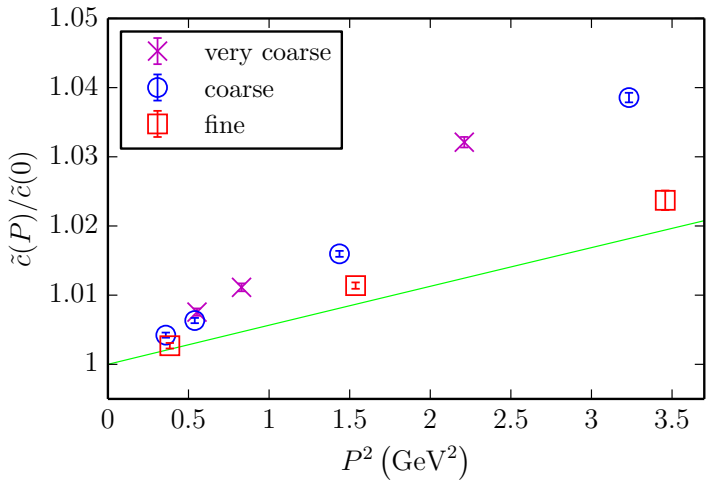

Figure 4.10: The ratios of the zero momentum amplitudes and amplitudes for mesons with momentum P from the leading current plotted against P^2 in GeV^2 for the temporal axial current. These matrix elements come from the η_b correlator amplitudes with a matching factor of 1 for relativistic behaviour. Points are shown for three ensembles – very coarse, coarse and fine – with $m_l/m_s = 0.2$. The green line shows the expected relativistic behaviour, $1 + P^2/4M^2$.

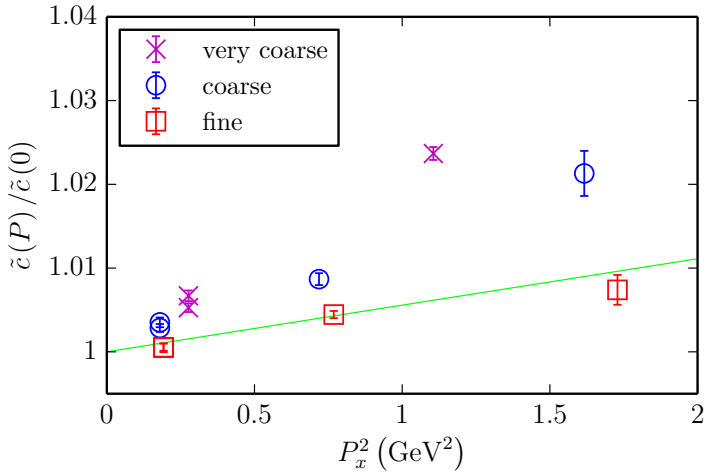

Figure 4.11: The ratios of the zero momentum amplitudes and amplitudes for mesons with momentum P from the leading current plotted against P^2 in GeV^2 for the Υ, with the factor $\left(\frac{m_b}{E} + \frac{P_x}{E(E+m_b)}\right)$ from equation 4.20 included. Points are shown for all three ensembles: very coarse, coarse and fine. The green line shows the expected relativistic behaviour, which in this case is $\sqrt{1 + P_x^2/M_\Upsilon^2}$.

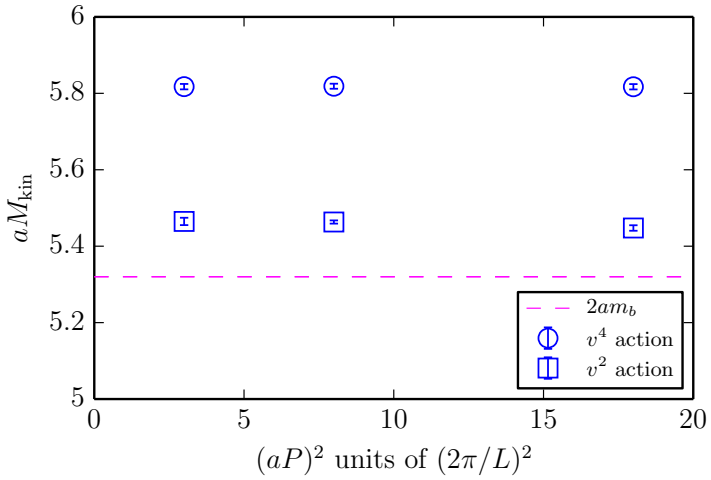

Figure 4.12: Kinetic mass on the coarse ensemble in lattice units comparing the v^2 action given in equation 3.30 with the action with only v^2 terms. The dashed line corresponds to twice the mass of the b quark in lattice units used in these calculations.

Kinetic Mass

Figures 4.12 and 4.13 show the effect of the full action compared with the v^2 action on the kinetic mass. Since there are no spin dependent terms in the v^2 action, the results from the numerical calculation for the Υ are actually the same as those for the η_b. The points corresponding to the v^4 action are those for the spin-average kinetic mass, $\overline{M}_{\text{kin}}$. The dashed line shown on each of the plots is twice the b quark mass in lattice units.

The result is that the kinetic mass using only the v^2 terms is much smaller than with the v^4 terms. The interaction terms in the v^4 action are required in order to have the correct binding energy fed into the mesons. This is contrasted with the kinetic mass for the v^2 terms which is closer to the case in which there is no binding energy as shown by the dashed line on each of the plots.

Amplitudes

Figures 4.14 and 4.15 show the amplitude ratios $c(P)/c(0)$ for the η_b on the coarse and fine ensembles respectively when using the v^4 action compared with the result when using the v^2 terms only. On the coarse ensemble, the amplitudes using the v^2 action grow more slowly than when using the v^4 action, while on the fine ensemble they even decrease with increasing P^2. Applying the factor for a pseudoscalar from equation 4.16 results

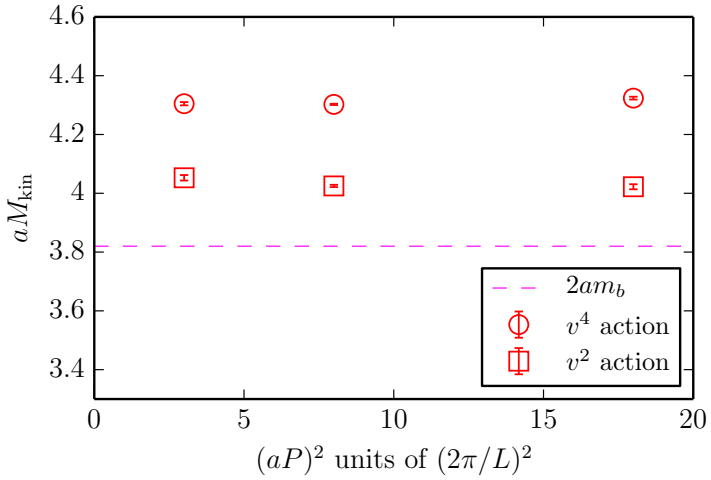

Figure 4.13: Kinetic mass on the fine ensemble in lattice units comparing the v^4 action given in equation 3.30 with the action with only v^2 terms. The dashed line corresponds to twice the mass of the b quark in lattice units used in these calculations.

in the corrected amplitude $\tilde{c}(P)$ decreasing with increasing P^2 for the v^2 action in both cases, while the v^4 action exhibits the expected relativistic behaviour as the lattice spacing decreases. This is demonstrated in figures 4.16 and 4.17 for the coarse and fine ensembles respectively.

From the kinetic mass and amplitude results contrasting the v^2 and v^4 actions, it is clear that it is important to include the v^4 terms so that binding energy is included and that correct relativistic behaviour can be obtained.

4.3 Υ Decay Constant & Leptonic Width

The leptonic width, Γ, of the $\Upsilon(nS)$ to two leptons can be measured experimentally to high precision. In the NRQCD calculation this is defined as,

$$\Gamma\left(\Upsilon^{(n)} \to e^+e^-\right) = 16\pi\alpha_{\rm em}^2 e_b^2 \frac{|\langle 0|J_{V,\rm NRQCD}|\Upsilon^{(n)}\rangle|^2}{M^2_{\Upsilon^{(n)}}} Z_V^2, \tag{4.21}$$

where e_b is the charge of the b quark in units of the electron charge, M_Υ is the mass of the Υ and Z_V is a renormalisation constant that matches the NRQCD vector current to the full QCD current. $\alpha_{\rm em}$ is the fine structure constant, and taken at the b quark mass is $\alpha_{\rm em}(m_b) = 1/132$ [69].

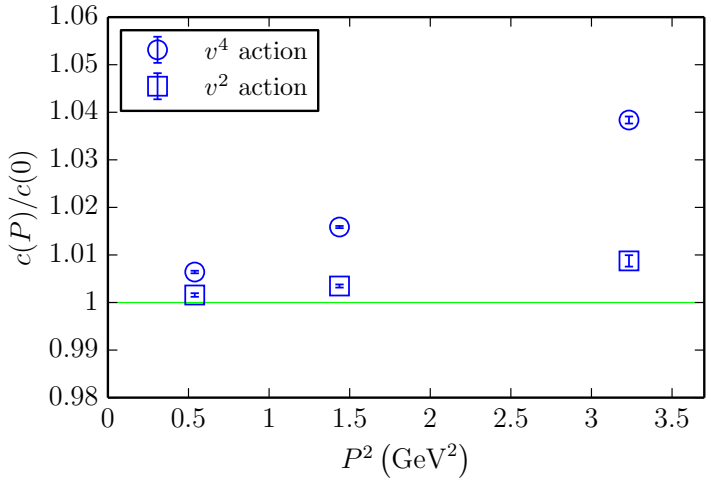

Figure 4.14: The ratios of the zero momentum amplitudes and amplitudes for mesons with momentum P from the leading current plotted against P^2 in GeV^2 for the η_b, comparing the effect of the v^4 action given in eq 3.30 with the action when only v^2 terms are included. Points are shown for the coarse ensemble. The green line shows the expected relativistic behaviour, which for the η_b is a constant.

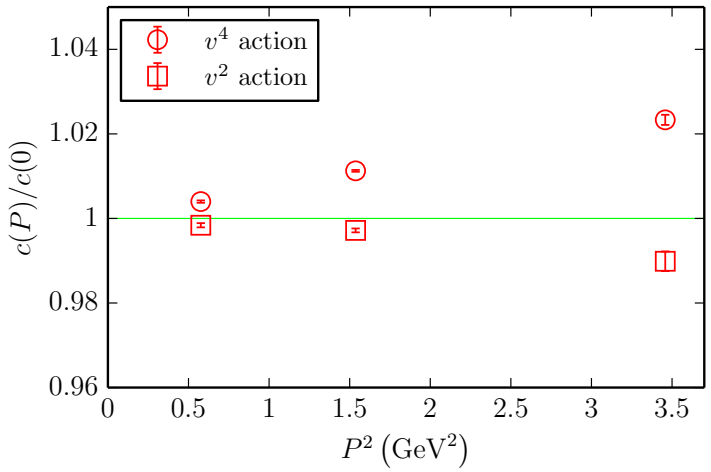

Figure 4.15: The ratios of the zero momentum amplitudes and amplitudes for mesons with momentum P from the leading current plotted against P^2 in GeV^2 for the η_b, comparing the effect of the v^4 action given in eq 3.30 with the action when only v^2 terms are included. Points are shown for the fine ensembles. The green line shows the expected relativistic behaviour, which for the η_b is a constant.

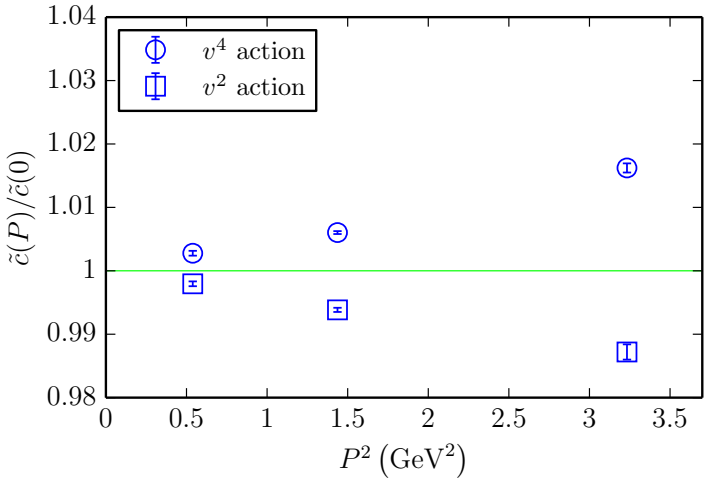

Figure 4.16: The ratios of the zero momentum amplitudes and amplitudes for mesons with momentum P from the leading current plotted against P^2 in GeV^2 for the η_b on set 4 where the factor $\frac{m_b}{E}$ has been included. The points compare the effect of the v^4 action given in eq 3.30 with the action when only v^2 terms are included on the coarse ensemble. The green line shows the expected relativistic behaviour, which for the η_b is a constant.

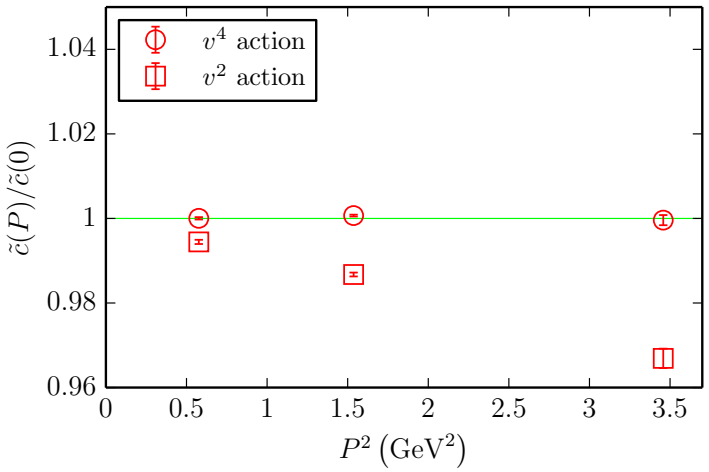

Figure 4.17: The ratios of the zero momentum amplitudes and amplitudes for mesons with momentum P from the leading current plotted against P^2 in GeV^2 for the η_b on set 7 where the factor $\frac{m_b}{E}$ has been included. The points compare the effect of the v^4 action given in eq 3.30 with the action when only v^2 terms are included on the fine ensemble. The green line shows the expected relativistic behaviour, which for the η_b is a constant.

However, it is more convenient to initially determine the hadronic parameter f_Υ – known as the decay constant – as it relates to the matrix element for creating an Υ by,

$$\langle 0|J_{V,i}|\Upsilon_j^{(n)}\rangle = f_{\Upsilon^{(n)}} M_{\Upsilon^{(n)}} \delta_{ij} \tag{4.22}$$

for polarisation j and vector current $J_{V,i}$. f_Υ is then related to the leptonic width by,

$$\Gamma\left(\Upsilon^{(n)} \to e^+e^-\right) = \frac{4\pi}{3}\alpha_{\mathrm{QCD}}^2 e_b^2 \frac{f^2_{\Upsilon^{(n)}}}{M_{\Upsilon^{(n)}}}. \tag{4.23}$$

The starting point to the calculation of these quantities is to match our NRQCD vector currents to QCD. Before we proceed to the matching procedure it is useful here to discuss the currents used.

4.3.1 Vector Currents

Suitable vector currents have to be calculated in NRQCD which then can be matched to QCD to any desired order. Here they are taken as in [70],

$$\mathbf{J_i} = \sigma \left(\frac{\Delta^2}{m_b^2}\right)^i, \tag{4.24}$$

such that the leading and next to leading currents are,

$$\begin{aligned} \mathbf{J_0} &= \sum_{x;i=1}^{3} \chi_x^\dagger \sigma \Psi_x \\ \mathbf{J_1} &= \sum_{x;i=1}^{3} \chi_x^\dagger \frac{\sigma}{(am_b)^2} \times (\Psi_{x+\hat{\imath}} + \Psi_{x-\hat{\imath}} - 2\Psi_x), \end{aligned} \tag{4.25}$$

where the bold face symbols imply that these are 3-vectors and m_b is the mass of the heavy quark. It should be noted that $\mathbf{J_1}$ is not gauge invariant, due to the absence of the U fields. However, the MILC gauge configurations in these calculations are fixed to Coloumb gauge allowing us to use this form of the current. It is equally possible to use a gauge invariant $\mathbf{J_1}$ where the U fields are included; the effect of which would be to change the coefficient for matching NRQCD to QCD. A method for calculating and matching NRQCD currents to QCD was considered initially and in this case the U fields were included. This alternative procedure and the resulting amplitudes for the leading and subleading currents are given in appendix A.

Matching the QCD matrix elements with the NRQCD matrix elements is done through,

$$\langle 0|\mathbf{J}^{\mathrm{QCD}}|\bar{Q}Q\rangle = \sum_i k_i \langle 0|\mathbf{J}_i|\bar{Q}Q\rangle \tag{4.26}$$

with k_i being the correct matching coefficients. The coefficients can be expanded as a power series in α_s:

$$k_i = \sum_n \alpha_s^n k_i^{(n)}. \tag{4.27}$$

For the Υ at tree level, $k_0^{(0)} = 1$ and $k_1^{(0)} = \frac{1}{6}$ [70].

4.3.2 Temporal Moments

To calculate the hadronic parameter correctly we have to construct an NRQCD vector current of the form,

$$J_V = Z_V J_{V,\mathrm{NRQCD}} \tag{4.28}$$

$$\equiv Z_V (J^{(0)}_{V,\mathrm{NRQCD}} + k_1 J^{(1)}_{V,\mathrm{NRQCD}}), \tag{4.29}$$

where k_1 is the coefficient given in equation 4.27. The vector normalisation factor Z_V can be determined through the matching of the NRQCD currents to continuum QCD perturbation theory current correlators since these are well calculated [71–75]. The method used to do this is similar to that in [76], although in that case a relativistic discretisation of the quark action was used so there are some differences. A determination of both k_1 and Z_V is possible nonperturbatively on the lattice.

Correlators $C_{V,\mathrm{NRQCD}}(t)$ are created using $J_{V,\mathrm{NRQCD}}$ from equation 4.29, which is itself comprised of the currents from equation 4.25 at both the source and the sink. The temporal moments are then defined as [77, 78]

$$G_n^{V,\mathrm{NRQCD}} \equiv 2 \sum_t (t/a)^n \, G^{V,\mathrm{NRQCD}}(t), \tag{4.30}$$

where $G(t)$ is the correlator at lattice time t corrected by an exponential factor,

$$G(t) \equiv C_{V,\mathrm{NRQCD}}(t) e^{(\overline{E_0} - \overline{M}_{\mathrm{kin}})t}. \tag{4.31}$$

The factor is required because of the energy offset in the NRQCD correlators due to the absence of a quark mass term. Its introduction replaces the ground state energy with the kinetic mass. In tuning the b quark mass, the spin averaged kinetic mass of the Υ and η_b, $\overline{M}_{\mathrm{kin}}$, was used, so it is that which is used here along with the spin averaged ground state energy, $\overline{E}_0$. The values used in the calculations are given in table 4.7. For the kinetic mass value, the meson with momentum $aP = (1, 1, 1)$ in units of $2\pi/L$ was used. The

Set	am_b	c_4	$a\overline{M}_{kin}$	$a\overline{E}_0$
1	3.297	1.0	7.087(8)	0.27823(5)
1	3.297	1.22	7.109(10)	0.25137(6)
1	3.42	1.0	7.303(15)	0.27669(5)
2	3.25	1.22	6.988(14)	0.24950(2)
3	2.66	1.0	5.761(14)	0.28458(2)
4	2.62	1.20	5.717(9)	0.25161(2)
5	1.91	1.0	4.264(11)	0.27767(2)

Table 4.7: The spin averaged kinetic masses and spin averaged energies used in the calculations of the temporal moments. The kinetic mass results have been calculated using the zero momentum correlators and those with $aP = (1,1,1) \times 2\pi/L$.

factor of 2 has to be inserted because the NRQCD correlators only propagate forward in time, rather than in both directions since it is an initial value problem with an evolution equation for each time step. The moment numbers $n \geq 4$ and take only even values.

The lattice correlators are related to the continuum correlators through the Z_V renormalisation factor by,

$$G_n^V = Z_V^2 G_n^{V,\mathrm{NRQCD}}, \tag{4.32}$$

up to discretisation and relativistic corrections. The moments in continuum QCD perturbation theory, g_n^V, are known through $\mathcal{O}(\alpha_s^3)$ up to moment $n = 22$ [73] and are derived from q^2-derivative moments of the heavy-quark vacuum polarisation function [77], calculable in perturbation theory [71–75] by,

$$G_n^V = \frac{g_n^V(\alpha_s, \mu/m_b)}{[a\overline{m}_b(\mu)]^{n-2}}. \tag{4.33}$$

A further quantity, the reduced moment, can be used to reduce errors from discretisation effects and from the tuning of the b quark. These are defined by,

$$\begin{aligned} R_n^V &\equiv G_n^V / G_n^{V,(0)} \\ &= r_n^V(\alpha_{\overline{\mathrm{MS}}}, \mu/m_b) \left[\frac{m_b}{\overline{m}_b(\mu)}\right] \end{aligned} \tag{4.34}$$

where $G_n^{V,(0)}$ are free moments,

$$G_n^{V,(0)} = 2\sum (t/a)^n C_{V,\mathrm{NRQCD},U=1}(t) e^{-2m_b t}, \tag{4.35}$$

n	$r_n^{(1)}$	$r_n^{(2)}$	$r_n^{(3)}$
4	0.7623	0.2750	-0.2347
6	0.7727	0.7190	-0.1865
8	0.6102	0.7990	-0.1398
10	0.3500	0.7170	-0.2420
12	0.0248	0.5907	-0.4147
14	-0.3475	0.5018	-0.5806
16	-0.7563	0.5096	-0.6972
18	-1.1935	0.6618	-0.7592
20	-1.6550	0.9958	-0.7894
22	-2.1360	1.5433	-0.8546

Table 4.8: Coefficients of the perturbative series $r_n^V = 1 + \sum_i r_n^{(i)} \alpha_s(\mu)$ for $\mu = \overline{m}_b(\mu)$. Results are taken from [71–75] using four light quarks in the sea and no heavy quarks, i.e. $n_l = 4$ and $n_h = 0$, except for $r_n^{(3)}$, which uses $n_l = 4$ and $n_h = 1$, as in [73].

where the U fields are set to the unit matrix in color space and all coefficients, c_i, are set to their tree level values of 1. The energy offset here is just twice m_b. r_n^V are reduced moments in continuum QCD perturbation theory, which is the ratio of the continuum moment g_n^V to the leading zeroth order coefficient. The ratio $m_b/\overline{m}_b$ is that of the NRQCD b quark mass to that in the $\overline{\rm MS}$ scheme.

The values for the perturbative coefficients for the perturbation series r_n^V are given in table 4.8 for values up to $\mathcal{O}(\alpha_s^3)$. α_s is determined using scale $\mu = m_b$ and $\alpha_{\overline{\rm MS}}(n_f = 4, m_b) = 0.2268(24)$ [1].

The quark mass can be cancelled by taking ratios with different moments to get Z_V such as,

$$Z_V = \left(\frac{G_n^V}{G_n^{V,(0)} r_n^V} \right)^{\frac{(n'-2)}{2(n-n')}} \left(\frac{G_{n'}^{V,(0)} r_{n'}^V}{G_{n'}^V} \right)^{\frac{(n-2)}{2(n-n')}}, \tag{4.36}$$

where we have simply taken $n' = n + 2$.

This matching has to be done for each lattice ensemble where a normalisation factor is determined for each moment number, n. Since a nonrelativistic discretisation of the quark action is being used, we are only matching to a finite order in a relativistic expansion, and so as well as discretisation errors, there are also relativistic errors that cannot be

untangled, therefore we cannot actually simply take a value of Z_V from a single moment number. In contrast, when matching using a relativistic treatment, Z_V from any moment number can be used since the errors are purely from discretisation effects, and in the continuum limit must disappear [76].

However, we can make a sensible choice of Z_V by first realising that at low moments, the low time behaviour of the current-current correlators are emphasised and so are more sensitive than the higher moments to higher internal spatial momentum [78].

At leading relativistic order, by multiplying the free quark and antiquark propagators together, the moments for the pseudoscalar or vector are,

$$G_n = 4 \int \mathrm{d}^4x\, t^n \int \frac{\mathrm{d}E_1 \mathrm{d}^3p_1}{(2\pi)^4} \frac{\mathrm{d}E_2 \mathrm{d}^3p_2}{(2\pi)^4} \frac{e^{-2mt} e^{i(E_1+E_2)t} e^{i(\mathbf{p_1}+\mathbf{p_2})\cdot\mathbf{x}}}{(iE_1 + p_1^2/2m)(iE_2 + p_2^2/2m)} \tag{4.37}$$

for quark mass m and moment number n. After integrating over $\mathbf{x}$ and $\mathbf{p}$ we get,

$$G_n = 4 \int \mathrm{d}t\, t^n \Theta(t) e^{-2mt} \int \frac{\mathrm{d}^3p}{(2\pi)^3} e^{(-p^2/m)t}, \tag{4.38}$$

where $\Theta(t)$ is the Heaviside step function. The contribution to the integral as a function of the square of the heavy quark velocity in the quark-antiquark pair, v^2, can be looked at after integrating over t. This gives,

$$G_n = \frac{n!}{\pi^2 2^{n+1} m^{n-2}} \int \frac{(v^2)^{1/2} \mathrm{d}(v^2)}{(1 + v^2/2)^{n+1}}. \tag{4.39}$$

The integrand here peaks when $v^2 = 1/(n + 1/2)$, getting smaller – as expected – as the moment number n increases.

In practice, this means that when this matching is done, a plot of the renormalisation constant Z_V against moment number n should show a plateau region indicating that the errors from the discretisation and relativistic effects have become small when compared with the missing higher order terms in the perturbation theory expansion of α_s.

Figures 4.18 to 4.20 show values of Z_V as determined using equation 4.36 for the leading current, $J^{(0)}_{V,\mathrm{NRQCD}}$. Notice that only the fine ensemble shows a reasonable plateau from which a Z_V can be extracted. On all of the ensembles, the matching to the low moments, which are more relativistic, varies significantly over the range of moments.

Figures 4.21 to 4.25 show the values for Z_V on each of the ensembles with the current $J^{(0)}_{V,\mathrm{NRQCD}} + k_1 J^{(1)}_{V,\mathrm{NRQCD}}$ using the tree level value of $k_1 = 1/6$. These moments are calculated from correlators that were constructed using point sources, where the correction of

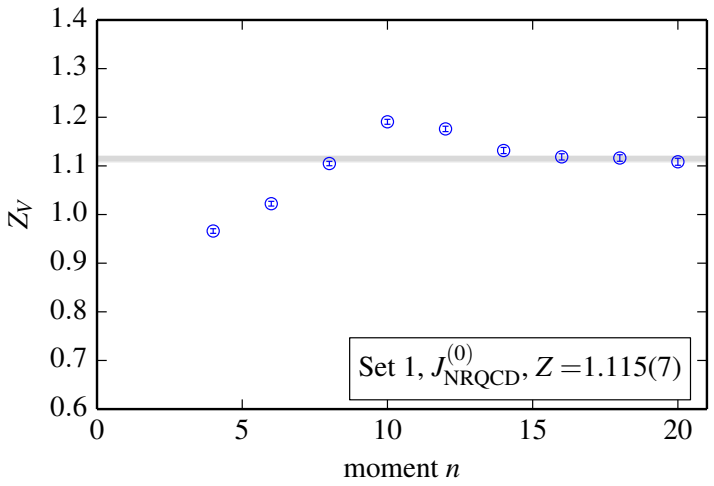

Figure 4.18: Values of Z_V for the leading current J_0 on the very coarse $m_l/m_s = 0.2$ ensemble. The band is the average value of Z between $n = 16$ and $n = 20$.

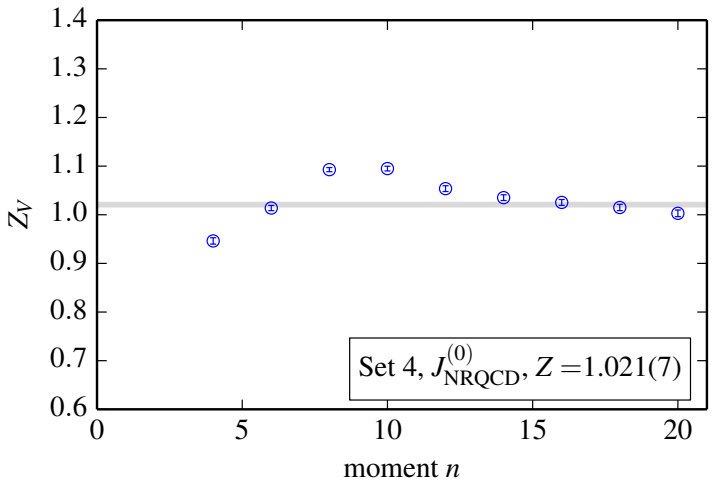

Figure 4.19: Values of Z_V for the leading current J_0 on the coarse $m_l/m_s = 0.2$ ensemble. The band is the average value of Z between $n = 16$ and $n = 18$.

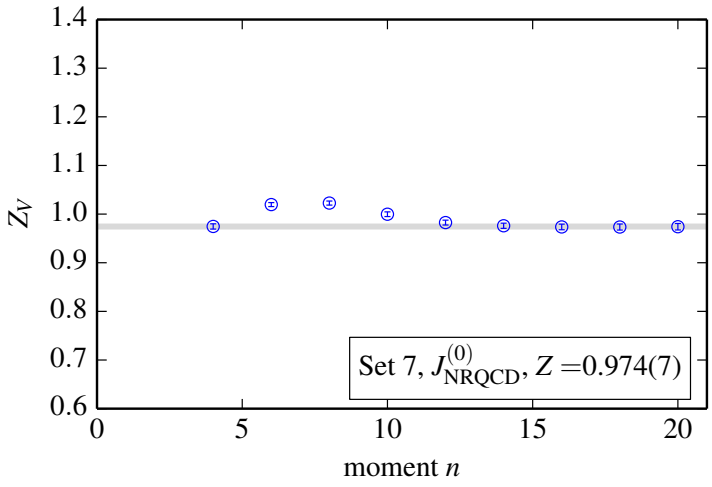

Figure 4.20: Values of Z_V for the leading current J_0 on the fine $m_l/m_s = 0.2$ ensemble. The band is the average value of Z between $n = 14$ and $n = 20$.

equation 4.25 were applied at both the source and the sink. This is also the way in which the free moments were constructed, but since there are no $\mathcal{O}(\alpha_s)$ terms in this case, the coefficients c_i in the action and the tadpole improvement parameter u_{0L} are set to 1.

By the addition of the current correction term $J^{(1)}_{V,\rm NRQCD}$ at tree level, the values of Z_V do not improve noticibly for most of the lattice ensembles. Although clearly the fine ensemble, set 7, shows a better plateau for low values of the moments than do the very coarse and coarse ensembles, which implies that the tree level coefficient for the $J^{(1)}_{V,\rm NRQCD}$ current, k_1, is more closely tuned for this ensemble.

To get the final value of Z_V we vary k_1 to give a better plateau and can achieve this down to moments of $n = 10$. The value of $k_1^{(0)}$, i.e. the tree level coefficient, is kept at $1/6$ for the free moments as they have no $\mathcal{O}(\alpha_s)$ terms included.

The central value chosen for k_1 is that which minimises the χ^2 value in a fit between $n = 10$ and $n = 20$ on each ensemble. Plots showing each of the Z_V values on each ensemble are shown in figures 4.26 to 4.30. With the tuned value of k_1 it is now possible to get reasonable plateaus on each one of the ensembles.

Table 4.9 gives these tuned values for the k_1 and the corresponding Z_V on each of the ensembles used, plus additional results on set 1 where the $\mathcal{O}(\alpha_s)$ value of $c_4 = 1.22$ is used and for the case where the b quark is mistuned to give estimates for the errors from these effects. The error on k_1 was obtained by varying its value until $\Delta\chi^2 = 1$ in each of the

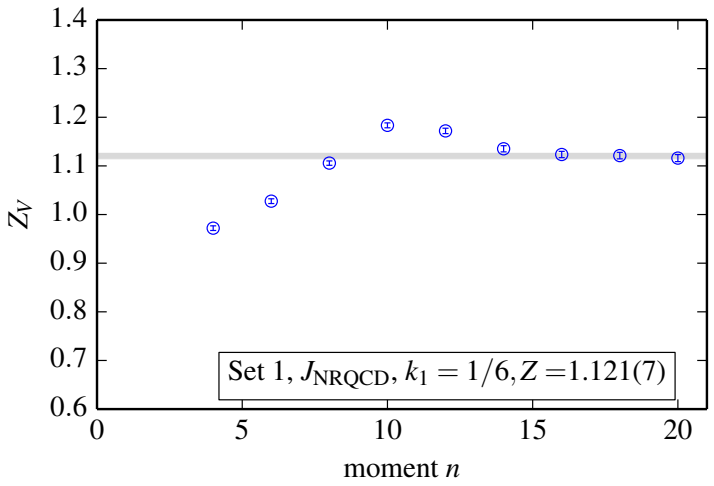

Figure 4.21: Values of Z_V for the leading current J_0 on the very coarse $m_l/m_s = 0.2$ ensemble. The band is the average value of Z between $n = 16$ and $n = 20$.

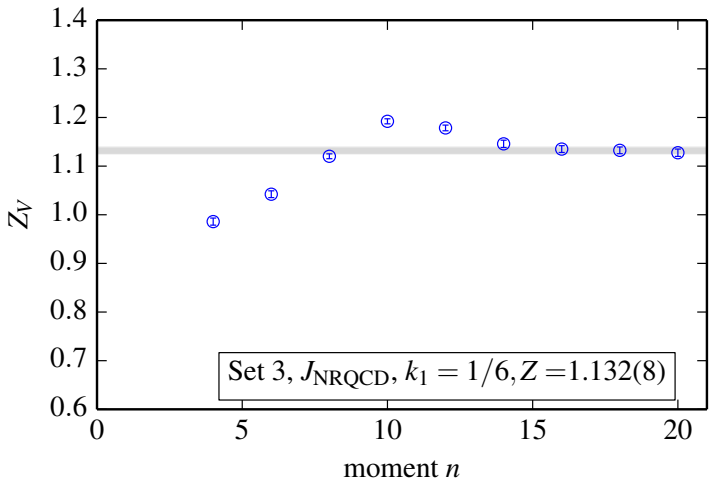

Figure 4.22: Values of Z_V for the leading current J_0 on the very coarse ensemble with physical m_l. The band is the average value of Z between $n = 16$ and $n = 20$.

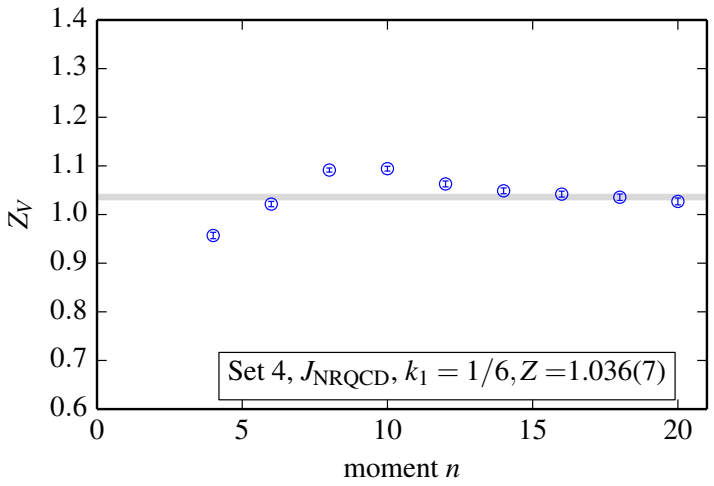

Figure 4.23: Values of Z_V for the leading current J_0 on the coarse $m_l/m_s = 0.2$ ensemble. The band is the average value of Z between $n = 16$ and $n = 20$.

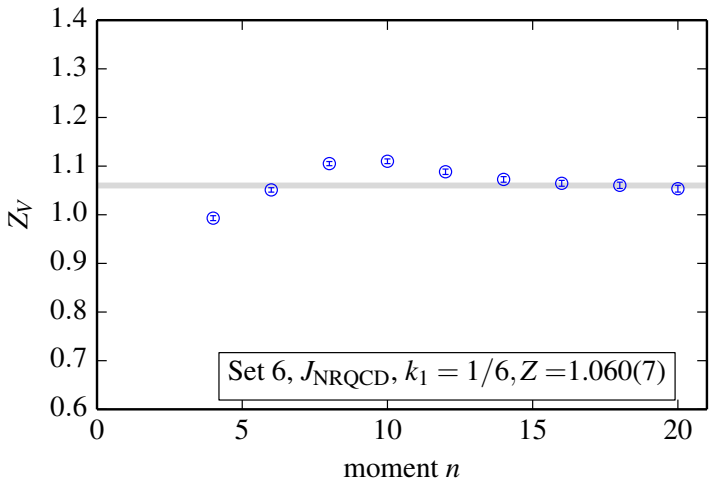

Figure 4.24: Values of Z_V for the leading current J_0 on the coarse ensemble with physical m_l. The band is the average value of Z between $n = 16$ and $n = 20$.

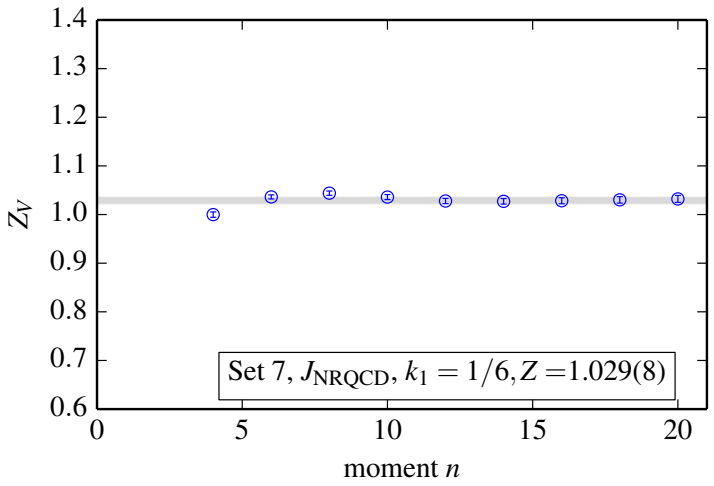

Figure 4.25: Values of Z_V for the leading current J_0 on the fine $m_l/m_s = 0.2$ ensemble. The band is the average value of Z between $n = 14$ and $n = 20$.

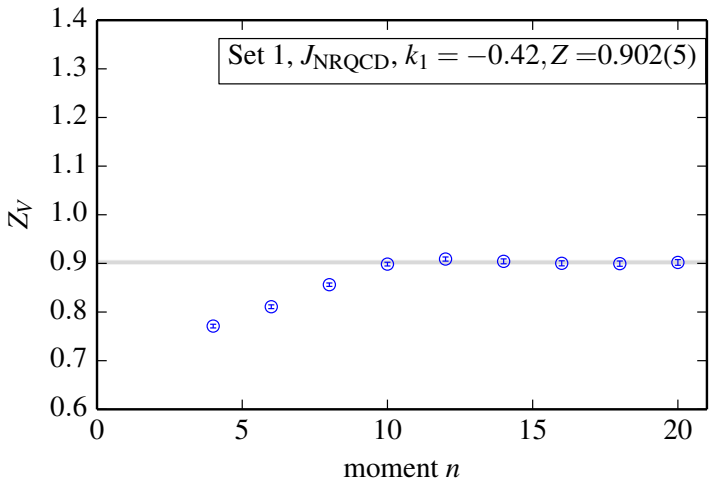

Figure 4.26: Values of Z_V for $J_0 + k_1 J_1$ on the very coarse $m_l/m_s = 0.2$ ensemble. The band is the average value of Z between $n = 10$ and $n = 20$.

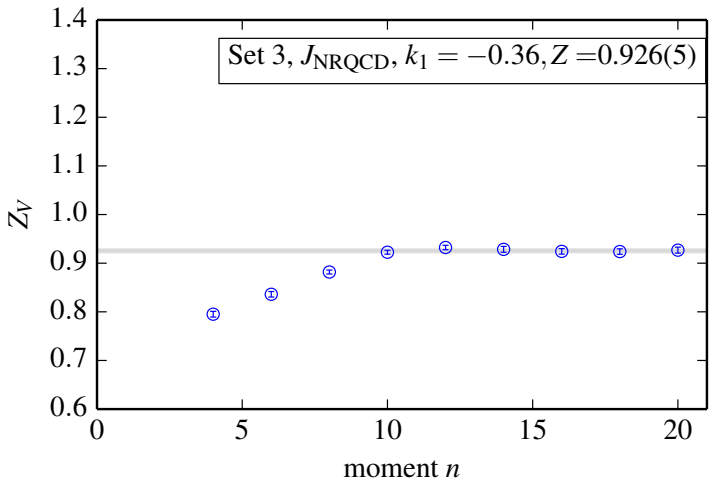

Figure 4.27: Values of Z_V for $J_0 + k_1 J_1$ on the very coarse ensemble with physical m_l. The band is the average value of Z between $n = 10$ and $n = 20$.

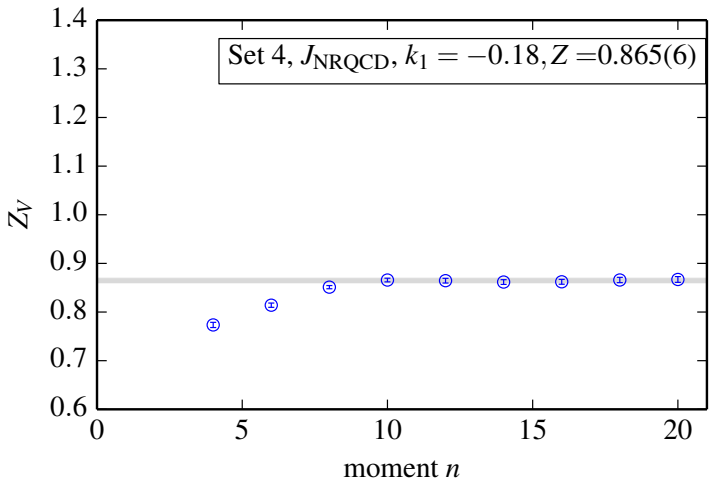

Figure 4.28: Values of Z_V for $J_0 + k_1 J_1$ on the coarse $m_l/m_s = 0.2$ ensemble. The band is the average value of Z between $n = 10$ and $n = 20$.

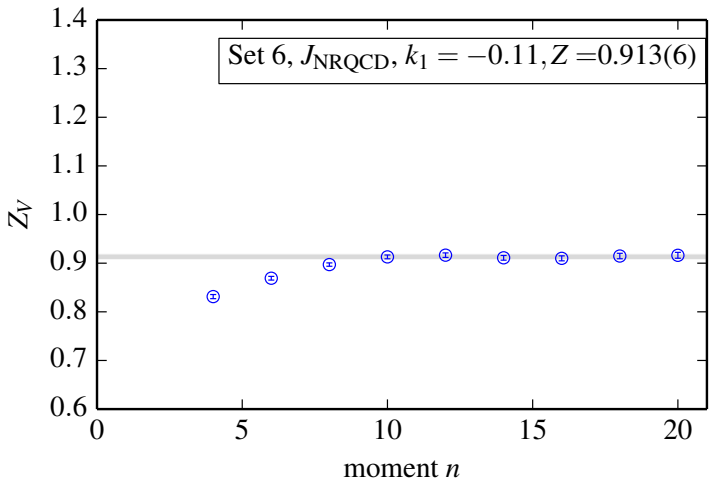

Figure 4.29: Values of Z_V for $J_0 + k_1 J_1$ on the coarse ensemble with physical m_l. The band is the average value of Z between $n = 10$ and $n = 20$.

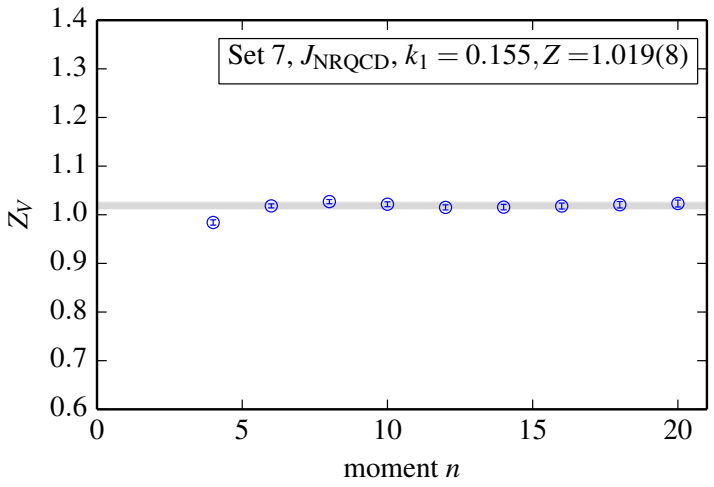

Figure 4.30: Values of Z_V for $J_0 + k_1 J_1$ on the fine $m_l/m_s = 0.2$ ensemble. The band is the average value of Z between $n = 10$ and $n = 20$.

Set	m_b	c_4	k_1	Z_V
1	3.297	1.0	-0.42(16)	0.902(5)(58)
1	3.297	1.22	-0.29(15)	0.963(5)(60)
1	3.42	1.0	-0.52(20)	0.890(5)(67)
3	3.25	1.22	-0.36(16)	0.926(5)(62)
4	2.66	1.0	-0.18(10)	0.865(6)(59)
6	2.62	1.20	-0.11(9)	0.913(6)(50)
7	1.91	1.0	0.155(35)	1.019(8)(35)

Table 4.9: The tuned values of k_1 on each of the ensembles and the corresponding values of Z_V. The two errors on Z_V correspond to the error on the central value of k_1 which arise due to the truncation errors in matching lattice NRQCD to perturbation theory, and from the error in k_1, respectively. The second error in Z_V is correlated with that uncertainty in k_1, making Z_V increase as k_1 increases.

fits. There are two errors quoted for Z_V: the first error is the error on the central value that comes from the truncation errors from matching to perturbation theory to a finite order, and the second – which dominates the overall error – is a result of the correlated error on k_1.

4.3.3 Υ Decay Constant and Leptonic Width

Having values for the Υ matching factor Z_V, it is now possible to make a determination of the decay constant f_Υ from which we can subsequently determine the leptonic width. To do this, correlators that correspond to $J^{(0)}_{V,\mathrm{NRQCD}} + k_1 J^{(1)}_{V,\mathrm{NRQCD}}$ with k_1 set to the values given in table 4.9 are constructed and fit using the usual Bayesian fit procedure to extract the ground state amplitude.

Our ground state amplitude relates to the matrix element between the Υ and the vacuum by,

$$c(J^{(0)}_{V,\mathrm{NRQCD}}, 0) = \frac{\langle 0|J|\Upsilon\rangle}{\sqrt{2M_\Upsilon}}. \tag{4.40}$$

Using equation 4.22, the value of $f_\Upsilon\sqrt{M_\Upsilon}$ in lattice units is obtained from the fit by taking the ground state amplitude and multiplying this by $\sqrt{2}$. Additionally, it must be multiplied by the matching factor Z_V so that it matches QCD.

Set	am_b	c_4	$c(J^{(0)}_{V,\mathrm{NRQCD}},0)$	$c(J^{(1)}_{V,\mathrm{NRQCD}},0)$	$a^{3/2}f_\Upsilon\sqrt{M_\Upsilon}$
1	3.297	1.0	0.9422(22)	-0.2439(6)	1.334(4)(33)
1	3.297	1.22	0.9194(24)	-0.2355(7)	1.346(4)(34)
1	3.42	1.0	0.9695(23)	-0.2373(6)	1.376(4)(40)
3	3.25	1.22	0.9087(21)	-0.2371(6)	1.304(3)(35)
4	2.66	1.0	0.7153(17)	-0.2360(6)	0.929(2)(26)
6	2.62	1.20	0.6821(18)	-0.2268(6)	0.914(3)(23)
7	1.91	1.0	0.4523(8)	-0.2109(4)	0.604(1)(11)

Table 4.10: The amplitudes for the ground state Υ where the $J^{(0)}_{V,\mathrm{NRQCD}}$ and $J^{(1)}_{V,\mathrm{NRQCD}}$ pieces have been separated and the value of $f_\Upsilon\sqrt{M_\Upsilon}$ from a fit to a set of single $J_{V,\mathrm{NRQCD}}$ correlators constructed with the appropiate values of k_1 taken from table 4.9.

The results here were determined by constructing complete correlators with the appropriate k_1 values and fitting those to get the ground state amplitude, but a 2×2 fit of the correlators was done to determine the $J^{(0)}_{V,\mathrm{NRQCD}}$ and $J^{(1)}_{V,\mathrm{NRQCD}}$ current amplitudes also. The values of these amplitudes and the values for $f_\Upsilon\sqrt{M_\Upsilon}$ from the fully constructed correlators are given in table 4.10. The first error quoted is a statistical error from the fitting of the central value and the second is the error from the renormalisation factor Z_V.

We have not yet explored the nonperturbative determination of renormalisation factor Z_P for matching of the pseudoscalar η_b NRQCD and QCD currents, but for completeness the amplitudes from the relevant currents $J^{(0)}_{P,\mathrm{NRQCD}}$ and $J^{(1)}_{P,\mathrm{NRQCD}}$ are given in table 4.11.

To compare to experiment, the values of $f_\Upsilon\sqrt{M_\Upsilon}$ are converted to physical units using the lattice spacings as given in table 2.1 and plotted against the square of the lattice spacing in figure 4.31. It is clear that there is little dependence on the lattice spacing or the sea quark mass.

As can be seen from the value where the c_4 coefficient on set 1 is set to 1.22, this coefficient has a negligible effect on the calculation. On the other hand, the value for the mistuned b quark mass ($m_b = 3.42$) has a noticeable effect which can be used to estimate errors coming from the tuning.

The lattice values must be fitted to a function of lattice spacing and sea quark mass in order to obtain a physical result. The method that is used is one used previously [18],

Set	m_b	c_4	$c(J^{(0)}_{\eta_b}, 0)$	$c(J^{(1)}_{\eta_b}, 0)$
1	3.297	1.0	1.0201(22)	-0.2843(6)
1	3.297	1.22	1.0293(23)	-0.2928(7)
1	3.42	1.0	1.0439(23)	-0.2736(6)
3	3.25	1.22	1.0232(17)	-0.2977(5)
4	2.66	1.0	0.8036(15)	-0.2977(6)
6	2.62	1.20	0.8034(15)	-0.3143(6)
7	1.91	1.0	0.5453(9)	-0.3186(7)

Table 4.11: Amplitudes for the leading current, $J^{(0)}_{\rm NRQCD}$, and next-to-leading current, $J^{(1)}_{\rm NRQCD}$, for the η_b on lattice ensembles with $m_l/m_s = 0.2$ and ensembles with physical light quarks, with zero meson momentum.

which takes into account discretisation errors coming from the gluon or light quark actions and also includes pieces that account for higher order discretisation errors in the NRQCD action that might depend on am_b. The form of the fit is

$$h(a, m_{sea}) = h_{\rm phys}[1 + b_l \delta m_{\rm sea}/(10m_s) + \sum_{j=1,3} c_j (a\Lambda)^{2j} + \sum_{j=1,2} (a\Lambda)^{2j} (c_{jb}\delta x_m + c_{jbb}(\delta x_m)^2)] \quad (4.41)$$

where h is the hadronic parameter we are interested in, which is $f_\Upsilon\sqrt{M_\Upsilon}$ in this case. The second term in square brackets is used to account for the effect of the sea quark masses in the lattice calculations, which is expected to follow a linear dependence at leading order. The value of $\delta m_{\rm sea}$ is the difference between twice the light quark mass plus the strange quark mass and the physical value of this. The physical values of the strange quark masses using the lattice spacings given in table 2.1 are given in [18]. The mass of the physical light quarks are taken to be $m_s/27.5$ [1]. The denominator – $10m_s$ – is used to introduce the chiral scale of 1 GeV. The third term in the fit function is for standard discretisation effects where we use the scale $\Lambda = 500$ MeV. The terms containing δx_m are those that deal with the discretisation effects that have some dependence on the b quark mass in the NRQCD action. To do this, δx_m is taken as $\delta x_m = (am_b - 2.7)/1.5$ so that it varies from -0.5 to 0.5 across the range of masses used and can then be fit with linear and quadratic terms.

This fit function uses a Bayesian fit approach like that described earlier where all priors for the coefficients are taken as 0.0(1.0) except for c_1 which has a prior of 0.0(0.5) since we expect the value here to be no more than $\mathcal{O}(\alpha_s)$. The width of the prior for $h_{\rm phys}$ is taken as 50%.

Performing this fit we get the result $f_\Upsilon\sqrt{M_\Upsilon} = 0.1995(90)$ GeV$^{3/2}$. To the error quoted here, some additional systematic errors that have not yet been included must be considered:

- missing higher order terms in the correction to the NRQCD current of $\mathcal{O}(v^4)$, estimated as 1%, using $v_\Upsilon^2 = 0.1$;
- mistuning of the b quark which mostly comes from the error in the determination of the lattice spacing. Using the results on set 1 and comparing the values for $am_b = 3.297$ and $am_b = 3.42$ this leads to an error of 1%;
- the lack of electromagnetic effects in our calculation mean these now have to be included. However, they are small and estimated from a potential model for quark and antiquark attraction gives an estimate of 0.2% on the decay constant [79];
- missing effects of having a b quark in the sea. This has a negligible effect [80], but b quarks in the sea results in a short-distance potential between heavy quarks [79].

Including these errors on the value gives a result of $f_\Upsilon\sqrt{M_\Upsilon} = 0.1995(94)$, shown as the grey band on figure 4.31. The majority of the error comes from the determination of the lattice spacing and from the error in Z_V. This is in good agreement with the experimental value of $f_\Upsilon\sqrt{M_\Upsilon} = 2.119(14)$ GeV$^{3/2}$ ($f_\Upsilon = 0.689(5)$ GeV) – within 1.5σ – also shown on the plot, which uses the value of leptonic width of 1.340(18) keV [1] and equation 4.23. Using the experimental value of M_Υ, this gives a final value for the Υ decay constant of

$$f_\Upsilon = 0.649(31) \text{ GeV}. \tag{4.42}$$

Using equation 4.23, this gives a result for the leptonic width of

$$\Gamma(\Upsilon \to e^+e^-) = 1.19(11) \text{ keV}, \tag{4.43}$$

again in good agreement with the result from experiment.

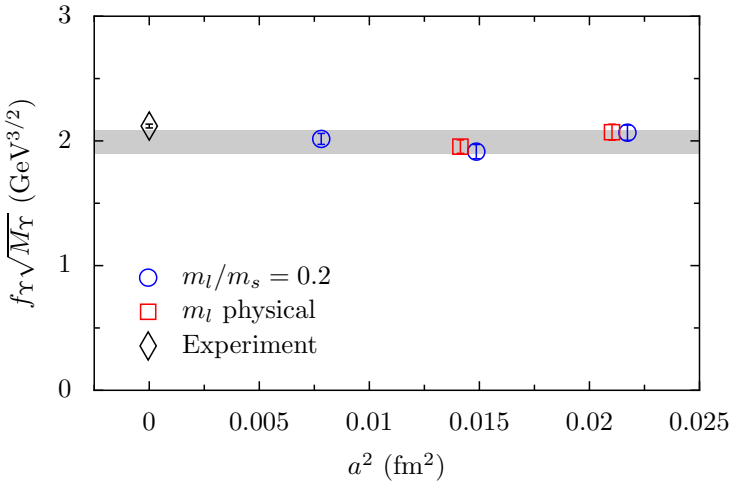

Figure 4.31: Decay constants for the Υ using the vector current $J_0 + k_1 J_1$. Shown are points for the ensembles where $m_l/m_s = 0.2$ and those with physical light quarks. The grey band shows the physical value obtained from a fit to these points with all errors included.

4.3.4 The Υ' Leptonic Width

Using the same correlators as before, it is also possible to get a result for the leptonic width of the first excited vector bottomonium state, the Υ'. This requires the ability to access results for the excited states in the correlator fits, which is not possible when using *only* point source correlators like those used in the preceding results. Instead a matrix fit to various smearing combinations must be carried out since, as described in section 3.4.1, different smearings exhibit different behaviour at low values of t so excited states can be accessed and amplitudes can be separated out.

Uncertainties from Z_V, the lattice spacing and tuning uncertainties can be reduced by calculating the ratio of the excited to the ground state amplitudes as

$$A = \frac{\langle 0|J_V|\Upsilon'\rangle}{\langle 0|J_V|\Upsilon\rangle} = \frac{f_{\Upsilon'}}{f_\Upsilon}\sqrt{\frac{M_{\Upsilon'}}{M_\Upsilon}} \tag{4.44}$$

from which the Υ' decay constant and leptonic width can be extracted using the previously calculated values for the Υ. This is a useful procedure because the matching factor Z_V cancels, and it was from this that a large portion of the error arose in the calculation of the Υ leptonic width.

We used a 3×3 fit to Υ correlators using a point source for the local operator $J^{(0)}_{V,\mathrm{NRQCD}}$, labelled l, generated with a random wall source and hydrogen-like smearings that we give

labels gs and es for ground and excited states [18],

$$\phi_l(r) = \delta_{r,0} \tag{4.45}$$

$$\phi_{gs}(r) = \exp(-r/a_{\rm sm}) \tag{4.46}$$

$$\phi_{es}(r) = (2a_{\rm sm} - r)\exp(-r/a_{\rm sm}), \tag{4.47}$$

where $a_{\rm sm}$ is the radius of the smearing. These were chosen so as to project onto different radially excited states and have been shown to work well [60].

Simultaneously, the correlators including the $J^{(1)}_{V,\rm NRQCD}$ piece of the current is included in the fit, which allows access to the ground state and first excited state of both parts of the amplitude required. Errors quickly grow, so only results up to and including the first excited state give good statistical accuracy. Since here we required ensembles with a random wall source in order to increase statistics, only sets 1, 4, and 7 have been used since they had the matrix of correlators available as described in [18]. Additionally, set 1 uses the mistuned value of $am_b = 3.42$, which is thus mistuned by 4%, but we do not expect this to make a big difference to the ratio.

Again, the prior on the energy difference is set to be 600 ± 300 MeV and the amplitude prior is set as 0.1 ± 1.0, which amounts to a width of 3 to 5 times the ground state amplitude.

The results for the matrix elements on each of the ensembles are given in table 4.12. Also given are the values for the ratio A calculated using the values of k_1 given in table 4.9. Figure 4.32 shows points for A plotted against the square of the lattice spacing. The grey band is the physical value as determined using a fit to the function given in equation 4.41, where this time the hadronic parameter is the ratio, A. The priors are the same as before, 0.0(1.0), this time including the c_1 term as this has been increased in this case since there is a clear strong dependence on a^2. We do not have much information for sea quark mass dependence since we are using ensembles with similar masses for the light sea quarks, but nevertheless we include sea quark mass dependent terms in our fit as before. The error coming from the sea quark masses in the fit contributes 3.5% of the overall error on the ratio.

The fitted value of the physical result shown as the grey band in the plot is determined to be 0.762(50). The only source of systematic error that is added to this is a 1% error from missing $\mathcal{O}(v^4)$ terms in the NRQCD vector current, giving a final result of 0.762(51).

	1	3	5
am_b	3.42	2.66	1.91
$c(J^{(0)},0)$	0.9720(2)	0.7160(1)	0.4523(1)
$c(J^{(1)},0)$	-0.2376(1)	-0.2362(1)	-0.2109(1)
$c(J^{(0)},1)$	0.791(8)	0.570(8)	0.360(2)
$c(J^{(1)},1)$	-0.277(4)	-0.261(5)	-0.225(1)
A	0.854(16)	0.813(14)	0.774(7)

Table 4.12: Amplitudes for the operators corresponding to the leading ($J^{(0)}$) and next-to-leading ($J^{(1)}$) pieces of the NRQCD vector current for both the Υ and Υ' mesons taken from a 3×3 matrix fit of correlators with various smearing combinations. A is the ratio given in equation 4.44. The error on A includes the error from the uncertainty in k_1. Results are on sets 1 (with $am_b = 3.42$), 4 and 7.

The reason that this is the only additional error is because, as mentioned, the other sources of error should cancel in the ratio.

The black diamond on the plot is the experimental value, calculated using their leptonic widths to leptons and masses from [1] and using equation 4.23. This gives an experimental value of $A_{\text{expt}} = 0.716(8)$, which agrees with our calculation, although the lattice QCD value is a lot less accurate.

Using the value of the Υ decay constant and converting to physical units, this gives a value for $f_{\Upsilon'}$ of

$$f_{\Upsilon'} = 0.481(39) \text{ GeV}, \tag{4.48}$$

which is in good agreement with the experimental value of 0.479(4) GeV. Translating this into the leptonic width value, this gives

$$\Gamma(\Upsilon \to e^+e^-) = 0.69(9) \text{ keV}, \tag{4.49}$$

again in good agreement with the experimental value of 0.612(11) GeV [1].

The results presented here are summarised along with other determinations of other decay constants in figure 4.33.

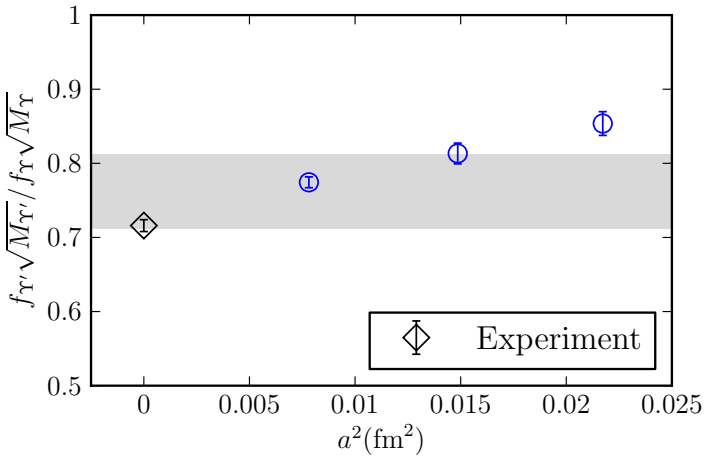

Figure 4.32: The ratio of the hadronic parameters $f\sqrt{M}$ for the Υ' to the Υ. The blue points are the results taken from sets 1, 4 and 7 where a random wall source was used and the next-to-leading order current $J^{(1)}_{V,\mathrm{NRQCD}}$ was generated at the sink. The black diamond is the result from the experimental leptonic widths, calculated using equation 4.21. The grey band gives our final fitted result with all errors included.

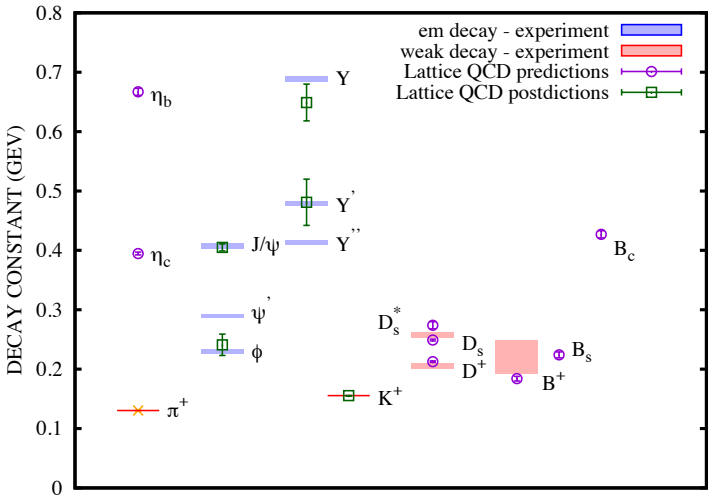

Figure 4.33: Summary of the decay constants for various mesons including the new results for the Υ and Υ'.

Set	am_b	c_4	$n=4$	$n=6$	$n=8$	$n=10$
1	3.297	1.0	0.0492(6)	0.193(2)	0.307(3)	0.399(4)
1	3.297	1.22	0.0487(6)	0.192(2)	0.306(3)	0.398(4)
1	3.42	1.0	0.0453(6)	0.185(2)	0.299(3)	0.387(4)
3	3.25	1.22	0.0500(7)	0.193(2)	0.306(3)	0.397(4)
4	2.66	1.0	0.0643(8)	0.203(2)	0.308(3)	0.401(4)
6	2.62	1.20	0.0635(7)	0.200(2)	0.302(2)	0.393(3)
7	1.91	1.0	0.0755(9)	0.198(2)	0.297(2)	0.391(3)

Table 4.13: Values for $(G_n)^{1/(n-2)}$ where they all have dimension GeV^{-1} for $n = 4$, 6, 8 and 10 for each ensemble. Values are also included for the $\mathcal{O}(\alpha_s)$ c_4 coefficient on set 1, plus the mistuned value of $am_b = 3.42$. Errors are from statistics, Z_V, k_1 and the determination of the lattice spacing.

4.3.5 $R_{e^+e^-}$

The low lattice time moments discussed in the section 4.3.2 can themselves be compared to the experimental values. We do this for $n = 4, 6, 8, 10$ after converting our results to $(G_n^V)^{1/n-2}$ so that they are all in the same dimension of GeV^{-1}. These results are presented in table 4.13 for each of the ensembles used, including two additional set 1 determinations where in one case the $\mathcal{O}(\alpha_s)$ value of c_4 is used and in the other, the b quark is at the mistuned value of $am_b = 3.42$.

The results for our chosen values of k_1 are shown in figure 4.34 against the square of the lattice spacing. The errors on the points come from the uncertainty in k_1, Z_V and from the lattice spacing.

To get a physical result, we again fit to the form given in equation 4.41 with the same priors as for the determination of $f_\Upsilon\sqrt{M_\Upsilon}$, i.e. 0.0(1.0), except for $n = 4$ where the prior on the c_1 coefficient is set to 0.0(3.0) due to the large dependency on the lattice spacing. This large dependency can be seen in figure 4.34 for $n = 4$, and this is expected as the spatial momenta at such a low moment is high.

Each of the moments are fitted separately and to each additional systematic errors again must be included from various sources:

- missing relativistic effects from the vector currents at $\mathcal{O}(v^4)$. These are estimated

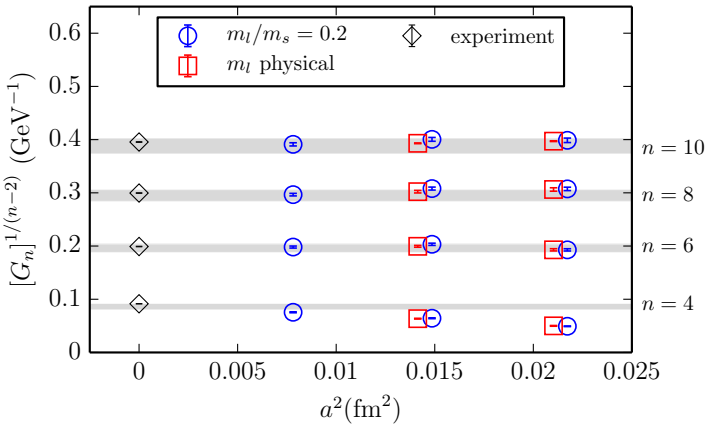

Figure 4.34: Fit results for the moments as calculated on the lattice using NRQCD, converted to GeV^{-1}. Results here are for the moments $n = 4$ to $n = 10$. The blue points are the lattice values for each moment on sets 1, 4, and 7 where $m_l/m_s = 0.2$ and the red points are those with physical light quark masses: sets 3 and 6. The black diamonds show the q^2 derivative moments of the b quark vacuum polarisation determined using experimental values for $R_{e^+e^-}$ in continuum QCD perturbation theory. The grey band shows the physical result from a fit to the data.

to be $v^2 \approx 1/n$. This can be tested by comparing the results of the moments with and without the $J^{(1)}_{V,\mathrm{NRQCD}}$ piece included in the currents. The result is to give errors slightly larger than those in this naive estimate, and for each moment on the fine ensemble, set 7 we get: $n = 4 : 25\%$, $n = 6 : 22\%$, $n = 8 : 18\%$ and $n = 10 : 15\%$. To get an estimate of the errors at $\mathcal{O}(v^4)$ we square these values, giving: $n = 4 : 6\%$, $n = 6 : 4\%$, $n = 8 : 3\%$ and $n = 10 : 2\%$. After taking the $1/(n-2)$th root, this gives the final additional uncertainty from missing $\mathcal{O}(v^4)$ corrections as $n = 4 : 3\%$, $n = 6 : 1\%$, $n = 8 : 0.5\%$ and $n = 10 : 0.4\%$.

- the b quark tuning has a noticeable effect as can be seen from comparing the mistuned and tuned values of am_b on set 1, with $n = 4$ being most effected. A value of 1.5% is taken for $n = 4$, and 0.5% for the other moments.

- In [76], effects from electromagnetic interactions were estimated for the case of the charm. These produced very small uncertainties, which because of the smaller electric charge of the b quark are even smaller here so no additional error is required

from this source.

This gives final values for the moments of,

$$(G_4^V)^{1/2} = 0.086(5)(3)\ \text{GeV}^{-1} \tag{4.50}$$

$$(G_6^V)^{1/4} = 0.196(8)(2)\ \text{GeV}^{-1} \tag{4.51}$$

$$(G_8^V)^{1/6} = 0.295(11)(2)\ \text{GeV}^{-1} \tag{4.52}$$

$$(G_{10}^V)^{1/8} = 0.388(15)(2)\ \text{GeV}^{-1}, \tag{4.53}$$

where the first error is that taken from the fit which takes into account lattice spacing dependence, and the second error comes from the sources given above. The grey band on figure 4.34 shows these fitted values including the errors.

These values can be compared to q^2-derivative moments, $\mathcal{M}_k$, where $n = 2k + 2$, of the b quark vacuum polarisation that can be calculated in continuum QCD perturbation theory, which uses experimental values for $R_{e^+e^-} = \sigma(e^+e^- \to \text{hadrons})/\sigma_{pt}$ [72]. These values, converted to GeV^{-1} for comparison with our results are

$$(M_1^{\text{exp}} 4!/(12\pi^2 e_b^2))^{1/2} = 0.0915(3)\ \text{GeV}^{-1} \tag{4.54}$$

$$(M_2^{\text{exp}} 6!/(12\pi^2 e_b^2))^{1/4} = 0.1991(5)\ \text{GeV}^{-1} \tag{4.55}$$

$$(M_3^{\text{exp}} 8!/(12\pi^2 e_b^2))^{1/6} = 0.2996(5)\ \text{GeV}^{-1} \tag{4.56}$$

$$(M_4^{\text{exp}} 10!/(12\pi^2 e_b^2))^{1/8} = 0.3955(6)\ \text{GeV}^{-1}. \tag{4.57}$$

In 4.34 these values are shown as black diamonds and it is clear that the errors are a lot smaller than those determined from the NRQCD correlators because of the systematic errors in NRQCD for such low moments.

4.3.6 Anomalous Magnetic Moment of the Muon

The magnetic moment of the muon is

$$\vec{M} = g_\mu \frac{e}{2m_\mu} \vec{S}, \tag{4.58}$$

where g_μ is the gyromagnetic ratio, which is predicted to be 2 from the Dirac equation [1, 81, 82]. However, there are small deviations to this value that come from self-interactions. This is known as the anomalous magnetic moment and parametrised as,

$$a_\mu = \left(\frac{g_\mu - 2}{2} \right). \tag{4.59}$$

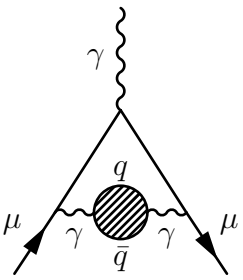

Figure 4.35: The hadronic vacuum polarisation contribution to the anomalous magnetic moment of the muon. The quark loop is shaded to indicate that there are internal QCD processes taking place.

This value can be measured to high precision in experiment with the average value of the μ^+ and μ^- anomalous magnetic moments being [1, 83],

$$a_\mu^{\text{exp}} = 116\,592\,091(54)(33) \times 10^{-11}, \tag{4.60}$$

where the first error is from statistical errors and the second is from systematic errors. This value currently shows tension with theoretical predictions and gives a discrepancy of around $25(9) \times 10^{-10}$.

The Standard Model prediction can be split into three distinct parts, so that

$$a_\mu^{\text{SM}} = a_\mu^{\text{QED}} + a_\mu^{\text{EW}} + a_\mu^{\text{Had}}, \tag{4.61}$$

for QED contributions, contributions from electroweak interactions and hadronic loops. The tools of lattice QCD can be used to make determinations of the values to the hadronic contribution to a_μ^{SM}. Figure 4.35 shows a diagram of this process.

Although this contribution is small, it is possible to use the moments that have been calculated to make a determination of the contribution of a b quark loop to the anomalous magnetic moment of the muon and was done so as described in [84]. The method used was developed previously in [85] for the calculation of the s and c quark contributions, and allows the moments to be converted to q^2-derivatives of the hadronic vacuum polarisation. From there, q^2-dependence of the integrand required for the b quark contribution to a_μ^{Had} can be determined.

Our lattice results give $a_\mu^b = 0.271(37) \times 10^{-10}$ [84]. The experimental moments given in equation 4.57 give a value of $a_\mu^b = 0.307(2) \times 10^{-10}$ using this same method. The contribution as calculated in QCD perturbation theory is $a_\mu^b = 0.29(1)$ [86].

The error we get is quite large, being dominated by NRQCD systematics. The reason for this is that the integral is dominated by the region with small q^2, and it is the fourth time moment that contributes most here, which is the temporal moment determined least well in our lattice calculation. However, the b quark contribution is very small compared to the hadronic vacuum polarisation contribution, which is $\approx 700 \times 10^{-10}$. Therefore even this relatively large error does not negatively impact the issue of reducing the Standard Model result for a_μ and provides an important cross-check of other methods by which to calculate it.

It is possible to calculate the contribution using relativistic b quarks, with preliminary results for this sort of calculation given in [87], which uses the HISQ formalism.

4.3.7 Determination of m_b

A further calculation that can be made using this data is the value of the b quark mass. Since QCD confinement prohibits quarks being detected directly, it is not possible to measure its mass directly either. Lattice QCD *can* be used in order to infer the mass of the quarks, and in particular, NRQCD can be used to determine the mass of the b quark.

We can use temporal moments to gain access to the b quark mass in the $\overline{\text{MS}}$ scheme. This is because the continuum moments relate to the perturbation series divided by the $\overline{\text{MS}}$ b quark mass.

By taking ratios of successive reduced moments we can cancel the renormalisation factors Z_V that were necessary in calculating the decay constant and leptonic widths. Factors of the lattice b quark mass can also be cancelled by multiplying in a ratio of the spin average value of the Υ and η_b meson mass, $\overline{M}_{\Upsilon,\eta_b}$, to twice am_b. This leaves the $\overline{\text{MS}}$ b quark mass as a ratio to $\overline{M}_{\Upsilon,\eta_b}$,

$$\overline{m}_b(\mu) = \frac{\overline{M}_{\Upsilon,\eta_b}}{2}\left[\frac{R_{n-2}r_n}{R_n r_{n-2}}\right]^{1/2}\frac{2m_b}{\overline{M}_{\text{kin}}} \tag{4.62}$$

where $m_b(\mu)$ is the physical mass of the b quark in the $\overline{\text{MS}}$ scheme at scale μ.

Figure 4.36 shows the results of this calculation as a function of n on the very coarse set 1 and fine set 5. As with the calculation of Z_V, a plateau develops where the NRQCD vector current becomes a good approximation to the continuum vector current. Table 4.14 gives the results for $n = 14, 18$ and 22 on each ensemble. The errors are significantly

Set	am_b	c_4	$n = 14$	$n = 18$	$n = 22$
1	3.297	1.0	4.187(11)	4.193(6)	4.192(5)
1	3.297	1.22	4.188(11)	4.194(5)	4.193(6)
1	3.42	1.0	4.189(13)	4.197(6)	4.193(5)
2	3.25	1.22	4.192(11)	4.197(6)	4.196(5)
3	2.66	1.0	4.209(10)	4.210(7)	4.208(4)
4	2.62	1.20	4.210(10)	4.214(7)	4.211(4)
5	1.91	1.0	4.207(9)	4.204(5)	4.202(3)

Table 4.14: Values for the b quark mass in GeV in the $\overline{MS}$ scheme, for $n = 14$, 18 and 22 on each set of configurations that we used. Additional values on set 1 are included for the $\mathcal{O}(\alpha_s)$ value of c_4 and for the mistuned value of the b quark. The errors are those from the uncertainty in k_1. The statistical errors from the calculation are negligibly small.

dominated by the uncertainty in k_1,which gets smaller for larger n as the moments become more nonrelativistic, and the statistical errors are very small.

For the determination of the physical value of the b quark mass, the results from $n = 18$ are used [84]. The values for each of the five ensembles are plotted in figure 4.37. The grey band shows the physical value, which was determined by fitting to the function in equation 4.41 where this time the hadronic parameter used was $\overline{M}_{\Upsilon,\eta_b}/2 - \overline{m}_b$. This parameter is the binding energy that results from the QCD interactions in the meson.

The fit at $n = 18$ gives

$$\overline{m}_b(\mu = 4.18 \text{ GeV}, n_f = 4) = 4.207(21) \text{ GeV}. \tag{4.63}$$

For comparison, performing the same fits at $n = 14$ and $n = 22$ gives,

$$\overline{m}_b(\mu = 4.18 \text{ GeV}, n_f = 4) = 4.209(22) \text{ GeV}, \quad n = 14 \tag{4.64}$$

$$\overline{m}_b(\mu = 4.18 \text{ GeV}, n_f = 4) = 4.204(20) \text{ GeV}, \quad n = 22. \tag{4.65}$$

Additional systematic errors that were not included in the fit must be added in from various sources:

- truncation of the perturbation theory means we include an error of $0.25\alpha_s$ for this, but since here we take the square root, this is divided by two. By leaving out the

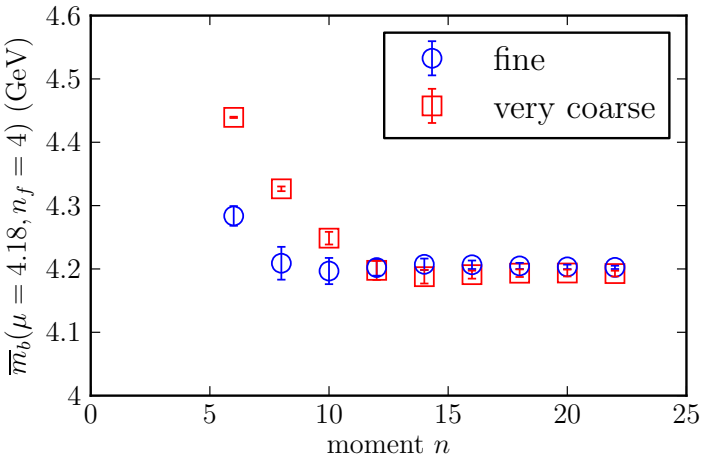

Figure 4.36: The mass of the b quark in the $\overline{\text{MS}}$ at scale 4.18 GeV and $n_f = 4$ for each value of the time moment n on very coarse set 1 and fine set 7.

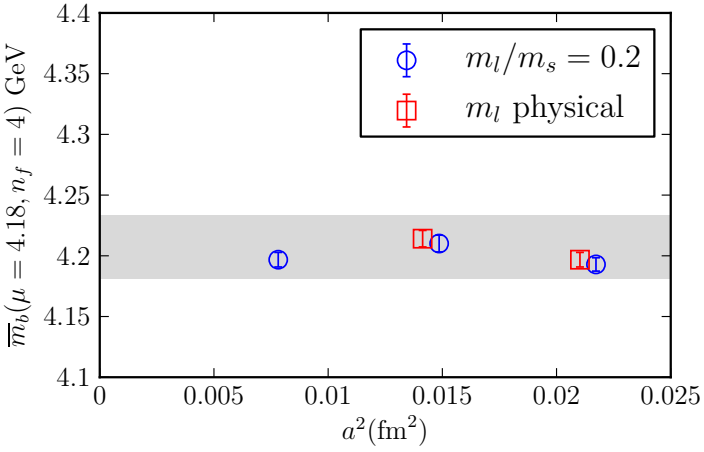

Figure 4.37: Result for the b quark mass in the $\overline{\text{MS}}$ scheme calculated from time moments of the current-current correlator at $n = 18$. The grey band is the result of the fit.

$\mathcal{O}(\alpha_s^3)$ coefficients in the perturbation theory, the value changes by 5 MeV, so we take a conservative error of 7 MeV to cover this;

- the error on α_s makes a small difference. A change of 1σ results in a 3 MeV shift in the b quark mass in opposition to the change of α_s;
- missing $\mathcal{O}(v^4)$ terms in the NRQCD action gives an estimated additional error of $(1/n)^2$. The effect of missing $\mathcal{O}(v^2)$ can be studied by using only the leading term in the current, which amounts to a 30 MeV shift in the mass on the very coarse ensembles and an 8 MeV shift on the fine ensemble, so taking a 13 MeV error for moment $n = 18$ is conservative for missing $\mathcal{O}(v^4)$ effects.
- there is an error from the mistuning of the b quark mass, but as can be seen in table 4.14, this effect is negligible;
- missing electromagnetic effects give a 1 MeV error on the determination of m_b which is negligible.

This gives a result for $n = 18$ of

$$\overline{m}_b(\mu = 4.18 \text{ GeV}, n_f = 4) = 4.207(26) \text{ GeV}, \tag{4.66}$$

when the additional errors are added in quadrature. This result has to be converted to an $n_f = 5$ result through perturbation theory [72], which gives a final value of

$$\overline{m}_b(\mu = \overline{m}_b \text{ GeV}, n_f = 5) = 4.196(23) \text{ GeV}. \tag{4.67}$$

Figure 4.38 gives a summary of determinations of the b quark mass using various methods in lattice QCD that include at least the u, d and s quarks in the sea, or with a c quark included also. The first of these determinations is the result given here. The second result, from [88], uses the relativistic HISQ formalism for the b quark and pseudoscalar current-current correlators. Low moments are compared to the results from continuum QCD perturbation theory for a range of quark masses including the b quark mass on the finest lattices. Calculations included $n_f = 3$ and $n_f = 4$ and these were combined for this value, providing an update for the calculation in [78]. The third result given again uses NRQCD, but this time calculates the mass of the b quark from the binding energy for Υ

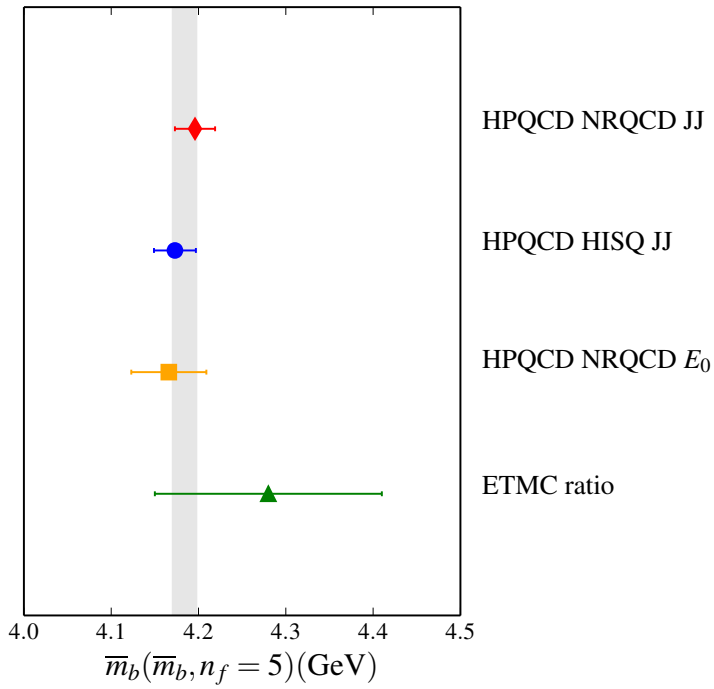

Figure 4.38: Results for $m_b(m_b)$ in the $\overline{\text{MS}}$ scheme for various lattice QCD determinations. These values are for $n_f = 5$ which were determined from perturbation theory as each of the values were calculated for either 3 or 4 quark flavours. The weighted average of the values is 4.184(15) GeV and is depicted by the grey band here.

and B_s mesons on gluon field configurations with $n_f = 3$ [89]. The fourth is the result of a calculation by the European Twisted Mass Collaboration [90].

Due to the very different systematic errors, a weighted average can be taken, giving a value of $\overline{m}_b(\overline{m}_b) = 4.184(15)$ GeV which appears as the grey band in figure 4.38. This compares with – but is more accurate than – the current value in the Particle Data Tables of $\overline{m}_b(\overline{m}_b) = 4.18(3)$ GeV [1].

Chapter 5

B Physics

The rôle of B physics is an important one in particle physics, both as a test of our understanding of the Standard Model itself and as a sector in which to detect signals of new physics beyond the Standard Model. Experiments such as LHCb at the Large Hadron Collider focus on physics involving b quarks as a test of CP violation [91], which aims to shed light on the question of why matter and antimatter have slightly different properties.

Lattice QCD can provide an input into these calculations by providing ways in which to constrain the CKM unitary triangle through the calculation of the CKM matrix elements. Determination of these matrix elements are not carried out here, but this work presents the first step towards this calculation. It is the decay of B and B_s mesons – both of which contain b valence quarks – into lighter mesons via the emission of a W boson that will be the focus of this chapter.

5.1 Semileptonic Decays

Semileptonic decays are those where a quark changes flavour, emitting a W boson, which in turn decays to a charged lepton and its neutrino. Here we will consider specifically the decays $B \to \pi\ell\nu$ and $B_s \to K\ell\nu$.

Some consideration will also be given to the fictitious $B_s \to \eta_s$ decay. The η_s does not exist in the real world but it can be simulated on the lattice and utilised in lattice QCD calculations [18, 19]. This particular decay involves the transition $b \to s$ that can happen via diagrams that are more complicated than the simple W boson decay. The η_s also gives a way for us to see the quark mass dependence.

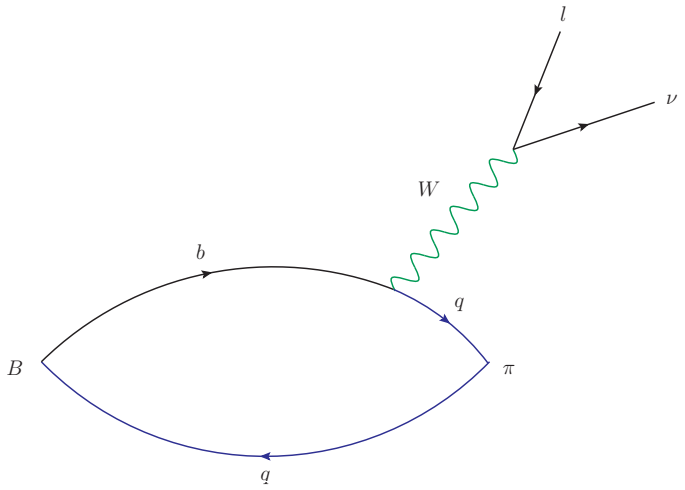

Figure 5.1: Schematic of the semileptonic decay of a B meson to a π, a charged lepton and a neutrino. The B meson is created at lattice time $t_0 - T$ and the π destroyed at lattice time t_0, between which a vector decay changes the flavour of the b quark into a u/d quark.

A diagram depicting the $B \to \pi$ decay is shown in figure 5.1, which is analogous to the other decays discussed in this chapter. The total distance between the creation of the B meson on the left of the image and the annihilation of the π on the right is T, in units of lattice time. The light quark the bottom of the diagram is known as the spectator as it has no actual role in the decay process itself. The spectator quark is used as a source for the b quark, which here is known as the extended propagator. The remaining light quark is known as the active quark. An appropriate current – a vector current for these semileptonic decays – is inserted between the active and extended propagator, which thus changes the flavour of the b quark to a u quark in this example.

These types of decays allow us to use the same NRQCD action used in bottomonium systems. The parameters used in the calculation for the valence quarks are given in table 5.1 as there are some slight differences between these values and those used in the bottomonium calculations. The MILC gluon field ensembles given in table 2.1 are used here again.

Set	am_b	am_l^{val}	am_s^{val}	u_{0L}	c_1	c_4	c_5	c_6
1	3.297	0.013	0.0641	0.8195	1.36	1.22	1.21	1.36
2	3.263	0.0064	0.0636	0.82015	1.36	1.22	1.21	1.36
3	3.25	0.00235	0.0628	0.819467	1.36	1.22	1.21	1.36
4	2.66	0.01044	0.0522	0.834	1.31	1.20	1.16	1.31
5	2.62	0.00507	0.0505	0.8349	1.31	1.20	1.16	1.31
6	2.62	0.00184	0.0507	0.834083	1.31	1.20	1.16	1.31
7	1.91	0.0074	0.0364	0.8525	1.21	1.16	1.12	1.21
8	1.89	0.0012	0.0360	0.851805	1.21	1.16	1.12	1.21

Table 5.1: Parameters used for B physics calculations. am_b is the bare lattice mass of the b quark simulated with the NRQCD action. am_l^{val} and am_s^{val} are the valence light and strange quark masses respectively, which use the HISQ formalism. u_{0L} is the Landau link value used for tadpole improvement. The parameters $c_{1,4,5,6}$ listed are the coefficients for the NRQCD action and include $\mathcal{O}(\alpha_s)$ corrections. The other coefficients, c_2 and c_3, are set to their tree level values of 1.

5.2 Lattice QCD Calculation

This section outlines the calculation of the $B \to \pi\ell\nu$ decay in lattice QCD, which is applicable to the $B_s \to K\ell\nu$ and $B_s \to \eta_s$ decays described later. It is necessary to calculate two point meson correlators on the lattice ensembles for each of the mesons involved in the process; that is, the B meson and the π meson. Additionally three point correlators on the same set of lattice ensembles are generated. Three point correlators create the initial state meson at time $t = 0$ and destroy the final state meson at $t = T$, with an appropriate current inserted at t for the process of interest. Both sets of two point correlators and the three point correlators are then fitted simultaneously to extract the relevant energies and amplitudes, much like in the two point fits for the heavy-heavy physics. This is necessary because there are amplitudes associated with the two mesons and with the vector current. The two amplitudes from the mesons are then divided out of the amplitude from the three point correlators leaving only the contribution from the vector current inserted between them.

5.2.1 Light Mesons

The same HISQ quarks used for the quarks in the sea of the MILC collaboration ensembles are used in these calculations for the valence quarks in the light mesons, i.e. the π, K and η_s [17]. The light valence quarks are given the same masses as they have in the sea, while the strange quark masses are given slightly different tuned masses so that they correspond more closely to their physical values [17, 18].

The fitting function for the light correlators for extracting the energies and amplitudes is

$$\begin{aligned} C(t) = & \sum_{k=0}^{n_{\text{exp}}-1} c_k^2 \left(e^{-E_k t} + e^{-E_k(T-t)}\right) \\ & - (-1)^{t/a} \sum_{ko=0}^{n_{\text{exp}}-1} \tilde{c}_{ko}^2 \left(e^{-\tilde{E}_{ko} t} + e^{-\tilde{E}_{ko}(T-t)}\right), \end{aligned} \tag{5.1}$$

where the second sum is an oscillating piece that results from using staggered quarks as described in section 2.2.3. However, it is only present for the K meson, because the valence quarks in the pion and η_s have the same mass, so the terms cancel for zero meson momentum.

The hadronic parameter we are interested in extracting is the decay constant $f_{a\bar{b}}$ for the meson with quark content $a\bar{b}$. This relates to the constituent valence quark masses and the ground state energy and amplitude from our fits by [92],

$$f_{ab} = (m_a + m_b)\sqrt{\frac{2}{E_0^3}} c_0, \tag{5.2}$$

where m_a and m_b are the masses of quarks a and b and E_0 is the ground state energy. In contrast to the NRQCD calculations, the ground state energies from these fits do correspond to the mass of the mesons.

Table 5.2 gives masses and the decay constants for each of the π, K and η_b mesons[1] in lattice units taken from [17] since the same two-point correlators are used in the results here. When fitting the correlators, the results were checked for agreement with these values.

[1] In the $B_s \to K\ell\nu$ and $B_s \to \eta_s$ decays, not all of the ensembles have been used, but the results for the masses and decay constants of these mesons on all ensembles are included for completeness.

Set	m_π	f_π	m_K	f_K	m_{η_s}	f_{η_s}
1	0.23644(15)	0.11184(10)	0.40006(19)	0.12585(10)	0.51511(16)	0.14009(7)
2	0.16614(7)	0.10508(6)	0.37948(10)	0.12177(4)	0.51080(9)	0.13840(4)
3	0.10172(4)	0.09938(6)	0.36557(8)	0.11837(4)	0.50656(6)	0.13720(2)
4	0.19158(9)	0.09077(6)	0.32789(11)	0.10189(5)	0.42358(11)	0.11318(4)
5	0.13414(6)	0.08452(5)	0.30756(10)	0.09788(4)	0.41474(8)	0.11119(3)
6	0.08154(2)	0.07990(3)	0.29843(5)	0.09532(2)	0.41478(4)	0.11065(2)
7	0.14062(10)	0.06618(5)	0.23919(11)	0.07424(4)	0.30871(10)	0.08236(3)
8	0.05716(2)	0.05784(3)	0.21855(5)	0.06921(2)	0.30480(4)	0.08053(2)

Table 5.2: Values of the π, K and η_s mass and decay constants in lattice units taken from [17] on each of the gluon field ensembles.

5.2.2 B and B_s Mesons

The two-point correlators for the B and B_s mesons required for the calculation presented here were generated previously by the HPQCD collaboration, and detailed results are contained in [62] and [93]. Again, these were checked for consistency when fitting the correlators. The hadronic parameter that we are interested in obtaining from the B meson is the decay constant f_B. This is defined from the temporal axial current between the pseudoscalar B meson and the vacuum as

$$\langle 0|A_0|B\rangle = f_B m_B, \tag{5.3}$$

where m_B is the mass of the B meson. The B meson uses a HISQ light valence quark and an NRQCD b quark generated on the usual gluon field ensembles that include HISQ quarks in the sea. The appropriate temporal axial currents are,

$$J_0^{(0)} = \bar{q}\gamma_5\gamma_0 Q \tag{5.4}$$

$$J_0^{(1)} = \frac{-1}{2m_b}\bar{q}\gamma_5\gamma_0\boldsymbol{\gamma}\cdot\boldsymbol{\nabla}Q \tag{5.5}$$

$$J_0^{(2)} = \frac{-1}{2m_b}\bar{q}\boldsymbol{\gamma}\cdot\overleftarrow{\boldsymbol{\nabla}}\gamma_5\gamma_0 Q. \tag{5.6}$$

where q is a light quark and Q is the heavy b quark. The properly renormalised temporal axial current constructed from the leading order and $1/m_b$ currents is given through $\mathcal{O}(\alpha_S)$

Set	z_0	z_1	z_2
1	0.024(2)	0.024(3)	−1.108(4)
2	0.022(2)	0.024(3)	−1.083(4)
3	0.022(1)	0.024(2)	−1.074(4)
4	0.006(2)	0.007(3)	−0.698(4)
5	0.001(2)	0.007(3)	−0.690(4)
6	0.001(2)	0.007(2)	−0.690(4)
7	−0.007(2)	−0.031(4)	−0.325(4)
8	−0.007(2)	−0.031(4)	−0.318(4)

Table 5.3: Coefficients for matching of the currents made of an NRQCD b quark and HISQ light quarks to full QCD. This parametrisation follows that in [62], where $z_0 = \rho_0 - \zeta_{10}$, $z_1 = \rho_1 - z_0$ and $z_2 = \rho_2$ using the values calculated in [94].

in perturbation theory by [62, 94],

$$\langle A_0 \rangle = (1 + \alpha_s z_0) \left(\langle J_0^{(0)} \rangle + (1 + \alpha_s z_1) \langle J_0^{(1)} \rangle + \alpha_s z_2 \langle J_0^{(2)} \rangle \right) \tag{5.7}$$

for renormalisation factors z_0, which are given in table 5.3. z_0 takes care of the effect of mixing between $J_0^{(0)}$ and $J_0^{(1)}$ at one loop level. These values are the same as those in [62], which come from the values calculated in [94] but with a reordered perturbation series. The $J_0^{(1)}$ and $J_0^{(2)}$ currents were applied at the sink in the results given here.

Like the heavy-heavy calculations, the b quarks in the heavy-light correlators utilise smearing functions. Those used for the b quark on each ensemble is listed in table 5.4 for two smearings a_{sm} – in addition to the point source also used – that take the form $\exp(-r/a_{\mathrm{sm}})$. Having these smearing combinations at the source and sink allows 3×3 matrix fits to be performed. The fitting function for the B and B_s mesons is

$$\begin{aligned} C(t) = & \sum_{k=0}^{n_{\mathrm{exp}}-1} c^*_{sc,k} c_{sk,k} e^{-E_k(t-t_0)} \\ & - \sum_{ko=0}^{n_{\mathrm{exp}}-1} \tilde{c}^*_{sc,ko} \tilde{c}_{sk,ko} (-1)^{(t-t_0)} e^{\tilde{E}_{ko}(t-t_0)} \end{aligned} \tag{5.8}$$

where this second piece is an oscillating term. The labels sc and sk refer to the smearing functions used at the source and the sink.

Set	a_{sm}		T		
1	2.0,	4.0	9,	12,	15
2	2.0,	4.0	9,	12,	15
3	2.0,	4.0	8,	11,	14
4	2.5,	5.0	13,	18,	23
5	2.0,	4.0	13,	18,	23
6	2.0,	4.0	13,	18,	23
7	3.425,	6.85	18,	23,	28
8	3.425,	6.85	19,	26,	33

Table 5.4: Parameters for three-point data. The values of a_{sm} are the parameters for the smearing functions used, which take the form $\exp(-r/a_{\mathrm{sm}})$. The values of T give the time in lattice units between the creation of the B meson in the initial state and the annihilation of the light meson in the final state in the decay calculations, which along with the various smearing combinations are fitted simultaneously.

From our fits, the quantity we get directly is the amplitude c_B which relates to the temporal axial matrix element by $c_B = \langle 0|A_0|B\rangle/(\sqrt{2}\sqrt{2m_B})$. The extra factor of $\sqrt{2}$ arises due to a factor of 2 in the HISQ propagator for the light quark. Since we cannot get the mass of the B meson from our correlators in a straightforward way due to the energy offset in the NRQCD action, it is most convenient to take $f_B\sqrt{m_B}$ as the hadronic parameter. The values of the B and B_s meson amplitudes, calculated in [62], are given in table 5.5. The factor of 2 is already included for relating them to $f_B\sqrt{m_B}$.

5.2.3 Three Point Correlators

The semileptonic transition of the b quark to a u quark takes place through the emission of the vector W boson, so a three-point correlation function where mesons are created and destroyed at either end of the process and a current is inserted for the decay between them is required. The appropriate current for the decays being discussed here is a temporal

Set	$c(J_B^{(0)})$	$c(J_B^{(1)})$	$c(J_{B_s}^{(0)})$	$c(J_{B_s}^{(1)})$
1	0.3720(10)	-0.0300(3)	0.3220	-0.0263(3)
2	0.3644(6)	-0.0291(3)	0.3093(11)	-0.0257(8)
3	0.3621(16)	-0.0288(2)	0.2986(17)	-0.0237(4)
4	0.2733(4)	-0.0234(2)	0.2373(9)	-0.0197(4)
5	0.2679(3)	-0.0234(1)	0.2272(7)	-0.0197(3)
6	0.2653(2)	-0.0229(1)	0.2193(8)	-0.0194(3)
7	0.1747(3)	-0.0170(1)	0.1525(8)	-0.0146(6)
8	0.1694(3)	-0.0167(0)	0.1386(5)	-0.0136(1)

Table 5.5: Results for the leading and next-to-leading amplitudes on each of the lattice ensembles for the B and B_s mesons. These values are taken from [62] and are used to construct the decay constants of the B and B_s with a renormalised temporal axial current using equations 5.10.

vector current. The temporal vector currents used take the form [62, 95],

$$\begin{aligned} J_0^{(0)} =& \bar{q}\gamma_0 Q \\ J_0^{(1)} =& \frac{-1}{2m_b}\bar{q}\gamma_0 \boldsymbol{\gamma}\cdot\boldsymbol{\nabla} Q \\ J_0^{(2)} =& \frac{-1}{2m_b}\bar{q}\boldsymbol{\gamma}\cdot\overleftarrow{\boldsymbol{\nabla}}\gamma_0 Q, \end{aligned} \tag{5.9}$$

for heavy quark Q and light quark q. The properly renormalised vector current constructed from the leading order and $1/m_b$ currents is given by [62, 94],

$$\langle V_0\rangle = (1+\alpha_s z_0)\left(\langle J_0^{(0)}\rangle + (1+\alpha_s z_1)\langle J_0^{(1)}\rangle + \alpha_s z_2\langle J_0^{(2)}\rangle\right) \tag{5.10}$$

where z renormalisation factors are the same as those in equation 5.7, given in table 5.3, because HISQ quarks have chiral symmetry.

The four momentum transferred to the leptons is $q^\mu = p_B^\mu + p_\pi^\mu$. In all of the calculations described, both the initial and final state mesons are at rest, so the momentum transferred to the leptons is maximal, $q_{\max}$. A consequence of this is that the $1/m_b$ currents, $\langle J_0^{(1)}\rangle$ and $\langle J_0^{(2)}\rangle$, are equal. An advantage that emerges is that it is only then necessary to fit one of these currents, which results in better fits that take less time to perform.

The fitting procedure for the correlators in semileptonic meson decays is very similar to the procedure for the two-point correlators as in the previous chapter. However, this

time two sets of two-point functions for each of the mesons are fitted simultaneously with three-point functions for the decay in order to capture the amplitude of the matrix element, therefore the fitting function from theory is slightly different for three-point function fits. Using the example of the $B \to \pi\ell\nu$ decay, the matrix element $\langle\pi|V^0|B\rangle$ is what we are interested in extracting. The fit function takes the form,

$$C^{(3\text{pt})}(t,T) = \sum_{k=0}^{n_\pi-1}\sum_{l=0}^{n_B-1}(-1)^{kt}(-1)^{l(T-t)}A^0_{kl}e^{-E_{k,\pi}t}e^{-E_{l,B}(T-t)} \tag{5.11}$$

where the sums determine the number of energy levels fitted for the B and π mesons. A^0_{kl} is the amplitude from the three point correlators that relates the k^{th} amplitude of the pion to the l^{th} amplitude of the B allowing access to the matrix elements $\langle\pi_k|V^0_{kl}|B_l\rangle$. As discussed previously, staggered quarks introduce oscillatory behaviour that must be taken into account when fitting. T is the lattice time between the B meson and pion at either end of the correlator. On each ensemble three values were used and are given in table 5.4.

When fitting the data, an approach was taken in which the two-point functions were fitted together without the three-point functions in order to achieve a quicker and better fit. The output parameters of this initial fit were passed as priors into a larger fit where the two-point correlators and three-point correlators for all values of T and the smearing combinations were fitted simultaneously.

For each of the fits described below, the prior values are similar, and only the ground state energy priors are adjusted for each of the mesons for the two-point correlators. The priors on the energy differences is taken to be 600(300) MeV, while the difference between the ground state energy and the first oscillation energy is 400(200) MeV. The priors on the two-point amplitudes are the same as for bottomonium: 0.1(1.0). For the three-point correlators the prior is allowed to vary further with 0.1(5.0). In each of these cases, this is a width of around three to five times the size of the ground state amplitudes.

5.3 $B \to \pi\ell\nu$ Semileptonic Decay

By taking the ratio $\frac{C_{3\text{pt}}(t)}{C_{2\text{pt},B}(t)C_{3\text{pt},\pi}(T-t)}$, the B meson oscillatory behaviour becomes evident[2]. An example of this is shown in Figure 5.2, which has been taken from set 4. This sort

[2]The values of t are the opposite way round from our earlier definition, with the B meson here at $t = 0$ and the pion at T. This is only a cosmetic rearrangement so that it is clear that different T values converge to the same result.

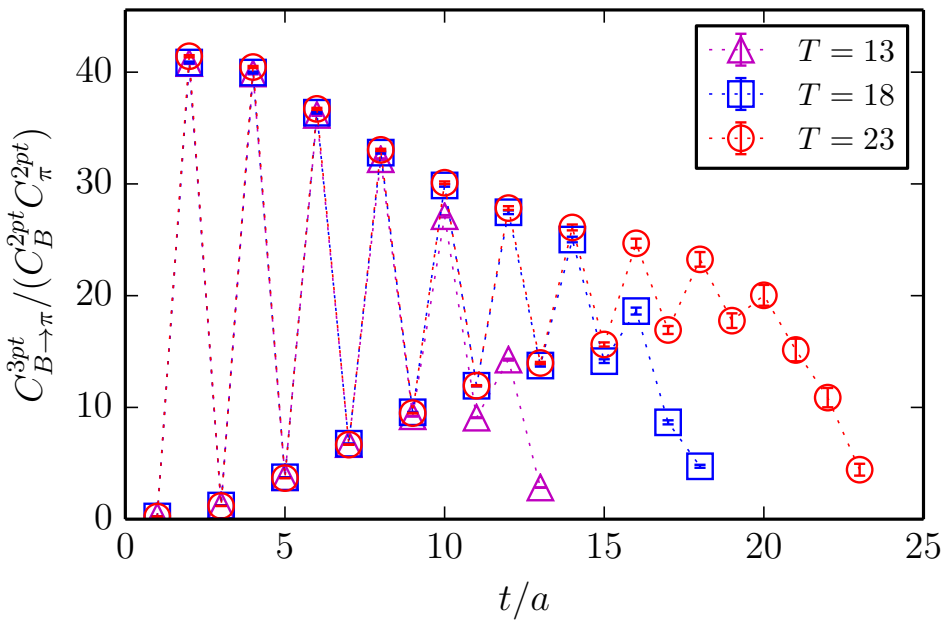

Figure 5.2: Ratio of the 3-point correlator for $B \to \pi$ decay to the 2-point correlators for the B meson and pion on coarse set 4. The statistical accuracy we have is clear and the results converge for different T values.

of plot demonstrates the statistical accuracy we have in our calculation and the fact that different T values converge to the same result.

5.3.1 Form Factors

The matrix element for the electroweak current between two pseudoscalar mesons is $\langle\pi|(V)^\mu|B\rangle$. This matrix element can be expressed as a function of the form factors $f_+(q)$ and $f_0(q)$,

$$\langle\pi(p_\pi)|V^\mu|B(p_B)\rangle = f_+(q^2)\left[p_B^\mu + p_\pi^\mu - \frac{M_B^2 - M_\pi^2}{q^2}q^\mu\right] \tag{5.12}$$

$$+ f_0(q^2)\frac{M_B^2 - M_\pi^2}{q^2}q^\mu, \tag{5.13}$$

where $q^\mu = p_B^\mu - p_\pi^\mu$. In the limit of zero recoil, when the B and the π are both at rest, this becomes,

$$\langle\pi|V^0|B\rangle = f_0(q^2_{\rm max})(m_B + m_\pi). \tag{5.14}$$

Another useful parametrisation used in some of the literature is in terms of form factors $f_\parallel$ and $f_\perp$,

$$\langle \pi(p_\pi)|V^\mu|B(p_B)\rangle = \sqrt{2m_B}\left[v^\mu f_\parallel + p_\perp^\mu\right], \tag{5.15}$$

where

$$v^\mu = \frac{p^\mu}{m_B}, \qquad p_\perp^\mu = p_\pi^\mu - (p_\pi \cdot v)v^\mu. \tag{5.16}$$

These form factors give the temporal and spatial parts of the form factors in equation 5.13 separately, so in the B meson rest frame we get,

$$\langle \pi|V^0|B\rangle = \sqrt{2m_B} f_\parallel \tag{5.17}$$

$$\langle \pi|V^k|B\rangle = \sqrt{2m_B} p_\pi^k f_\perp. \tag{5.18}$$

At q^2_{max}, the spatial piece disappears and the temporal piece here relates $f_\parallel$ and $f_0(q^2_{\mathrm{max}})$ as defined in equation 5.14 by

$$f_0(q^2_{\mathrm{max}}) = \frac{\sqrt{2m_B}}{m_B + m_\pi} f_\parallel. \tag{5.19}$$

Table 5.6 gives the leading and next-to-leading pieces of the three-point current V_{00}, the amplitude that matches with the ground state B and π mesons, taken directly from the fits and then multiplied by a factor of $4/\sqrt{2}$. This normalising factor comes from the use of the MILC code to generate the light HISQ quark in the three point function: there are two hisq propagators, each carrying an extra factor of 2. The B meson also has to be multiplied by this factor due to a single HISQ quark in that case, resulting in the $\sqrt{2}$ in the denominator. The improved current is constructed using the amplitudes and renormalisation factors as in equation 5.10 and is given in the final column of the table.

This amplitude must be related to the matrix element $\langle \pi|V^0|B\rangle$ in order to extract $f_0(q^2_{\mathrm{max}})$. They relate by

$$V_{00} = \frac{\langle \pi|V^0|B\rangle}{2\sqrt{m_\pi m_B}}. \tag{5.20}$$

Using equation 5.14 we get

$$f_0(q^2_{\mathrm{max}})\sqrt{m_B}\left(1 + \frac{m_\pi}{m_B}\right) = \frac{4}{\sqrt{2}}\sqrt{m_\pi} V_{00}, \tag{5.21}$$

where the factor of $4/\sqrt{2}$ is the same as that discussed previously. We leave the factor of $1 + m_\pi/m_B$ in our results since, as a result of the NRQCD action being used, there is again an energy offset, so we cannot get the mass of the B meson directly from our fits.

Set	$V_{00}^{(0)}$	$V_{00}^{(1)}$	V_{00}
1	1.655(37)	-0.092(6)	1.609(37)
2	2.195(42)	-0.134(5)	2.124(42)
3	3.178(92)	-0.240(60)	3.050(100)
4	1.750(40)	-0.107(2)	1.670(40)
5	2.339(51)	-0.160(3)	2.214(51)
6	3.530(52)	-0.266(4)	3.321(52)
7	1.887(66)	-0.130(20)	1.766(69)
8	3.753(28)	-0.327(3)	3.451(27)

Table 5.6: Fit results of the temporal vector amplitude from the 3 point fits for the process $B \to \pi\ell\nu$. Given are the leading currents and the next to leading order correction. The value of $V_{00}^{(2)} = V_{00}^{(1)}$, so is not included in the table. The final column is the value of the improved and renormalised current as given in equation 5.10. It has been provided separately here as, since the errors between the leading and subleading currents are correlated, the error on the improved current is taken directly from the fit.

Table 5.7 gives these values in lattice units for each of the lattice ensembles. The second column gives the result using only the leading current, $J^{(0)}$ while the third column gives the improved value with $J^{(1)}$ and $J^{(2)}$ included using equation 5.10.

Figure 5.3 shows the values of $f_0(q^2_{\rm max})\sqrt{m_B}\left(1+\frac{m_\pi}{m_B}\right)$ for each of the lattice ensembles for the leading current $J^{(0)}$ in physical units of $\mathrm{GeV}^{1/2}$ against m_π and figure 5.4 gives the values for the improved current. The effect of including the $J^{(1)}$ and $J^{(2)}$ currents is to give a slightly lower determination of this parameter.

5.3.2 Soft Pion Theorem

Soft pion theorems state that in the $m_\pi \to 0$ limit [96, 97],

$$f_0(q^2_{\rm max}) = \frac{f_B}{f_\pi} \tag{5.22}$$

Previous studies of this decay in the quenched approximation noted that it did not seem to hold well [98, 99], giving a ratio of $f_0(q^2_{\rm max})/(f_B/f_\pi) \sim 0.5$.

Results for this ratio are given in table 5.8 for each of the lattice ensembles. Results are given for the leading currents for each of the B meson decay constant and the vector

Set	$f_0^{(0)}(q^2_{\rm max})\sqrt{m_B}\left(1+\frac{m_\pi}{m_B}\right)$	$f_0(q^2_{\rm max})\sqrt{m_B}\left(1+\frac{m_\pi}{m_B}\right)$
1	1.609(35)	1.565(35)
2	1.789(34)	1.732(34)
3	2.027(58)	1.944(64)
4	1.532(35)	1.461(35)
5	1.713(37)	1.622(38)
6	2.016(30)	1.896(30)
7	1.415(50)	1.325(51)
8	1.793(45)	1.648(44)

Table 5.7: Hadronic parameter $f^0(q^2_{\rm max})\sqrt{m_B}$ multiplied by $\left(1+\frac{m_\pi}{m_B}\right)$ on each of the lattice ensembles in lattice units. The numbers in the second column correspond to results for only the $J^{(0)}$ current. The third column gives the result for the renormalised improved value where the $J^{(1)}$ and $J^{(2)}$ currents have been included.

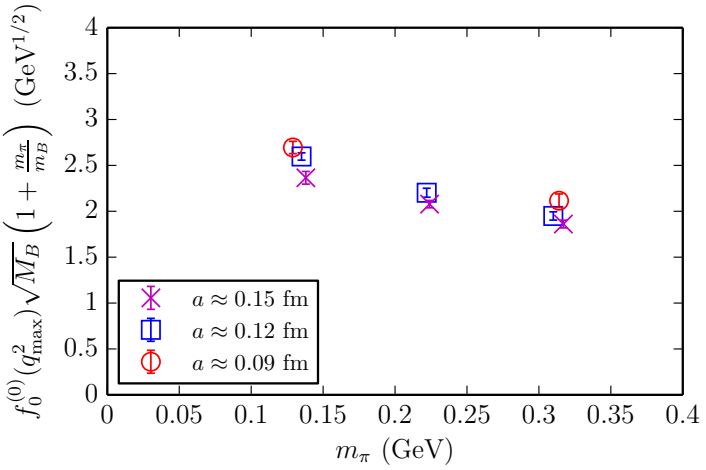

Figure 5.3: Results for the hadronic parameter $f_0^{(0)}(q^2_{\rm max})\sqrt{M_B}(1+\frac{m_\pi}{m_B})$, which used only the $J^{(0)}$ vector current on each of the lattice ensembles for the $B\to\pi\ell\nu$ decay in physical units of GeV$^{1/2}$.

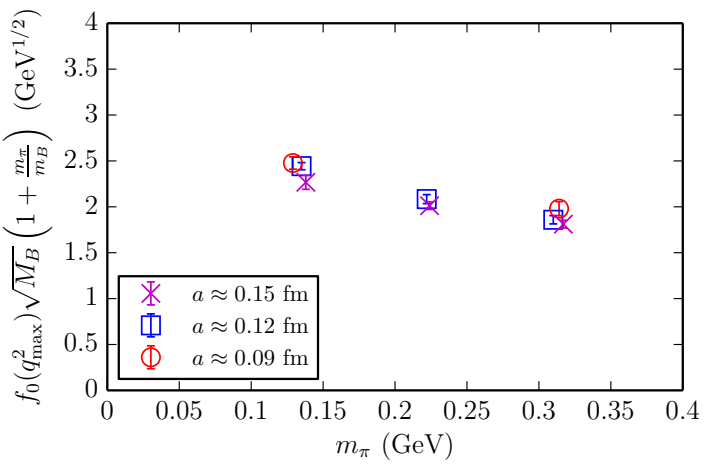

Figure 5.4: Results for the hadronic parameter $f_0\left(q^2_{\rm max}\right)\sqrt{M_B}\left(1+\frac{m_\pi}{m_B}\right)$ on each of the lattice ensembles for the $B \to \pi\ell\nu$ decay in physical units of GeV$^{1/2}$.

current in the three point function in the second column. The third column gives the improved values of the ratio where the $1/m_b$ currents, $J^{(1)}$ and $J^{(2)}$ are included in the calculation and are correctly renormalised as in equation 5.10.

A fit was performed to show the behaviour of the ratio of the form factor to the decay constants in the chiral limit, i.e. in the case where $m_\pi \to 0$, in order to test the soft pion theorem. The fit function took the form,

$$\Gamma(a, m_\pi) = \Gamma_{\rm phys}\left(1 + \sum_{j=1,3}\left(c_j(a\Lambda)^{2j} + b_j m_\pi^j\right)\right. \tag{5.23}$$

$$+ \left(\frac{\Lambda}{m_b}\right)^2\left((a\Lambda)^2 c_b \delta x_m + (a\Lambda)^2 c_{bb}(\delta x_m)^2\right) \tag{5.24}$$

$$\left. + da^2 m_\pi^2 - l\left(\frac{m_\pi}{1.6}\right)^2 \log(m_\pi^2)\right), \tag{5.25}$$

where in the sum there are standard discretisation errors and a term accounting for the mass of the pion. Λ is the scale for QCD which we have set as 400 MeV. The terms involving δx_m account for the mass of the b quark and has been taken to be $\delta x_m = (m_b - 2.7)/1.5$ so that it varies between -0.5 and 0.5. All of these terms are given prior values of 0.0(1.0) except the linear m_π term, which is 0.0(5.0). The final term accounts for chiral logs that arise in chiral perturbation theory [100, 101]. The expectation is that this would have a coefficient of 4, but the fit parameter l is used with the prior value 4.0(1.0).

Figure 5.5 shows the $f_0(q^2_{\rm max})/(f_B/f_\pi) \times (1 + m_\pi/m_B)$ results for all ensembles using

Set	$f_0^{(0)}(q^2_{\rm max})/(f_B^{(0)}/f_\pi)$	$f_0(q^2_{\rm max})/(f_B/f_\pi)$
1	0.558(9)	0.567(13)
2	0.619(12)	0.627(13)
3	0.693(21)	0.695(24)
4	0.589(15)	0.602(16)
5	0.636(14)	0.646(16)
6	0.739(11)	0.747(12)
7	0.618(22)	0.637(25)
8	0.757(20)	0.771(23)

Table 5.8: Ratio of the form factor $f_0(q^2_{\rm max})$ to the ratio of the decay constants f_B and f_π for each of the lattice sets. The numbers in the second column correspond to result for just the leading currents for the B meson and the vector current in three point correlators, i.e. only the $J^{(0)}$ current. The third column gives the result for the renormalised improved value where the $J^{(1)}$ and $J^{(2)}$ currents have been included both for the B decay constant and the vector current in the three point correlators.

only the leading currents for the B meson decay constant and the vector current in the three point function. The grey band gives the result from the fit in this case as $m_\pi \to 0$. Figure 5.6 gives these values where the $J^{(1)}$ and $J^{(2)}$ currents have been included, again with a grey band with the fit result. The final value for the ratio at $m_\pi \to 0$ is 1.01(5); consistent with the soft pion theorem. At the physical pion mass of 139.5 MeV, $f_0(q^2_{\rm max})/(f_B/f_\pi) \times (1 + m_\pi/m_B) = 0.79(2)$.

5.4 $B_s \to K\ell\nu$ Decay

A similar decay to the $B \to \pi\ell\nu$ process is the process $B_s \to K\ell\nu$. The same $b \to u$ transition via the emission of a vector boson takes place, with the only difference being in the spectator, which is an s quark. There has not yet been an observation of this decay in any experiments, although the LHCb collaboration plan a measurement of it, and it is also possible that it could be observed in a run at BelleII.

Since they include the same quark transition, this decay can, like the $B \to \pi\ell\nu$, give results that can be used as an input for the determination of the CKM matrix element V_{ub}

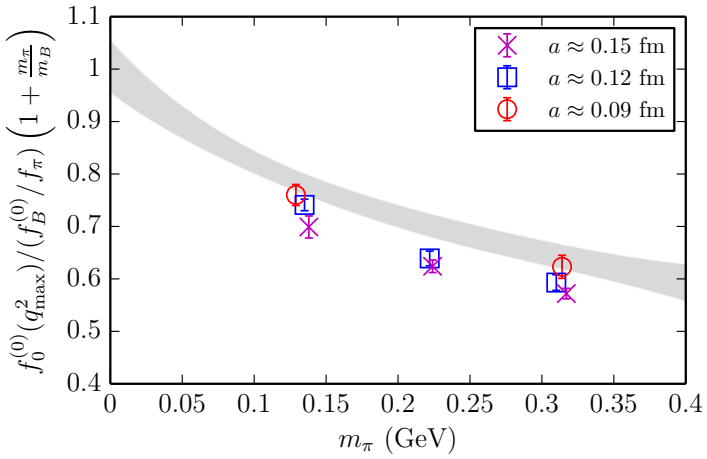

Figure 5.5: Results for the ratio $f_0^{(0)}(q^2_{\max})/(f_B^{(0)}/f_\pi)\left(1+\frac{m_\pi}{m_B}\right)$ on each of the lattice ensembles against m_π in GeV where only the $J^{(0)}$ currents have been used for the three point correlators and the B meson two point correlators. The grey band shows the result of our fit in the limit $m_\pi \to 0$.

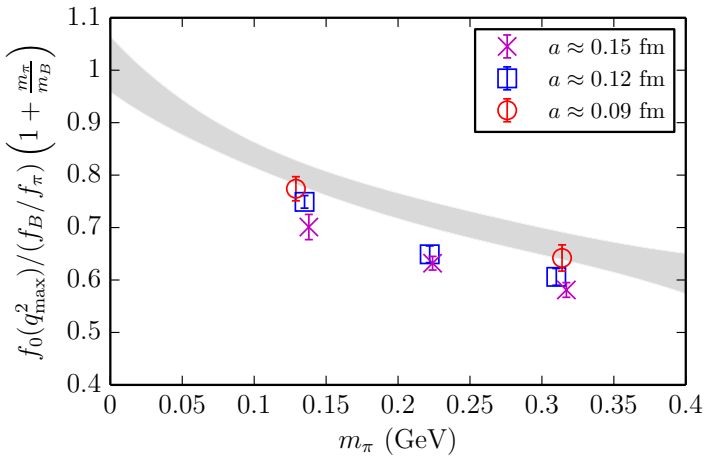

Figure 5.6: Results for the ratio $f_0(q^2_{\max})/\left(f_B/f_\pi\right)\left(1+\frac{m_\pi}{m_B}\right)$ on each of the lattice ensembles against m_π in GeV for the improved and renormalised currents. The grey band shows the result of our fit as $m_\pi \to 0$.

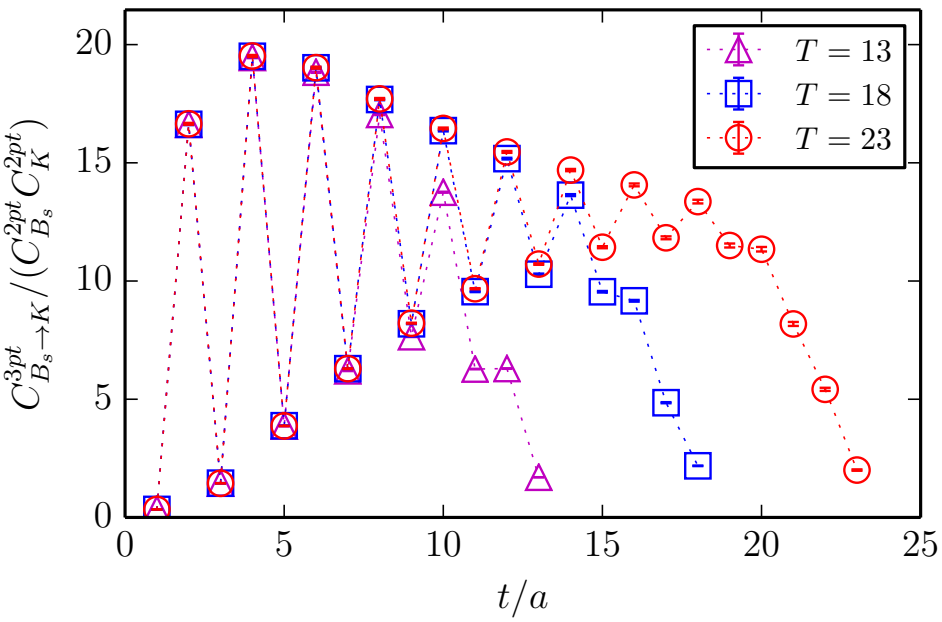

Figure 5.7: Ratio of the 3-point correlator for $B \to K$ decay to the 2-point correlators for the B_s meson and K on coarse set 4. The statistical accuracy we have is clear and the results converge for different T values.

and the first results for a range of q^2 values have recently been presented by the HPQCD collaboration using 2+1 AsqTad configurations generated by the MILC collaboration [102].

The same sort of oscillatory behaviour that could be seen in ratios of the three point functions to the two point functions in the $B \to \pi\ell\nu$ decay can be seen in this decay. This is shown in figure 5.7, again on coarse ensemble set 4.

Results for the currents $V_{00}^{(0)}$ and $V_{00}^{(1)}$ from the three-point fits are given in table 5.9 where they have again been multiplied by the normalisation factor $4/\sqrt{2}$. The value for $f_0(q^2_{\rm max})\sqrt{m_{B_s}}\left(1+\frac{m_K}{m_{B_s}}\right)$ obtained using equation 5.14 are given in table 5.10 for the leading and improved and renormalised currents. The latter values are plotted in figure 5.8 in physical units of $\mathrm{GeV}^{1/2}$.

The ratios $f_0(q^2_{\rm max})/(f_{B_s}/f_K)\times(1+m_K/m_{B_s})$ are given in table 5.10 as in the $B \to \pi\ell\nu$ decay. The values where the currents $J^{(1)}$ and $J^{(2)}$ are included are plotted in figure 5.9. The grey band shows the result at $m_\pi = 0$ using the fit function,

$$\Gamma(a, m_\pi) = \Gamma_{\rm phys}\left(1 + \sum_{j=1,3}(c_j a\Lambda)^{2j} + b(a\Lambda)^2 m_\pi^2 \right. \tag{5.26}$$

Set	$V_{00}^{(0)}$	$V_{00}^{(1)}$	V_{00}
1	1.002(14)	-0.040(2)	0.985(14)
2	1.043(19)	-0.043(3)	1.023(19)
4	1.078(8)	-0.050(1)	1.041(7)
6	1.144(15)	-0.056(1)	1.144(15)
8	1.262(8)	-0.076(2)	1.191(8)

Table 5.9: Fit results of the temporal vector amplitude from the 3 point fits for the process $B_s \to K\ell\nu$. Given are the leading currents and the next-to-leading order correction. The value of $V_{00}^{(2)} = V_{00}^{(1)}$, so is not included in the table. The final column is the value of the improved current as given in equation 5.10. It has been provided separately here as, since the errors between the leading and subleading currents are correlated, the error on the improved current is taken directly from the fit.

Set	$f_0^{(0)}(q^2_{\rm max})\sqrt{m_{B_s}}\left(1+\frac{m_K}{m_{B_s}}\right)$	$f_0(q^2_{\rm max})\sqrt{m_{B_s}}\left(1+\frac{m_K}{m_{B_s}}\right)$
1	1.267(18)	1.246(18)
2	1.284(23)	1.261(23)
4	1.235(9)	1.192(9)
6	1.250(17)	1.202(17)
8	1.180(8)	1.114(8)

Table 5.10: Hadronic parameter $f_0(q^2_{\rm max})\sqrt{m_{B_s}}$ multiplied by $\left(1+\frac{m_K}{m_B}\right)$ in lattice units. The numbers in the second column correspond to results for only the $J^{(0)}$ current. The third column gives the result for the renormalised improved value where the $J^{(1)}$ and $J^{(2)}$ currents have been included.

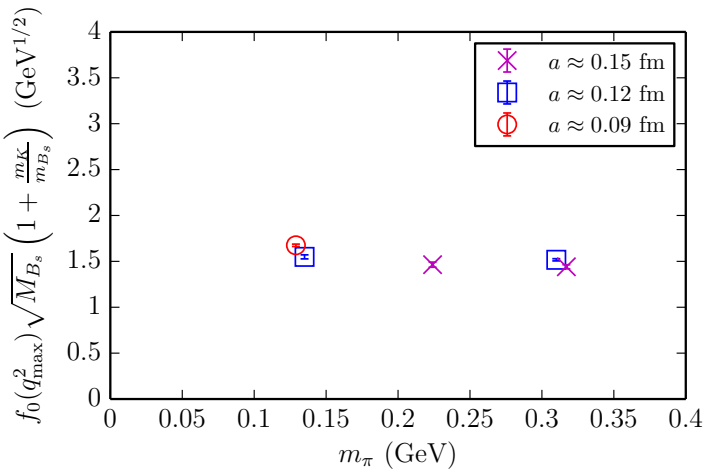

Figure 5.8: Results for the hadronic parameter $f_0(q^2_{\rm max})\sqrt{M_B}\left(1+\frac{m_K}{m_B}\right)$ on each of the lattice ensembles for the $B \to K\ell\nu$ decay in physical units of GeV$^{1/2}$.

$$+\left(\frac{\Lambda}{m_b}\right)^2\left(c_b(a\Lambda)^2\delta x_m + c_{bb}(a\Lambda)^2(\delta x_m)^2\right) \tag{5.27}$$

$$+\sum_{k=1,2}\left(d_k m_\pi^{2k} + l_k M_K^{2k}\right)\Bigg), \tag{5.28}$$

The prior on $\Gamma_{\rm phys}$ is set to 0.6(0.3). All other priors are set to 0.0(1.0) except c_1, which is given 0.0(0.5). Λ is taken as 400 MeV and Λ/m_b is taken as 0.1. At $m_\pi = 0$, $f_0\left(q^2_{\rm max}\right)/\left(f_{B_s}/f_K\right)\left(1+\frac{K}{B_s}\right) = 0.530(8)$, and at physical m_π the ratio is 0.535(8).

5.5 $B_s \to \eta_s$

In the same way that calculations of the $B \to \pi\ell\nu$ transition can be calculated, so too can the $B_s \to \eta_s$ transition. This is a special process that can be studied happily on the lattice, but is not a real-world process due to the presence of the η_s meson, which, as a result of mixing with the u and d quarks does not exist in reality. Therefore it should be viewed to be the same as the $B \to \pi\ell\nu$ with the spectator and active quark masses simply being increased to that of the s.

Figure 5.10 shows the ratio of the $B_s \to \eta_s$ three point correlators to the meson two point correlators. As with the $B \to \pi$ and $B_s \to K$ decays, the oscillatory behaviour is clear and the different T values converge to the same result.

Results for the currents $V_{00}^{(0)}$ and $V_{00}^{(1)}$, the leading and next-to-leading parts of the

Set	$f_0^{(0)}(q^2_{\text{max}})/(f^{(0)}_{B_s}/f_K)$	$f_0(q^2_{\text{max}})/(f_{B_s}/f_K)$
1	0.429(6)	0.440(6)
2	0.430(8)	0.441(8)
4	0.462(4)	0.478(4)
6	0.449(6)	0.463(7)
8	0.482(3)	0.501(4)

Table 5.11: Ratio of the form factor $f_0(q^2_{\text{max}})$ to the ratio of the decay constants f_{B_s} and f_{η_s} for each of the lattice sets. The numbers in the second column correspond to result for just the leading currents for the B meson and the vector current in three point correlators, i.e. only the J^0 current. The third column gives the result for the renormalised improved value where the $J^{(1)}$ and $J^{(2)}$ currents have been included for the B and the vector current in the three point correlators.

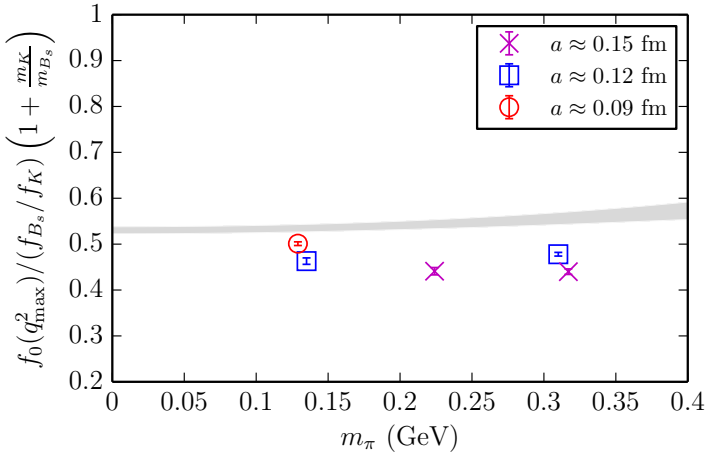

Figure 5.9: Results for the ratio $f_0\left(q^2_{\text{max}}\right)/\left(f_{B_s}/f_K\right)\left(1+\frac{m_K}{m_{B_s}}\right)$ on each of the lattice enmsembles against m_π in GeV.

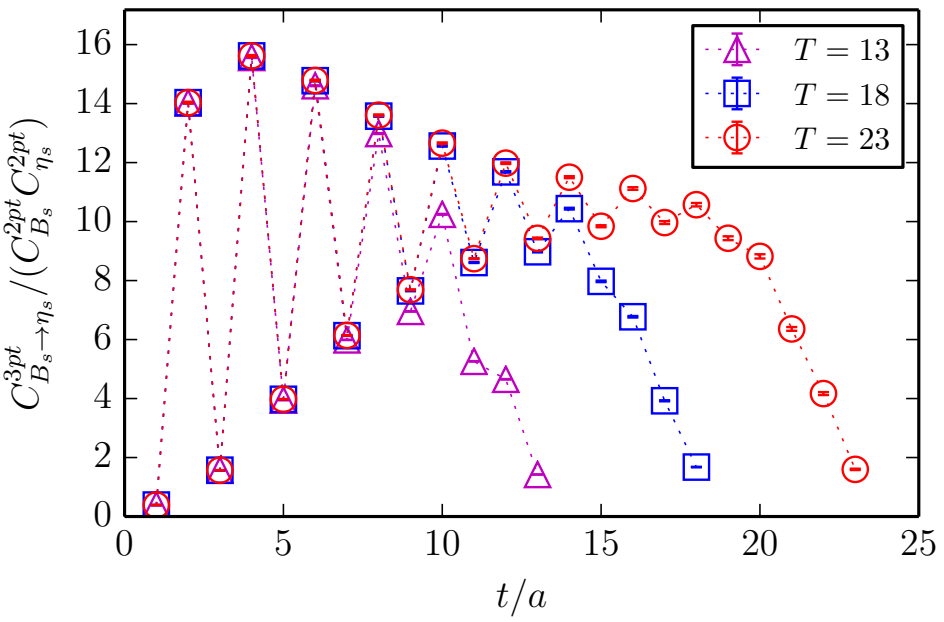

Figure 5.10: Ratio of the 3-point correlator for $B \to \eta_s$ decay to the 2-point correlators for the B_s meson and η_s on coarse set 4. The statistical accuracy we have is clear and the results converge for different T values.

three-point amplitude, and the improved and renormalised current V_{00} are given in table 5.12. Again, these have a normalisation factor of $4/\sqrt{2}$ included.

Table 5.13 gives the values of $f_0(q^2_{\text{max}})\sqrt{m_B}(1 + m_{\eta_s}/m_{B_s})$ in lattice units. The second column in the table gives the result for the leading current only. The third column is the result where the improved and renormalised B_s and vector currents are used. These values have been converted to GeV and are shown in figure 5.11 against the mass of the pion.

Finally, ratios of the form factor to the ratio of the B_s and η_s decay constants are given in table 5.14. The first result is for the leading current terms only, while the second result is from the improved and renormalised three point and B_s meson currents. In either case, the results do not depend on the pion mass, which should be expected here since there are no light valence quarks and the strange quarks are already tuned to their physical masses. The ratios for the improved and renormalised B_s and vector current are showing in figure 5.12, again with a fit band for $m_\pi = 0$ using the fit function from equation 5.28 substituting M_K terms with M_{η_s} terms. The parameters are the same, except in this case the QCD scale Λ is taken as 700 MeV. At $m_\pi = 0$, $f_0\left(q^2_{\text{max}}\right) / \left(f_{B_s}/f_{\eta_s}\right)\left(1 + \frac{\eta_s}{B_s}\right) = 0.605(13)$, and

Set	$V_{00}^{(0)}$	$V_{00}^{(1)}$	V_{00}
1	0.796(10)	-0.025(1)	0.787(10)
2	0.795(7)	-0.025(1)	0.785(7)
4	0.869(4)	-0.033(0)	0.845(4)
6	0.873(1)	-0.034(0)	0.847(1)
8	0.990(2)	-0.048(0)	0.944(2)

Table 5.12: Fit results of the temporal vector amplitude from the 3 point fits for the process $B_s \to \eta_s$. Given are the leading currents and the next-to-leading order correction. The value of $V_{00}^{(2)} = V_{00}^{(1)}$, so is not included in the table. The final column is the value of the improved and renormalised current as given in equation 5.10. It has been provided separately here as, since the errors between the leading and subleading currents are correlated, the error on the improved current is taken directly from the fit.

Set	$f_0^{(0)}(q^2_{\rm max})\sqrt{m_{B_s}}\left(1+\frac{m_{\eta_s}}{m_{B_s}}\right)$	$f_0(q^2_{\rm max})\sqrt{m_{B_s}}\left(1+\frac{m_{\eta_s}}{m_{B_s}}\right)$
1	1.143(14)	1.130(15)
2	1.136(10)	1.122(10)
4	1.130(5)	1.099(5)
6	1.125(2)	1.091(2)
8	1.093(2)	1.042(2)

Table 5.13: Hadronic parameter $f_0(q^2_{\rm max})\sqrt{m_{B_s}}$ multiplied by $\left(1+\frac{m_{\eta_s}}{m_B}\right)$ in lattice units. The numbers in the second column correspond to results for only the $J^{(0)}$ current. The third column gives the result for the renormalised improved value where the $J^{(1)}$ and $J^{(2)}$ currents have been included.

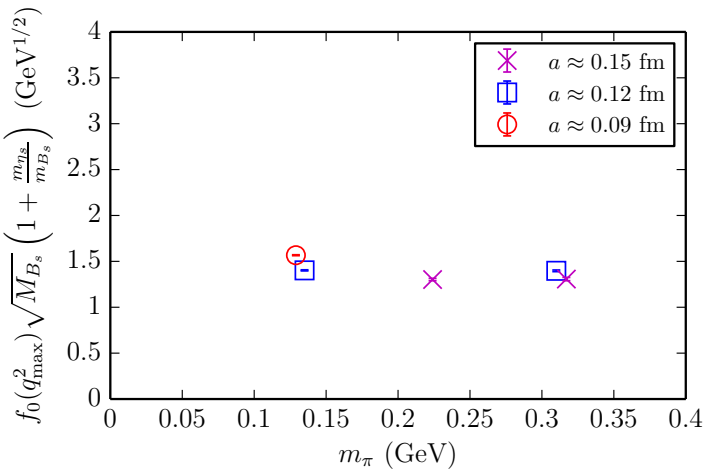

Figure 5.11: Results for the hadronic parameter $f_0\left(q^2_{\rm max}\right)\sqrt{M_{B_s}}\left(1+\frac{m_{\eta_s}}{m_{B_s}}\right)$ on each of the lattice ensembles for the $B_s \to \eta_s$ decay in physical units of GeV$^{1/2}$.

at physical m_π the ratio is 0.610(11).

Set	$f_0^{(0)}(q^2_{\rm max})/(f_{B_s}^{(0)}/f_{\eta_s})(1+m_{\eta_s}/m_{B_s})$	$f_0(q^2_{\rm max})/(f_{B_s}/f_{\eta_s})(1+m_{\eta_s}/m_{B_s})$
1	0.430(9)	0.444(6)
2	0.432(4)	0.446(4)
4	0.469(2)	0.488(3)
6	0.469(1)	0.489(1)
8	0.521(1)	0.546(1)

Table 5.14: Ratio of the form factor $f_0(q^2_{\rm max})$ to the ratio of the decay constants f_{B_s} and f_{η_s} for each of the lattice sets multiplied by the factor $(1+m_{\eta_s}/m_{B_s})$. The numbers in the second column correspond to result for just the leading currents for the B_s meson and the vector current in three point correlators, i.e. only the $J^{(0)}$ current. The third column gives the result for the renormalised improved value where the $J^{(1)}$ and $J^{(2)}$ currents have been included for the B_s and the vector current in the three point correlators.

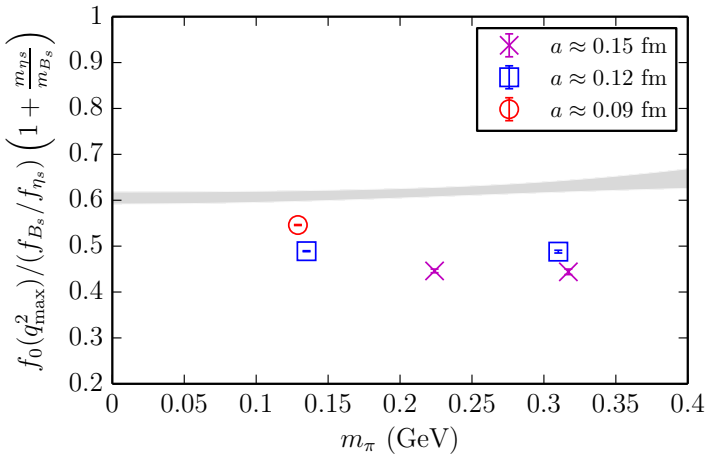

Figure 5.12: Results for the ratio $f_0(q^2_{\rm max})/\left(f_{B_s}/f_{\eta_s}\right)\left(1+\frac{m_{\eta_s}}{m_{B_s}}\right)$ on each of the lattice ensembles against m_π in GeV for the improved and renormalised currents.

Chapter 6

Conclusions

The use of NRQCD for b quarks is a powerful tool in lattice QCD calculations, because heavy quarks in bound systems are nonrelativistic and this is particularly true of b quarks. An advantage to using this method rather than a relativistic formalism is that the b quark can be simulated at its physical mass, eliminating the need to extrapolate to the physical mass at a later stage and thus reducing errors. NRQCD is also very fast, requiring only a relatively straightforward evolution equation to simulate the b quarks.

Results in this thesis have utilised gluon field configurations generation by the MILC collaboration that include $2+1+1$ flavours of quarks in the sea, and including u/d quarks down to their physical masses. Using these new state-of-the-art ensembles, energies and amplitudes have been obtained in order to calculate an array of hadron properties.

6.1 Bottomonium

We calculated the kinetic masses of η_b and Υ mesons on various lattice ensembles, which demonstrated how stable it is over a range of momenta. Comparisons were given that showed the effect of the v^4 radiative terms in the action.

We presented a complete nonperturbative determination of the Υ and Υ' decay constants and leptonic widths using full lattice QCD for the first time. By matching lattice temporal moments to those from continuum perturbative QCD and including corrections to the leading current term we could determination the matrix elements between the Υ

states and the vacuum required for these calculation. These results are

$$f_\Upsilon = 649(31)\ \text{GeV}$$
$$f_{\Upsilon'} = 481(39)\ \text{GeV} \tag{6.1}$$

and

$$\Gamma(\Upsilon \to e^+e^-) = 1.19(11)\ \text{keV}$$
$$\Gamma(\Upsilon' \to e^+e^-) = 0.69(9)\ \text{keV}. \tag{6.2}$$

These same moments were used in the calculation of the quark mass m_b to give

$$\bar{m}_b(\bar{m}_b, n_f = 5) = 4.196(23)\ \text{GeV} \tag{6.3}$$

which is among the best lattice QCD determinations of this quantity. The errors we obtain are dominated by the lattice spacing dependence. Future work will aim to include terms in our formalism to reduce these errors further.

6.2 B Physics

Heavy-light decays can be studied on the lattice where the heavy quark is simulated using NRQCD and the light quark is simulated with an appropriate lattice quark action. In the work presented here, HISQ quarks were used for the light quark. The form factor $f_0(q^2_{\text{max}})$ was calculated for the $B \to \pi\ell\nu$ semileptonic decay on the MILC ensembles, including those with physical light quarks. The main result was in demonstrating that the soft pion theorem, which says $f_0(q^2_{\text{max}})$ should equal the ratio of the B and π decay constants in the chiral limit – that is, when $m_\pi \to 0$ – holds. This resolves the issue of it seeming not to hold in previous studies where lattice ensembles that did not account for the behaviour of quarks in the sea were used or where the calculations involved heavy pion masses. Our calculations on ensembles with physical light quarks helps overcome this issue.

The work here can be expanded by generating the same data for a range of q^2 values, allowing a determination of the form factor $f_+(q^2)$. By doing so, this would allow access to the CKM matrix element $|V_{ub}|$ through the experimentally measurable differential partial decay rate of, for example the $B \to \pi\ell\nu$, by,

$$\frac{\mathrm{d}\Gamma}{\mathrm{d}q^2} = \frac{G_F^2}{24\pi^3} p_\pi^3 |V_{ub}|^2 |f_+(q^2)|^2, \tag{6.4}$$

where G_F is the Fermi constant and p_π is the momentum of the pion in the rest frame of the B meson.

The determination of $|V_{ub}|$ is not well known, and by comparing the value from exclusive processes – where a particular final state is considered – in lattice QCD and inclusive processes where all $b \to u$ transitions are taken, there is some controversy over the value. In order to resolve this issue, it is important to improve the accuracy of the lattice QCD calculation. The calculation presented here is the first step in this direction.

6.3 Outlook

All of the results presented in this thesis can be built upon in various ways. Work is already underway to perform calculations in NRQCD including the effects of v^6 terms and four-quark operators in the action. Further study of the current corrections will also help in achieving greater precision in our calculations; particularly in the Υ and Υ' leptonic widths.

The study of $B \to \pi\ell\nu$ and $B_s \to K\ell\nu$ decays can be expanded from the work presented here in order to give a determination of the V_{ub} CKM matrix element. This would involve performing calculations over a range of q^2 to extract the form factor $f_+(q^2)$ in particular.

Appendix A

Current Corrections

Initially, a different approach was taken to try to determine the correction coefficients k_1 from chapter 4.3.1. This method was to use a slightly altered correction current,

$$\mathbf{J_i} = \sigma \left(\frac{\Delta^2}{m_b^2} \right)^i, \tag{A.1}$$

where,

$$\mathbf{J_1} = \sum_{x;i=1}^{3} \chi_x^\dagger \frac{\sigma}{(am_b)^2} \times (U_i(x)\Psi_{x+\hat{i}} + U_i^\dagger(x-\hat{i})\Psi(x-\hat{i}) - 2\Psi(x)). \tag{A.2}$$

This is identical to the current given in equation 4.25 but with the addition of U fields. In this case, the correction was applied only to the sink and utilised a random wall source in contrast to the other set of corrections where the correction was applied to both the source and the sink with no random wall source.

The methodology that was used for the results in chapter 4.3.1 matched the lattice temporal moments calculated from bottomonium correlators at zero momentum to temporal moments from continuum perturbation theory by adjusting the value of k_1. In this calculation, correlators were generated for mesons with finite momentum as well as zero momentum so that the behaviour of the amplitudes could be compared to the expected relativistic behaviour and k_1 tuned such that the NRQCD currents correctly normalised.

The values of the amplitudes for the matrix elements $\langle 0|J^{(0)}_{V,\mathrm{NRQCD}}|\Upsilon\rangle$ and $\langle 0|J^{(1)}_{V,\mathrm{NRQCD}}|\Upsilon\rangle$ are given in tables A.1, A.2 and A.3 for the very coarse, coarse and fine ensembles with $m_l/m_s = 0.2$ respectively. These values were determined by fitting all of the various momenta simultaneously for each meson and with correlators corresponding to $\langle 0|[J_0^\dagger]J_0|0\rangle$ and $\langle 0|[J_1^\dagger]J_0|0\rangle$ so that the leading and current correction amplitudes components could be separated.

	η_b		Υ	
P	$c(J^{(0)}_{\eta_b}, 0)$	$c(J^{(1)}_{\eta_b}, 0)$	$c(J^{(0)}_{\Upsilon}, 0)$	$\langle 0\|J_1\|\Upsilon\rangle$
(0,0,0)	1.0473(4)	-0.2109(1)	0.9726(6)	-0.1770(1)
(1,1,0)	1.0552(4)	-0.2186(1)	0.9793(6)	-0.1840(1)
(1,1,1)	1.0590(4)	-0.2224(1)	0.9823(7)	-0.1875(2)
(2,2,0)	1.0810(7)	-0.2422(2)	1.0023(11)	-0.2057(3)
(3,3,0)	1.1254(30)	-0.2827(9)	1.0344(71)	-0.2409(18)

Table A.1: Values of the amplitudes for the currents J_0 and J_1 for the η_b and Υ mesons on the very coarse ensemble, set 1 using the mistuned value of $am_b = 3.42$. The correction piece, J_1, was determined by equation A.2 being applied to the sink only. The Υ values are those taken from the x polarisation.

	η_b		Υ	
P	$c(J^{(0)}_{\eta_b}, 0)$	$c(J^{(1)}_{\eta_b}, 0)$	$c(J^{(0)}_{\Upsilon}, 0)$	$\langle 0\|J_1\|\Upsilon\rangle$
(0,0,0)	0.8035(2)	-0.2248(1)	0.7153(4)	-0.1694(1)
(1,1,0)	0.8068(2)	-0.2294(1)	0.7183(4)	-0.1734(1)
(1,1,1)	0.8086(2)	-0.2317(1)	0.7196(5)	-0.1754(1)
(2,2,0)	0.8163(3)	-0.2431(1)	0.7240(12)	-0.1848(3)
(3,3,0)	0.8344(5)	-0.2672(2)	0.7386(21)	-0.2055(7)

Table A.2: Values of the amplitudes for the currents J_0 and J_1 for the η_b and Υ mesons on the coarse ensemble, set 4. The correction piece, J_1, was determined by equation A.2 being applied to the sink only. The Υ values are those taken from the x polarisation.

	η_b		Υ	
P	$c(J^{(0)}_{\eta_b}, 0)$	$c(J^{(1)}_{\eta_b}, 0)$	$c(J^{(0)}_{\Upsilon}, 0)$	$\langle 0\|J_1\|\Upsilon\rangle$
(0,0,0)	0.5455(1)	-0.2396(1)	0.4527(2)	-0.1449(1)
(1,1,0)	0.5470(2)	-0.2432(1)	0.4536(3)	-0.1477(1)
(2,2,0)	0.5517(2)	-0.2541(1)	0.4571(3)	-0.1564(1)
(3,3,0)	0.5584(8)	-0.2718(4)	0.4613(9)	-0.1705(4)

Table A.3: Values of the amplitudes for the currents J_0 and J_1 for the η_b and Υ mesons on the fine ensemble, set 7. The correction piece, J_1, was determined by equation A.2 being applied to the sink only. The Υ values are those taken from the x polarisation.

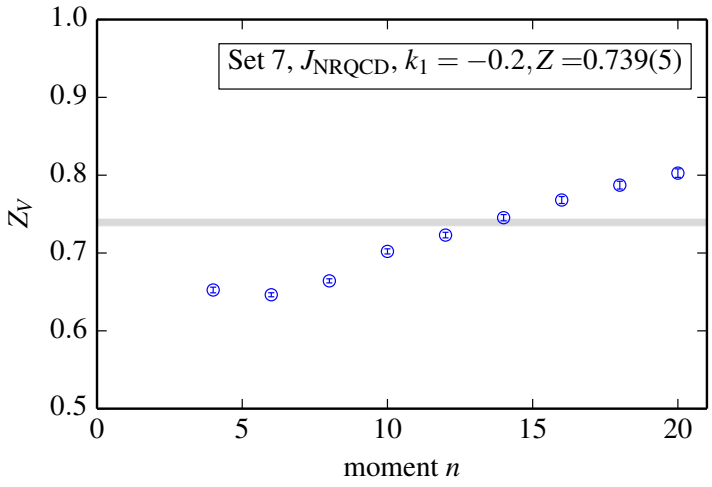

Figure A.1: Values of Z_{match} against moment number on fine ensemble set 7 with k_1 determined by fitting ratios of the amplitudes at finite momentum to amplitudes at zero momentum such that it matches the expected relativistic behaviour. It is clear that no plateau is achieved using this method, with k_1 having the opposite sign to that obtained using our other method. The grey band shows the average value of Z_{match} between $n = 10$ and $n = 20$, but this is obviously not a good fit.

In order to make a determination of the value of k_1 using this method, a fit was performed using ratios of the amplitudes at the finite momenta with the amplitudes at zero momentum as the input data and k_1 as a fit parameter with the aim of tuning k_1 to give the expected relativistic behaviour of $\tilde{c}(p)/\tilde{c}(0) = \sqrt{1 + P^2/M^2}$, where $\tilde{c}(p) = c(J^{(0)}_{V,\mathrm{NRQCD}}, p) + k_1 c(J^{(1)}_{V,\mathrm{NRQCD}}, p)$.

Unfortunately, this approach did not result in the correct sign for the k_1 value on the fine ensemble, the result of which can be seen in figure A.1 where no plateau is achieved. This is because the major part of the finite momentum correction comes from the terms in section 4.2.1 which this method fails to pick up.

Bibliography

[1] Particle Data Group, J. Beringer *et al.*, Phys. Rev. D **86**, 010001 (2012).

[2] ATLAS Collaboration, G. Aad *et al.*, Phys.Lett. **B716**, 1 (2012), 1207.7214.

[3] CMS Collaboration, S. Chatrchyan *et al.*, Phys.Lett. **B716**, 30 (2012), 1207.7235.

[4] F. Englert and R. Brout, Phys. Rev. Lett. **13**, 321 (1964).

[5] P. W. Higgs, Phys. Rev. Lett. **13**, 508 (1964).

[6] G. S. Guralnik, C. R. Hagen, and T. W. B. Kibble, Phys. Rev. Lett. **13**, 585 (1964).

[7] F. Mandl and G. Shaw, *Quantum field theory* (John Wiley & Sons, 2010).

[8] D. J. Gross and F. Wilczek, Phys. Rev. Lett. **30**, 1343 (1973).

[9] H. D. Politzer, Phys. Rev. Lett. **30**, 1346 (1973).

[10] D. J. Gross and F. Wilczek, Phys. Rev. D **8**, 3633 (1973).

[11] R. P. Feynman, Rev. Mod. Phys. **20**, 367 (1948).

[12] S. W. Herb *et al.*, Phys. Rev. Lett. **39**, 252 (1977).

[13] W. R. Innes *et al.*, Physical Review Letters **39**, 1240 (1977).

[14] BaBar Collaboration, B. Aubert *et al.*, Phys.Rev.Lett. **101**, 071801 (2008), 0807.1086.

[15] BaBar Collaboration, B. Aubert *et al.*, Phys.Rev.Lett. **103**, 161801 (2009), 0903.1124.

[16] HPQCD and UKQCD Collaborations, A. Gray *et al.*, Phys. Rev. D **72**, 094507 (2005), hep-lat/0507013.

[17] R. Dowdall, C. Davies, G. Lepage, and C. McNeile, (2013), 1303.1670.

[18] HPQCD Collaboration, R. J. Dowdall *et al.*, Phys. Rev. D **85**, 054509 (2012), 1110.6887.

[19] HPQCD Collaboration, C. Davies, E. Follana, I. Kendall, G. P. Lepage, and C. McNeile, Phys.Rev. **D81**, 034506 (2010), 0910.1229.

[20] K. G. Wilson, Phys. Rev. D **10**, 2445 (1974).

[21] C. Gattringer and C. B. Lang, *Quantum chromodynamics on the lattice: an introductory presentation* (Springer, 2009).

[22] K. Symanzik, Nuclear Physics B **226**, 187 (1983).

[23] M. G. Alford, W. Dimm, G. Lepage, G. Hockney, and P. Mackenzie, Phys.Lett. **B361**, 87 (1995), hep-lat/9507010.

[24] G. Curci, P. Menotti, and G. Paffuti, Physics Letters B **130**, 205 (1983).

[25] M. Lüscher and P. Weisz, Communications in Mathematical Physics **97**, 59 (1985).

[26] K. Wilson, Quarks and strings on a lattice, in *New Phenomena in Subnuclear Physics*, edited by A. Zichichi, , The Subnuclear Series Vol. 13, pp. 69–142, Springer US, 1977.

[27] H. J. Rothe, *Lattice gauge theories* (World Scientific, 2012).

[28] H. Nielsen and M. Ninomiya, Physics Letters B **105**, 219 (1981).

[29] D. B. Kaplan, Chiral Symmetry and Lattice Fermions, 2009, 0912.2560.

[30] B. Sheikholeslami and R. Wohlert, Nuclear Physics B **259**, 572 (1985).

[31] M. Lüscher, Advanced lattice QCD, 1998, hep-lat/9802029.

[32] G. P. Lepage, Phys.Rev. **D59**, 074502 (1999), hep-lat/9809157.

[33] S. Naik, Nuclear Physics B **316**, 238 (1989).

[34] E. Follana *et al.*, Phys. Rev. D **75**, 054502 (2007).

[35] S. Hashimoto and T. Onogi, Ann.Rev.Nucl.Part.Sci. **54**, 451 (2004), hep-ph/0407221.

[36] C. McNeile, Heavy quarks on the lattice, in *Heavy Quark Physics*, pp. 100–128, Springer, 2004.

[37] C. Davies, PoS **LATTICE2011**, 019 (2011), 1203.3862.

[38] HPQCD Collaboration, C. McNeile *et al.*, PoS **LAT2009**, 116 (2009), 0910.2921.

[39] E. Eichten and B. Hill, Physics Letters B **234**, 511 (1990).

[40] H. Georgi, Physics Letters B **240**, 447 (1990).

[41] B. Grinstein, Nuclear Physics B **339**, 253 (1990).

[42] T. Mannel, W. Roberts, and Z. Ryzak, Nuclear Physics B **368**, 204 (1992).

[43] M. Neubert, Physics Reports **245**, 259 (1994).

[44] MILC Collaboration, A. Bazavov *et al.*, Phys.Rev. **D87**, 054505 (2013), 1212.4768.

[45] MILC collaboration, A. Bazavov *et al.*, Phys. Rev. D. **82**, 074501 (2010).

[46] HPQCD Collaboration, A. Hart, G. von Hippel, and R. Horgan, Phys.Rev. **D79**, 074008 (2009), 0812.0503.

[47] B. A. Thacker and G. P. Lepage, Phys. Rev. D **43**, 196 (1991).

[48] L. L. Foldy and S. A. Wouthuysen, Physical Review **78**, 29 (1950).

[49] S. Tani, Progress of Theoretical Physics **6**, 267 (1951).

[50] J. G. Krner and G. Thompson, Physics Letters B **264**, 185 (1991).

[51] F. J. Ynduráin, *The theory of quark and gluon interactions* (Springer, 2007).

[52] S. Meinel, *Heavy quark physics on the lattice with improved nonrelativistic actions*, PhD thesis, University of Cambridge, 2010.

[53] G. P. Lepage, L. Magnea, C. Nakhleh, U. Magnea, and K. Hornbostel, Phys. Rev. D **46**, 4052 (1992).

[54] G. P. Lepage and P. B. Mackenzie, Physical Review D **48**, 2250 (1993).

[55] H. D. Trottier, Phys. Rev. D **55**, 6844 (1997).

[56] P. Lepage, Nucl.Phys.Proc.Suppl. **60A**, 267 (1998), hep-lat/9707026.

[57] M. G. Alford, T. R. Klassen, and G. P. Lepage, Phys.Rev. **D58**, 034503 (1998), hep-lat/9712005.

[58] N. H. Shakespeare and H. D. Trottier, Phys.Rev. **D58**, 034502 (1998), hep-lat/9802038.

[59] UKQCD Collaboration, C. Davies *et al.*, Phys.Rev. **D58**, 054505 (1998), hep-lat/9802024.

[60] A. Gray *et al.*, Phys.Rev. **D72**, 094507 (2005), hep-lat/0507013.

[61] R. Dowdall, C. Davies, T. Hammant, and R. Horgan, (2013), 1309.5797.

[62] HPQCD Collaboration, R. Dowdall, C. Davies, R. Horgan, C. Monahan, and J. Shigemitsu, (2013), 1302.2644.

[63] S. Meinel, Phys. Rev. D **85**, 114510 (2012).

[64] S. Meinel, Phys. Rev. D **82**, 114502 (2010).

[65] I. Kendall, *Lattice QCD Studies of Upsilon Physics*, PhD thesis, University of Glasgow, UK, 2010.

[66] G. P. Lepage *et al.*, Nuclear Physics B - Proceedings Supplements **106-107**, 12 (2002).

[67] J. J. Dudek, R. G. Edwards, and D. G. Richards, Phys. Rev. D **73**, 074507 (2006).

[68] G. T. Bodwin and A. Petrelli, Phys.Rev. **D66**, 094011 (2002), hep-ph/0205210.

[69] J. Erler, Phys.Rev. **D59**, 054008 (1999), hep-ph/9803453.

[70] A. Hart, G. M. von Hippel, and R. R. Horgan, Phys. Rev. D **75**, 014008 (2007).

[71] R. Boughezal, M. Czakon, and T. Schutzmeier, Phys.Rev. **D74**, 074006 (2006), hep-ph/0605023.

[72] K. Chetyrkin, J. H. Kuhn, and C. Sturm, Eur.Phys.J. **C48**, 107 (2006), hep-ph/0604234.

[73] Y. Kiyo, A. Maier, P. Maierhofer, and P. Marquard, Nucl.Phys. **B823**, 269 (2009), 0907.2120.

[74] A. Maier, P. Maierhofer, and P. Marqaurd, Phys.Lett. **B669**, 88 (2008), 0806.3405.

[75] A. Maier, P. Maierhofer, P. Marquard, and A. Smirnov, Nucl.Phys. **B824**, 1 (2010), 0907.2117.

[76] G. Donald *et al.*, Phys.Rev. **D86**, 094501 (2012), 1208.2855.

[77] HPQCD Collaboration, I. Allison *et al.*, Phys. Rev. D **78**, 054513 (2008).

[78] HPQCD Collaboration, C. McNeile, C. T. H. Davies, E. Follana, K. Hornbostel, and G. P. Lepage, Phys. Rev. D **82**, 034512 (2010).

[79] C. Davies *et al.*, Phys.Rev. **D82**, 114504 (2010), 1008.4018.

[80] C. McNeile, C. Davies, E. Follana, K. Hornbostel, and G. Lepage, Phys.Rev. **D86**, 074503 (2012), 1207.0994.

[81] M. E. Peskin and D. V. Schroeder, *An introduction to quantum field theory* (Westview, 1995).

[82] D. H. Perkins, *Introduction to high energy physics* (Cambridge University Press, 2000).

[83] Muon G-2 Collaboration, G. Bennett *et al.*, Phys.Rev. **D73**, 072003 (2006), hep-ex/0602035.

[84] B. Colquhoun, R. Dowdall, C. Davies, K. Hornbostel, and G. Lepage, (2014), 1408.5768.

[85] B. Chakraborty *et al.*, (2014), 1403.1778.

[86] S. Bodenstein, C. Dominguez, and K. Schilcher, Phys.Rev. **D85**, 014029 (2012), 1106.0427.

[87] C. Davies *et al.*, PoS **LATTICE2013**, 438 (2013), 1312.5874.

[88] B. Chakraborty *et al.*, (2014), 1408.4169.

[89] HPQCD Collaboration, A. Lee *et al.*, Phys.Rev. **D87**, 074018 (2013), 1302.3739.

[90] N. Carrasco *et al.*, (2013), 1311.2837.

[91] P. Ball *et al.*, (2000), hep-ph/0003238.

[92] HPQCD Collaboration, UKQCD Collaboration, E. Follana, C. Davies, G. Lepage, and J. Shigemitsu, Phys.Rev.Lett. **100**, 062002 (2008), 0706.1726.

[93] R. Dowdall, C. Davies, T. Hammant, and R. Horgan, Phys.Rev. **D86**, 094510 (2012), 1207.5149.

[94] C. Monahan, J. Shigemitsu, and R. Horgan, Phys.Rev. **D87**, 034017 (2013), 1211.6966.

[95] S. Collins *et al.*, Phys.Rev. **D63**, 034505 (2001), hep-lat/0007016.

[96] G. Burdman and J. F. Donoghue, Physics Letters B **280**, 287 (1992).

[97] G. Burdman, Z. Ligeti, M. Neubert, and Y. Nir, Phys.Rev. **D49**, 2331 (1994), hep-ph/9309272.

[98] S. Hashimoto, K.-I. Ishikawa, H. Matsufuru, T. Onogi, and N. Yamada, Phys. Rev. D **58**, 014502 (1998).

[99] S. Hashimoto, Nucl.Phys.Proc.Suppl. **83**, 3 (2000), hep-lat/9909136.

[100] C. Aubin and C. Bernard, Phys.Rev. **D76**, 014002 (2007), 0704.0795.

[101] C. Aubin and C. Bernard, Phys.Rev. **D73**, 014515 (2006), hep-lat/0510088.

[102] C. Bouchard, G. P. Lepage, C. Monahan, H. Na, and J. Shigemitsu, (2014), 1406.2279.